N-3 POLYUNSATURATED FATTY ACIDS ALTER MOUSE $CD4^+$ T CELL ACTIVATION BY MODIFYING THE LIPID BILAYER PROPERTIES

A Dissertation

by

TIM YU-TIEN HOU

Submitted to the Office of Graduate and Professional Studies of
Texas A&M University
in partial fulfillment of the requirements for the degree of

DOCTOR OF PHILOSOPHY

Chair of Committee,	Robert S. Chapkin
Co-Chair of Committee,	Stephen H. Safe
Committee Members,	David N. McMurray
	Gonzalo M. Rivera
	Hays S. Rye
Head of Department,	Gregory D. Reinhart

December 2014

Major Subject: Biochemistry

ABSTRACT

Epidemiological and clinical studies have shown that very long chain n-3 polyunsaturated fatty acids (n-3 PUFA) such as eicosapentaenoic acid (EPA) and docosahexaenoic acid (DHA) possess anti-inflammatory properties. The mechanisms by which n-3 PUFA exert their anti-inflammatory effects remain undefined. Extending earlier observations that actin remodeling at the immunological synapse (IS) is suppressed in $CD4^+$ T cells supplemented with n-3 PUFA, we hypothesized that the lipid mediator phosphatidylinositol-(4,5)-bisphosphate [$PI(4,5)P_2$], which modulates actin remodeling, is perturbed by n-3 PUFA. Utilizing the transgenic *Fat-1* mouse model that synthesizes n-3 PUFA *de novo* and enriches the plasma membrane with n-3 PUFA, and wild type (WT) mice fed either a 5% corn oil (CO, control) or a 4% DHA triglyceride-enriched diet, we found that splenic $CD4^+$ T cells from *Fat-1* mice and WT mice fed a DHA-enriched diet, when compared to WT and CO-fed $CD4^+$ T cells, exhibited i) decreased $PI(4,5)P_2$; ii) unchanged $PI(4,5)P_2$ upon activation; and iii) suppressed actin remodeling, as assessed by immunofluorescence, upon activation, which was rescued in *Fat-1* $CD4^+$ T cells by incubation with exogenous $PI(4,5)P_2$. Mechanistically, recruitment of the Wiskott-Aldrich syndrome protein (WASP), an actin-remodeling protein regulated by $PI(4,5)P_2$, to the IS upon anti-CD3/anti-CD28 coated bead stimulation was inhibited in *Fat-1* $CD4^+$ T cells.

Since discrete pools of $PI(4,5)P_2$ may exist in the plasma membrane, we also determined whether n-3 PUFA modulate the spatial organization of $PI(4,5)P_2$ relative to

raft and non-raft domains by transducing $CD4^+$ T cells from WT and *Fat-1* mice with fluorescence resonance energy transfer (FRET) lipid raft probes Lck(N10) and LAT(ΔCP), and the non-raft probe Src(N15). Co-clustering of PH(PLC-δ1), a $PI(4,5)P_2$ probe, and Lck(N10) or LAT(ΔCP), was not affected by n-3 PUFA; however, co-clustering of PH(PLC-δ1) and Src(N15) exhibited a decrease in *Fat-1* $CD4^+$ T cells, suggesting that n-3 PUFA alter the spatial organization of $PI(4,5)P_2$. Incubation with exogenous $PI(4,5)P_2$ rescued the effects on the non-raft $PI(4,5)P_2$ pool, and reversed the corresponding suppression of T cell proliferation in *Fat-1* $CD4^+$ T cells.

Previous research has shown that n-3 PUFA can inhibit Fyn palmitoylation. Therefore, we proposed an alternative hypothesis that n-3 PUFA affect the palmitoylation, and hence activation, of signaling proteins upon T cells activation. Using a newly developed technique in which palmitoylated proteins are coupled to biotin via Click chemistry, we demonstrated that n-3 PUFA do not affect the palmitoylation of signaling proteins, such as LCK, in *Fat-1* $CD4^+$ T cells.

DEDICATION

To my parents Hou Yun-Tai and Tsao Chun-Yen.

ACKNOWLEDGEMENTS

I would first like to thank my PI, Dr. Robert S. Chapkin, for providing me the opportunity to work on my doctoral research in his lab. Dr. Chapkin's patience, compassion, guidance, and leadership were instrumental in my development from a PhD student to an independent scientist. Dr. Chapkin's unwavering commitment to his students was an inspiration for me to reach for the stars and achieve my full potential.

I would also like to thank my committee members. Dr. Stephen Safe, the co-chair of my committee, for his support in my research endeavors, and his career advice; Dr. David McMurray, for attending update meetings and showing me the importance of extending my research beyond biochemistry and into physiological relevance; Dr. Gonzalo Rivera, for sharing his expertise in actin remodeling and lentiviral transduction with me; and Dr. Hays Rye, for helping me with my FRET experiments and controls.

Additionally, I could not have completed my PhD studies without Dr. Rola Barhoumi, her tireless efforts in imaging all the slides and FRET samples for me, as well as Dr. Rami Hannoush, for providing me with the reagents to initiate the post-translational modification studies.

I am grateful to the lab moms, Dr. Laurie Davidson, Dr. Yang-Yi Fan, Ms. Evelyn Callaway, and Ms. Jennifer Goldsby. Their unselfishness in teaching me new techniques, helping me analyze data, maintaining animal colonies, was paramount in my PhD studies. More importantly was their compassion in listening to me in time of need, and celebrating with me during time of success. I could not have completed this

dissertation without their wonderful support and friendship. I would also like to thank members of the Chapkin Lab; Dr. Jennifer Monk, thank you for your friendship and knowledge. I know that we will always be able to sing our way out of challenging experiments in front of us.

I would not be here without the loving support of my family. I would first like to thank my father, Hou Yun-Tai, and my mother, Tsao Chun-Yen, for making sacrifices and venturing into the unknown courageously to provide new opportunities for me and my sisters. Thanks to my sisters, Jenny, Jennifer, and Vicky for their unwavering love and support.

Lastly, I would like to acknowledge all the Buddhas in the ten directions, for showing me wisdom and compassion. Thank you for giving me courage and calmness when doubt crept in during my PhD studies.

This PhD research was generously supported by two fellowships: National Science and Engineering Research Council of Canada Pre-Doctoral Fellowship, and the Texas A&M Health Science Center, College of Medicine Microbial Pathogenesis Training Grant Faculty Pre-Doctoral Fellowship.

NOMENCLATURE

µm	Micrometer
AA	Arachidonic acid
Ag	Antigen
APC	Antigen presenting cell
AICD	Activation-induced cell death
BAR	Bin-amphiphysin-Rvs
Ca^{2+}	Calcium
CCL	CC chemokine ligand
CD	Cluster of differentiation
CFSE	Carboxyfluorescein succinimidyl ester
CO	Corn oil
cSMAC	Central supramolecular activation cluster
DAG	Diacylglycerol
DHA	Docosahexaenoic acid
DNA	Deoxyribonucleic acid
DOPE	1,2-dioleoyl-*sn*-glycero-3-phosphoethanolamine
DPA	Docosapentaenoyl acid
ECFP	Enhanced cyan fluorescent protein
EGFR	Epidermal growth factor receptor
ENTH	Epsin N-terminal homology

EPA	Eicosapentaenoic acid
ER	Endoplasmic reticulum
F-actin	Filamentous actin
FERM	Four-point one, ezrin, radixin, moesin
FRAP	Fluorescence recovery after photobleaching
FRET	Fluorescence resonance energy transfer
G-actin	Globular actin
GADS	Grb2 (growth-factor-receptor-bound protein 2)-related adaptor protein
GM1	Monosialotetrahexosylganglioside
GPR	G-protein coupled receptor
IBD	Inflammatory bowel disease
IFN-γ	Interferon-gamma
IL	Interleukin
Inp54p	Inositol polyphosphate 5-phosphatase
IP3	Inositol (1,4,5)-trisphosphate
IS	Immunological synapse
ITK	Interleukin-2 inducible T-cell kinase
kDa	Kilodalton
LAT	Linker of activated T cells
Lck	Lymphocyte-specific protein tyrosine kinase
LKU	Lipid kinase unique

Lo	Liquid-ordered
MARCKS	Myristoylated alanine-rich C kinase substrate
MHCII	Major histocompatibility class II
Na^+	Sodium
NCK	Non-catalytic region of tyrosine kinase adaptor protein
NLRP	NOD-like receptor family, pyrin domain containing
Nm	Nanometer
NMR	Nuclear magnetic resonance
NSAIDs	Non-steroidal anti-inflammatory drugs
OA	Oleic acid
PAK	p21-activated kinase
PALM	Photoactivation localization microscopy
PH	Pleckstrin homology domain
PI	Propidium iodide
PI(4)P	Phosphatidylinositol-4-phosphate
$PI(4.5)P_2$	Phosphatidylinositol-(4,5)-bisphosphate
PI(5)P	Phosphatidylinositol-5-phosphate
PIP	Phosphoatidylinositol phosphate
PIP4KII	Type II phosphatidylinositol-5-phosphate 4-kinases
PIP5KI	Type I phosphatidylinositol-4-phosphate 5-kinases
PLC	Phospholipase C
PMA	Phorbol 12-myristate 13-acetate

PPARγ	Peroxisome proliferator-activated receptor-γ
pSMAC	Peripheral supramolecular activation cluster
PTEN	Phosphatase and tensin homolog
PUFA	Polyunsaturated fatty acids
RNA	Ribonucleic acid
RXRα	Retinoid X receptor-α
SLP76	SH2 (Src homology 2) domain-containing leukocyte protein of 76 kDa
Src	Sarcoma proto-oncogene tyrosine-protein kinase
STIM1	Stromal interaction molecule 1
T_C	Cytotoxic T lymphocytes
TCR	T cell receptor
TGFβ	Transforming growth factor-beta
T_H	Helper T lymphocytes
TPN	Total parenteral nutrition
VAV1	VAV1 guanine nucleotide exchange factor
WASP	Wiskott-Aldrich syndrome protein
WT	Wild type
YPet	Yellow fluorescent protein for energy transfer
ZAP70	Zeta (ζ)-chain (TCR)-associated protein kinase of 70 kDa

TABLE OF CONTENTS

Page

Page

Page

Page

LIST OF FIGURES

CHAPTER I

INTRODUCTION AND LITERATURE REVIEW

1.1 Plasma membrane and the cytoskeleton

The cell, a basic unit of life, is composed of macromolecules such as carbohydrates, DNA, RNA, protein, and lipids. These macromolecules sustain life by processing complex chemicals in the environment into simple compounds to be used for energy metabolism. As well, the cell replicates by faithfully preserving its genetic materials. The cell membrane, composed mainly of a phospholipid bilayer, constitutes the outer boundary of the cell; not only does the cell membrane control molecule transport, but also regulates the transmission of signals into and out of the cell. Thus, it represents the first line of defense against external threats, while providing the compartment for the cell to perform biochemistry.

The first model of the plasma membrane was proposed in 1972 by Singer and Nicolson (1). In this model, coined the fluid mosaic model, the phospholipid bilayer is thought of as a fluid, dynamic, passive solvent in which proteins either transverse across (i.e. integral proteins), or loosely associate (i.e. peripheral proteins), with the phospholipid bilayer. The heterogeneity of the proteins and phospholipids that comprise the plasma membrane allow the cell to perform a diverse spectrum of biochemistry. Although the contribution of the protein heterogeneity to the function of a cell can be easily understood, the heterogeneity of the lipids in the plasma membrane is less well studied, leading to questions about the role these lipids play at the cellular level.

The heterogeneity of proteins results in the classical four levels of protein structures (i.e. primary, secondary, tertiary, and quaternary) to describe the three-dimensional structures of the proteins, and linking them to protein functions. Lipids, however, lack this system of classification to describe how these hydrophobic molecules interact with each other to form higher order structures, and ultimately how these lipid structures function in the cell. The plasma membrane is composed of amphiphilic phospholipids, which contain both hydrophobic and hydrophilic components, to create an energetically favorable bilayer. Analogous to the primary structure of proteins, where twenty amino acids are the building blocks of the polypeptide, phospholipids in the plasma membrane are generally characterized by three functional groups attached to a glycerol backbone.

The plasma membrane contains three classes of amphiphilic lipids: phospholipids, glycolipids, and sterols. These lipids are further subdivided into various fatty acids and headgroups at the *sn-1*, *sn-2*, and *sn-3* positions (2). For example, a major species of phosphatidylinositol-(4,5)-bisphosphate [$PI(4,5)P_2$] is composed of a saturated C18:0 fatty acid at the *sn-1* position, an unsaturated $C20:4^{\Delta 5,8,11,14}$ fatty acid at the *sn-2* position, and *myo*-inositol 4,5-bisphosphate at the *sn-3* position. With all these layers of complexity, could lipids in the plasma membrane form local structures, analogous to secondary structures such as alpha-helices and beta-sheets found in proteins?

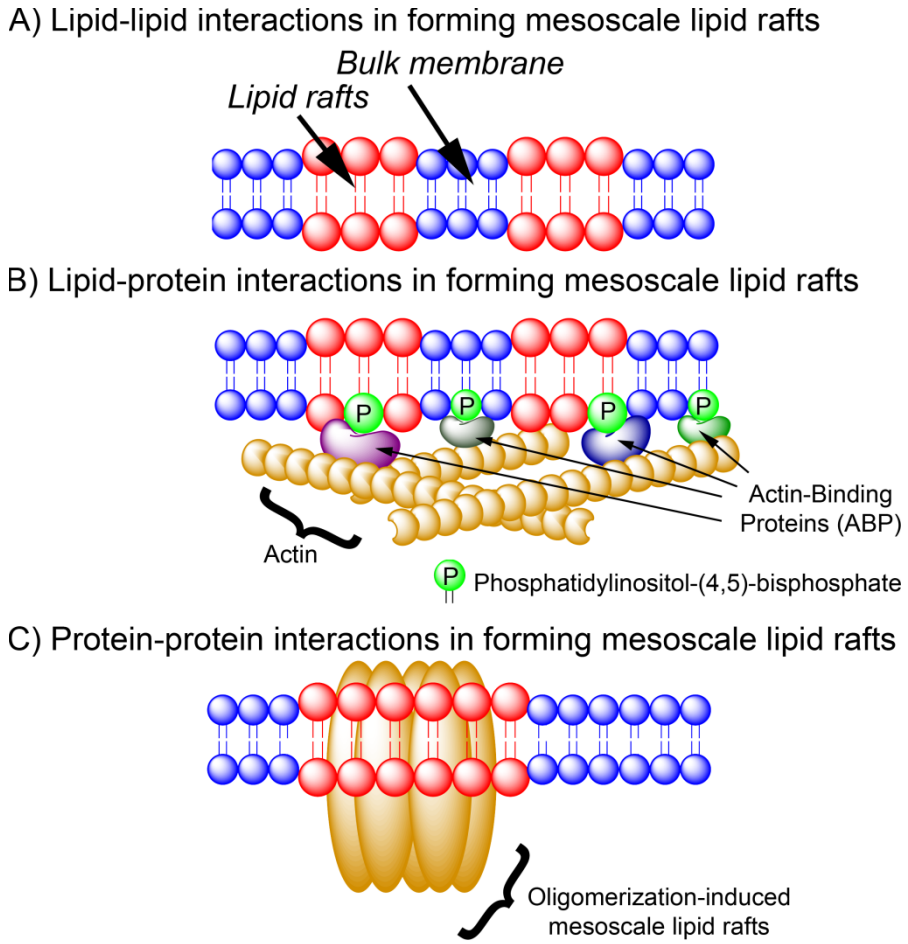

Figure 1.1. Three-tiered organization of the plasma membrane. A) Favorable interactions between cholesterol, sphingolipids, and saturated fatty acids result in the formation of "lipid rafts" in the plasma membrane. These domains are heterogeneous in nature, dynamic, but are important for localization of signaling proteins. B) Lipid-protein interactions between phosphatidylinositol-(4,5)-bisphosphate and actin-binding proteins can stabilize these mesoscale lipid rafts by the actin cytoskeleton. C) Protein-protein interactions via the formation of signaling complex can also induce mesoscale lipid raft formation in the plasma membrane.

1.1.1 Lipid rafts are mesoscale domains generated by lipid-lipid interactions in the plasma membrane

In a simple model system where two lipids (one high melting temperature, one low melting temperature) and cholesterol are mixed together, micron-scale domains phase separate and are easily visualized using conventional fluorescence microscopy (3). These micron-sized microdomains, one example of local structures in the plasma

membrane, can be observed in epithelial cells, where the apical plasma membrane is enriched in sphingolipids, while the basolateral plasma membrane is enriched in phosphatidylcholine (4). Small invaginations in the plasma membrane, enriched with cholesterol, sphingolipids, and the caveolin protein, can also be found in many cells such as endothelial cells and adipocytes (5). Smaller, highly dynamic, nanoscale lipid rafts enriched in sphingolipids, cholesterol, and saturated fatty acids, have been proposed to play a role in signal transduction (**Figure 1.1**). In fact, stable nanodomains can be visualized in yeast vacuole membranes upon various stresses such as nutrient deprivation and pH change; proteins that sort to these vacuolar membranes also segregate to one of two domains, similar to what would be predicted by the simple system composed of two lipids and cholesterol (5). These nanodomains are thought to organize select proteins to optimize their signaling capacity upon ligand engagement. For example, receptors such as epidermal growth factor receptor (EGFR) and the Fas receptor localize into lipid rafts of the plasma membrane, and their association with lipid rafts is critical for downstream signaling transduction upon engagement with their respective ligands (6-9). In fact, computer simulations suggest that in order for lipid rafts to promote protein-protein interactions, these mesoscale domains must be small (6 to 14 nm in diameter) to operate as protein concentrators in the plasma membrane (3).

Due to the diffraction limitation of conventional optical microscopy widely employed to study cells such as confocal and epifluorescence microscopy (lateral resolution ~ 200 nm), lipid rafts have yet to be visualized in contrast to phase-separated vesicles composed of two lipids and cholesterol. Thus, one criticism of the lipid raft

model is that these mesoscale domains have not been visualized in intact cells. Further, early history of lipid rafts defined these structures as resistant to detergent extraction (so-called detergent-resistant fraction), and/or under cold temperature, possibly introducing artifacts for identifying proteins that localize in lipid rafts; similarly, using cross-linking reagents to biochemically prepare detergent extraction can also introduce artificial localization into detergent-resistant fractions. On a cellular level, experiments extracting cholesterol, one component of the lipid rafts, from the plasma membrane with methyl-β-cyclodextrin to disrupt lipid rafts may result in additional artifacts since methyl-β-cyclodextrin can interact with not only cholesterol, but other phospholipids and membrane proteins as well (4).

Recently, using a technique known as secondary ion mass spectrometry imaging (lateral resolution ~50 nm), in which the primary ion is bombarded onto the cell surface, and the secondary ions ejected from the plasma membrane are collected and analyzed, sphingolipid-enriched domains were detected in primary fibroblasts, supporting the existence of lipid rafts; however, these sphingolipid-enriched domains were not enriched with cholesterol (10, 11). In addition, the emergence of super-resolution microscopy, in which lateral resolution of ~50 nm can be achieved, has provided further insight into the biophysical properties of these lipid rafts. By using photoactivation localization microscopy (PALM), in which only a few fluorescent probes are activated at each pulse of activating light to reconstruct the final image, and lipid-binding domains for cholesterol and sphingomyelin, it was recently determined that cholesterol-enriched microdomains are ~118 nm in diameter, while sphingomyelin-enriched microdomains

are ~124 nm in HeLa cells (12). Interestingly, the same study demonstrated that both microdomains were sensitive to cholesterol depletion, but only sphingomyelin-enriched microdomains were affected by sphingomyelin depletion, corroborating the results from secondary ion mass spectrometry imaging studies.

1.1.2 Lipid rafts and actin cytoskeleton are mesoscale domains stabilized by lipid-protein interactions

Although lipid rafts can associate and dissociate as a mechanism to regulate the formation of raft phases in the plasma membrane, one way to achieve a stabilized raft phase (i.e., stabilize the size and/or lifetime of the raft) is the presence of the actin cytoskeleton. Monomeric actin is a 42 kDa globular protein (G-actin) that is capable of polymerization to form long, complex filamentous actin (F-actin) that can provide the force required for organelle movement, and the scaffold required for stabilization of membrane raft phases. F-actin is bridged to the plasma membrane by interacting with integral and membrane-associated proteins; an example is the various protein-actin cytoskeleton interactions in erythrocytes (13). One current model is that these "membrane skeletons" form the "fences" in the plasma membrane, impeding the diffusion of membrane proteins and lipids (14).

The participation of the actin cytoskeleton in the formation of mesoscale domains was first postulated when it was observed that the coefficient of diffusion of phospholipid probes were significantly lower in live cells (15, 16), than those estimated in artificial membranes (17, 18). This difference was also observed for transmembrane protein markers and glycosylphosphatidylinositol-anchored protein markers (14). One

suggestion to explain the difference in the diffusion coefficient is the presence of the membrane cytoskeleton in live cells compared to artificial membranes. Indeed, it was observed that the lipid probe 1,2-dioleoyl-*sn*-glycero-3-phosphoethanolamine (DOPE) had a macroscopic (i.e. across the whole membrane) diffusion coefficient of 9.4 $\mu m^2/s$ in large unilamellar vesicles, but this diffusion coefficient was reduced to 0.99 $\mu m^2/s$ in normal rat kidney fibroblasts, suggesting that component(s) of the cell could interact with the cellular membrane, and compartmentalize membrane macromolecules such as lipids and proteins. Treatment of live cells with trypsin (removes extracellular matrix), methyl-β-cyclodextrin (removes cholesterol), or jasplakinolide (stabilizes the actin cytoskeleton) did not affect the size of the compartmentalized DOPE probe. However, the mesoscale domain increased in size by treating the live cells with latrunculin-A (sequesters G-actin to suppress actin polymerization), suggesting that actin cytoskeleton plays a crucial role in the generation of mesoscale domains in the plasma membrane (19). The requirement for the actin cytoskeleton in maintaining the properties of mesoscale domains was also observed using secondary ion mass spectrometry, in which treatment of NIH 3T3 mouse fibroblasts with latrunculin A resulted in a random distribution of sphingomyelin instead of sphingomyelin-enriched microdomains in control fibroblasts (11).

The actin cytoskeleton is bridged to membranes through interactions with integral proteins, or through proteins recruited to the plasma membrane by specific phospholipids. One such phospholipid is phosphatidylinositol-(4,5)-bisphosphate [$PI(4,5)P_2$], which comprises 5% of the total phosphatidylinositol species, and 1% of the

total plasma membrane phospholipid (20). Classically, $PI(4,5)P_2$ is important in signal transduction because the products of hydrolysis by phospholipase C are diacylglycerol (DAG), which is important for the recruitment of protein kinase C to the plasma membrane, and inositol (1,4,5)-trisphosphate (IP_3), which diffuses into the cytosol in order to bind to the endoplasmic reticulum (ER) inositol trisphosphate receptor that releases Ca^{2+} upon activation. These two classical second messengers amplify signal transduction from the plasma membrane. In addition to the generation of second messengers, $PI(4,5)P_2$ can also recruit proteins to specific sites like a second messenger. For example, recently, it has been found that $PI(4,5)P_2$ can interact with ion channels at the plasma membrane to activate and open these channels (21).

One of the functions of $PI(4,5)P_2$ is to recruit actin remodeling proteins to localized sites at the plasma membrane. It is typically thought that $PI(4,5)P_2$ activate actin-regulatory proteins that induce actin polymerization, while concurrently inhibiting those proteins that promote actin disassembly. Indeed, the increase in local $PI(4,5)P_2$ results in stress-fiber formation, indicative of increased actin filament formation (20). Due to multiple acidic phosphate groups on $PI(4,5)P_2$, basic protein domains are thought to play a role in recruiting proteins to the plasma membrane. For example, the Wiskott-Aldrich syndrome protein (WASP) is released from its autoinhibitory conformation when the basic domain binds to $PI(4,5)P_2$ (22). Talin utilizes the basic cleft in the FERM domain (four-point one, ezrin, radixin, moesin) to interact with $PI(4,5)P_2$ (23). Additional motifs such as the pleckstrin-homology (PH) domain are also known to interact with $PI(4,5)P_2$ (24, 25). Similarly, $PI(4,5)P_2$ can recruit and activate Rho family

GTPase through its polybasic region, of which some small GTPases play a role in cytoskeletal remodeling (23). $PI(4,5)P_2$ is not exclusively involved in the recruitment of actin remodeling proteins. It is known that in $CD4^+$ T cells, the ER Ca^{2+} channel STIM1 is coupled to its plasma membrane counterpart Orai1 through interaction between the polybasic domain of STIM1 and the plasma membrane $PI(4,5)P_2$ (26, 27). $PI(4,5)P_2$, and its role in regulating the actin cytoskeleton is further described in **Section 1.2**.

1.1.3 Lipid rafts and higher-ordered protein complexes form mesoscale domains formed by protein-protein interactions

A third interaction to consider in the formation and organization of optimal mesoscale lipid rafts, is the role of higher-ordered protein complexes (i.e., protein-protein interactions), as proposed by Kai Simons and Akihiro Kusumi (28, 29). As an example, epidermal growth factor receptor (EGFR) undergoes conformational change and dimerization upon binding of its ligand, epidermal growth factor, resulting in downstream signaling (7, 30). Optimal EGFR signaling, however, takes place in lipid rafts, highlighting the role of protein-protein interactions in driving the formation and organization of optimal lipid rafts for cellular signaling. Another example is the Fas-mediated cell death receptor. Similar to EGFR, Fas receptor (FasR) localizes in lipid rafts, and upon engagement with its ligand, Fas ligand (FasL), FasR undergoes oligomerization to induce favorable interactions between lipid rafts, again highlighting how protein-protein interactions can mediate lipid raft formation and organization (8, 9, 31).

1.2 Phosphatidylinositol-(4,5)-bisphosphate

$PI(4,5)P_2$ is generated from the phosphorylation of phosphatidylinositol-4-phosphate [PI(4)P] by type I phosphatidylinositol-4-phosphate 5-kinases (PIP5KI). The phosphorylation of phosphatidylinositol-5-phosphate PI(5)P by type II phosphatidylinositol-5-phosphate 4-kinases (PIP4KII) also contributes to a minor portion of $PI(4,5)P_2$. There are three isoforms of PIP5KI (α, β, γ), with PIP5KIα containing three, PIP5KIβ containing two, and PIP5KIγ containing three splicing variants. The most identifiable domain in the PIP5KI family is the catalytic kinase domain, but it is known that the PIP5KI family is activated by phosphatidic acid (20, 32). The C-terminal seems to play a role in the targeting of the various PIP5KI to cellular compartments and for substrate specificity. Due to the different isoforms and the splicing variants, the localization of PIP5KI remains unclear; however, it is believed that these kinases are recruited to the plasma membrane from the cytoplasm. Recent studies have demonstrated that PIP5KIα can be found at the nucleus to interact with the non-canonical poly(A) polymerase Star-PAP to regulate the expression of mRNAs (33).

PI4KII has two isoforms (α and β), which contain the kinase and the lipid kinase unique (LKU) domains seen in $PI(4,5)P_2$ 3-kinase PI3K. The α isoform also contains a nuclear localization sequence and a PH domain, while the β isoform contains a Rab-association domain that may be important for its translocation from the Golgi to the plasma membrane. In the rat, PI4KIIα has been found to localize to various membrane organelles, including ER, mitochondria, vesicles, and nucleus (34, 35), whereas PI4KIIβ

is localized to the early Golgi compartments in the MDCK cell line and the nucleus in NIH 3T3 cells (34, 36, 37).

$PI(4,5)P_2$ can also be generated from the dephosphorylation of $PI(3,4,5)P_3$ by the phosphatase and tensin homolog (PTEN). PTEN has attracted a lot of attention due to its ability to suppress tumor development; conversely, mutations in PTEN have been implicated in cancer development (38). PTEN contains the 3-phosphatase domain (CX_5R) conserved in other 3-phosphatases, as well as other domains that are known for recruitment of PTEN to the plasma membrane (C2 domain), for protein-protein interactions (PDZ domain), and for proteolytic control (proline-glutamine-serine-threonine PEST domain). $PI(4,5)P_2$ generated by PTEN is mostly considered the by-product of the regulation of $PI(3,4,5)P_3$ (32).

$PI(4,5)P_2$ regulates the recruitment and activity of actin-binding proteins that contain domains such as PH, ENTH, or BAR domains (23). Actin-binding proteins serve to promote the polymerization of G-actin into F-actin (i.e. Arp2/3 complex), to stimulate the severing and depolymerization of F-actin (i.e. ADF/cofilin), or to regulate the actin dynamics by interacting with G- or the F-actin (i.e. profiling, actin capping proteins). Additionally, actin-binding proteins are involved in the higher-ordered structure of actin filaments by promoting cross-linking and bundling of actin filaments. Presently, it is thought that $PI(4,5)P_2$ promotes the polymerization of F-actin since many actin-binding proteins that promote polymerization are activated by $PI(4,5)P_2$, whereas those that promote depolymerization are inhibited by $PI(4,5)P_2$.

Evidence for a role of $PI(4,5)P_2$ in regulating the spatial organization of mesoscale domains comes from studies using membrane-targeted inositol polyphosphate 5-phosphatase (Inp54p) that dephosphorylates $PI(4,5)P_2$ in either raft or non-raft membrane compartments (39). By targeting Inp54p to the raft to deplete the raft pool of $PI(4,5)P_2$, the number of filopodia in Jurkat T cells, cytoplasmic protrusions that contain extensive actin cytoskeleton, were decreased. Conversely, targeting Inp54p to the non-raft region of the plasma membrane increased the number of filopodia in Jurkat T cells, suggesting that i) different pools of $PI(4,5)P_2$ exist at the plasma membrane; and ii) different pools of $PI(4,5)P_2$ regulate distinct actin cytoskeleton processes (39). In fact, Inp54p targeted to the raft pool of $PI(4,5)P_2$ suppressed not only the formation of F-actin at the immunological synapse, but also increased the number of membrane blebs that is indicative of the dissociation of actin cytoskeleton from the plasma membrane, further supporting the concept that $PI(4,5)P_2$ regulates actin cytoskeleton processes and the organization of mesoscale domains in the plasma membrane (39-41).

Parallel to using targeted phosphatases to examine the different pools of $PI(4,5)P_2$ in regulating actin cytoskeleton, it has been proposed that different type I phosphatidylinositol-4-phosphate 5-kinases (PIP5KI) synthesize the different pools of $PI(4,5)P_2$. For example, overexpression of PIP5KIβ increased $PI(4,5)P_2$ in both detergent-resistant and detergent-soluble membrane fractions, whereas overexpression of PIP5KIγ increased $PI(4,5)P_2$ in only the detergent-soluble membrane fraction in RBL-2H3 mast cells, suggestive of different pools of $PI(4,5)P_2$ present at the plasma membrane (42). From a functional perspective, increasing both pools of $PI(4,5)P_2$ by

PIP5KIβ increased the association of STIM1 and Orai1 in RBL-2H3 mast cells, while increasing the detergent-soluble fraction of $PI(4,5)P_2$ by PIP5KIγ decreased the association of STIM1 and Orai1, providing further evidence of the different pools of $PI(4,5)P_2$. The role of various PIP5KI isoforms in regulating actin cytoskeleton is also highlighted by the fact that only the loss of PIP5KIγ, and no other forms of PIP5KI, alters the association of the actin cytoskeleton and plasma membrane in megakaryocytes and platelets, further supporting the role of $PI(4,5)P_2$ in organizing mesoscale domains by regulating the membrane actin cytoskeleton (43, 44).

Controversy exists in regard to the presence of specific pools of $PI(4,5)P_2$ at the plasma membrane. Examination of the diffusion coefficient of $PI(4,5)P_2$ at the inner leaflet of plasma membrane showed a two-fold decrease when compared to another phospholipid, phosphatidylethanolamine (45), demonstrating a restricted lateral diffusion. Interestingly, the restricted lateral diffusion of $PI(4,5)P_2$ can be abrogated by actin depolymerization (46), suggesting that cytoskeleton and/or cytoskeletal proteins can play a role in restricting simple diffusion of $PI(4,5)P_2$. This observation is consistent with the hop-fence model proposed by Dr. Akihiro Kusumi where actin-based membrane “fences” are anchored at the plasma membrane by transmembrane protein pickets to form confinements (28). Experiments have suggested that $PI(4,5)P_2$ is enriched in microdomains of the cells associated with caveolin, and this pool is sensitive to agonist stimulation (47). Further studies have demonstrated the localization of $PI(4,5)P_2$ in lipid rafts outside of caveolin (48); however, these early studies used detergent extraction to localize $PI(4,5)P_2$, which in itself may generate experimental

artifacts. Regardless, proteins can sequester $PI(4,5)P_2$ at specific sites. One of these proteins is the myristoylated alanine-rich C kinase substrate (MARCKS). The polybasic region of MARCKS can bind to three $PI(4,5)P_2$ to induce $PI(4,5)P_2$ clustering. The cellular level of MARCKS in the neuronal tissue is similar to that of $PI(4,5)P_2$, suggesting that MARCKS can sequester a significant amount of $PI(4,5)P_2$ (49). These findings indicate the likelihood of distinct pools of $PI(4,5)P_2$ that can activate proteins, recruit site-specific actin remodeling, and generate second messengers locally.

Interestingly, $PI(4.5)P_2$ has been localized to the nucleus, where it may play a role in transcriptional regulation (50). As mentioned earlier, PIP5Kα associates with the non-canonical poly(A) polymerase Star-PAP to regulate mRNA expressions (33). Specifically, $PI(4,5)P_2$ stimulated the poly(A) polymerase activity of Star-PAP. $PI(4,5)P_2$ may also regulate cytoskeletal control of transcription in the nucleus. For example, there are reports of nuclear cytoskeletal proteins that bind to nuclear $PI(4,5)P_2$ (51). There are also evidence that $PI(4,5)P_2$ may control chromatin remodeling by interacting with various chromatin remodeling complexes, such as BRG1 (52). The role of $PI(4,5)P_2$ in the nucleus is still rather unclear, as there is also evidence of distinct pools of $PI(4,5)P_2$ that are not associated with the membrane (53), thus there remain many questions about the nuclear pool of $PI(4,5)P_2$, and phosphatidylinositols, in general.

1.3 $CD4^+$ T Cells

The mammalian immune system is critical in defending the host against foreign pathogens. Under normal conditions, T lymphocytes circulate around the body in order

to survey for foreign antigens and target them for destruction. However, under pathophysiological conditions such as autoimmune diseases, the adaptive immune system is unable to differentiate between self and foreign antigens, resulting in aberrant T lymphocyte activation and response. This could manifest itself in autoimmune diseases such as inflammatory bowel disease (IBD), i.e. Crohn's disease and ulcerative colitis (54), and affect the patient's quality of life. Additionally, the adaptive immune system may become over-reactive against foreign antigens and unable to resolve appropriately, resulting in pathophysiological chronic inflammation such as Rheumatoid arthritis. The mammalian immune system is comprised of the innate and the adaptive system; within the adaptive immune system, there are two predominant cell types: i) B lymphocytes, responsible for antibody mediated (humoral) immunity; and ii) T lymphocytes, responsible for the regulation of humoral and cell mediated immunity. T lymphocytes can be separated into cytotoxic T lymphocytes ($CD8^+$ T lymphocytes, or T_C lymphocytes), and helper T lymphocytes ($CD4^+$ T lymphocytes, or T_H lymphocytes). While $CD8^+$ T lymphocytes play an important role in host defense and autoimmune disease, $CD4^+$ T lymphocytes due to their ability to further differentiate into other effector cell types (T_H1, T_H2, T_{reg}, T_H17), have opposing roles in autoimmune diseases such as IBD (54).

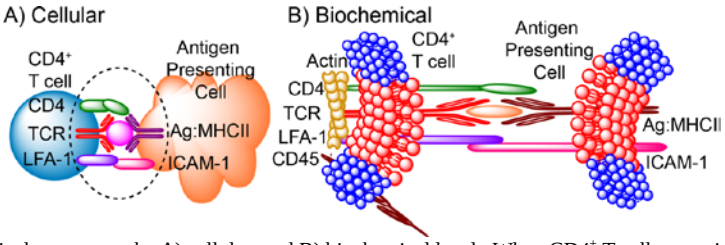

Figure 1.2. Immunological synapse at the A) cellular; and B) biochemical level. When $CD4^+$ T cell recognizes cognate antigen presented by the antigen presenting cell, an immunological synapse is formed at the cellular level. At the biochemical level, major lipididomic and proteomic rearrangement occurs to propagate T cell activation. At the lipidomic level, lipids found to be associated with lipid rafts are found to coalesce at the immunological synapse (represented in red). Adhesion molecules, such as LFA-1, are important for the stabilization of the immunological synapse, while CD45, which is required to terminate T cell activation, is excluded from the immunological synapse. Additionally, the actin cytoskeleton is important for T cell activation by stabilizing the immunological synapse.

1.3.1 Role of lipid rafts in $CD4^+$ T cell activation

The engagement of the T cell receptor (TCR) with antigen presented in the major histocompatibility complex II (MHCII) molecule results in the formation of the immunological synapse (IS, **Figure 1.2**), where proteins essential for propagating the signal are enriched to form the central supramolecular activation cluster (cSMAC), and where adhesion molecules necessary to stabilize the IS form the peripheral supramolecular activation cluster (pSMAC); this patterning leads to the "bull's eye" description of the IS (55, 56). Proteins that regulate T cell activation, such as phosphatases that can abrogate signaling, are excluded from the cSMAC and pSMAC in order for T cell activation to take place. At the IS, tyrosine kinases Lck and ZAP70 are activated and subsequently phosphorylate the adaptor protein linker for activation of T cells (LAT), leading to the assembly of the signalsome comprised of many proteins, including GADS, SLP76, NCK, ITK, VAV1, PAK, and PLC-γ1 (57). The proper formation of the IS, required for sustained T cell activation, is stabilized by the actin cytoskeleton (58-60). When the adhesion proteins coalesce to form the pSMAC, the

actin cytoskeleton is bridged to the IS by proteins such as talin, vinculin, and WASp. The dynamics of the actin cytoskeleton, however, are also important for sustained T cell activation. It is thought that the centripetal flow of F-actin to the initial engagement site between TCR and MHCII is important for the strength and duration of T cell activation; indeed, disruption of T cell activation can be achieved by inhibiting actin polymerization (61-64).

Lipid rafts in the plasma membrane are thought to be critical in $CD4^+$ T cell activation, where the interaction between Ag:MHCII and TCR on the surface of the antigen presenting cell (APC) and the T cell, respectively, results in the major reorganization of the mesoscale lipid rafts and signaling proteins, forming the immunological synapse (IS) (60, 65, 66). The reconfiguration of lipid rafts to form the IS involves changes to lipid-lipid interactions in the membranes; specifically, liquid ordered (Lo) lipids such as cholesterol and sphingolipids accumulate at the IS (67-69). The involvement of lipid rafts in $CD4^+$ T cell activation is conclusive; disruption of lipid rafts with various agents such as methyl-β-cyclodextrin (70), 7-ketocholesterol (71), or n-3 PUFA such as EPA (discussed below, 67) resulted in suppressed T cell activation.

1.3.2 Role of lipid rafts in $CD4^+$ T cell differentiation

Activated $CD4^+$ T cells differentiate into the pro-inflammatory effector subsets in the presence of the cytokines in the microenvironment such as interferon-γ (IFN-γ) and interleukin-12 (IL-12) for T_H1 $CD4^+$ T cells, and Tumor growth factor-β (TGFβ), interleukin-6 (IL-6), and interleukin 21 (IL-21) for T_H17 $CD4^+$ T cells (72). The role of

the plasma membrane, however, in directing the differentiation of $CD4^+$ T cells is underappreciated.

Early reports suggest that different effector $CD4^+$ T cell populations have distinct plasma membrane characteristics, and utilize these distinct membrane properties. For example, treatment of T cells with methyl-β-cyclodextrin as a proxy for lipid raft dependence, demonstrated that T_H1, but not T_H2, $CD4^+$ T cells were more sensitive to disturbance in lipid rafts as detected by suppressed Ca^{2+} influx upon antigen stimulation (73). Indeed, later studies demonstrated that T_H1 and T_H2 $CD4^+$ T cells have distinct IS. The T_H1 $CD4^+$ T cell IS is characterized by the bull's eye IS where the cSMAC, comprised of Ag:MHCII/TCR interactions, is surrounded by the pSMAC populated with adhesion molecules. Meanwhile, T_H2 $CD4^+$ T cell IS is described as multifocal and dependent on the concentration of antigens (74). Furthermore, individual human $CD4^+$ T cell can be categorized into three classes based on the lipid order of its plasma membrane (low, intermediate, and high), as determined by the generalized polarization of di-4-ANEPPDHQ, a probe that changes fluorescence intensities at 570 nm and 620 nm based on the lipid order of its surrounding microenvironment upon incorporation into the plasma membrane (75). $CD4^+$ T cells with intermediate membrane order were associated with IFN-γ production (i.e. T_H1 phenotype), while high membrane order was associated with IL-4 production (i.e. T_H2 phenotype); low membrane order $CD4^+$ T cells were associated with increased apoptosis. When $CD4^+$ T cells were cultured in either T_H1 or T_H2-polarizing conditions, the membrane order of the $CD4^+$ T cells changed to the corresponding T cell subset; intermediate membrane order was observed under T_H1

condition, while high membrane order was seen under T_H2 condition. To further link the role of membrane order with $CD4^+$ T cell differentiation, the reduction of membrane order with 7-ketoxycholesterol resulted in an increase in the number of $CD4^+$ T cell producing IFN-γ, indicative of a switch to an intermediate membrane order, associated with T_H1 phenotype. Clinically, $CD4^+$ T cells isolated from human patients with systemic lupus erythematosus, Sjogrens Syndrome, or rheumatoid arthritis have an increased population of intermediate membrane order $CD4^+$ T cells, associated with IFN-γ production and pro-inflammatory phenotype (75, 76). T_H17 $CD4^+$ T cells are also known to be affected by membrane order. By lowering glycosphingolipid, a lipid known to be associated with lipid rafts, in $CD4^+$ T cells, resulted in decreased T_H17 differentiation (77). These studies demonstrate the structural importance of membrane mesoscale domains in directing $CD4^+$ T cell differentiation.

1.4 n-3 polyunsaturated fatty acids

Very long chain n-3 polyunsaturated fatty acids (n-3 PUFA) such as eicosapentaenoic acid (EPA, $20:5^{\Delta5,8,11,14,17}$) and docosahexaenoic acid (DHA, $22:6^{\Delta4,7,10,13,16,19}$) are thought to be the major bioactive components of fish oil, the commercial value of which is predicted to reach $1.7 billion dollars globally in 2018 according to the Transparency Market Research (Albany, N.Y.). EPA and DHA are incorporated into the two major classes of phospholipids in the plasma membrane, phosphatidylenthanolamine and phosphatidylcholine at the *sn-2* position (68, 78), consistent with the observation that saturated fatty acids occupy the *sn-1* position of phospholipids, while unsaturated fatty acids are inserted at the *sn-2* position. Studies on

DHA, with 22 carbons and 6 double bonds, demonstrate that DHA is highly disordered and adopts various conformations on the subnanosecond time scale (79, 80). By eliminating the double bond at the n-3 position to generate docosapentaenoyl acid (DPA, $22:5^{\Delta 4,7,10,13,16}$), chain dynamics of the fatty acid are reduced (79), suggesting that the unsaturation at the n-3 position affords unique properties to EPA and DHA in the plasma membrane.

1.4.1 Biophysical properties of n-3 polyunsaturated fatty acids

Studies on ion channels have demonstrated that n-3 PUFA such as EPA and DHA can modulate membrane protein properties. The incorporation of docosahexaenoic acid into the lipid bilayer resulted in a decrease in bilayer stiffness without changing the negative curvature of the bilayer (81). Functionally, DHA increased the appearance and lifetime of gramicidin channels, and decreased the free energy for channel formation; the fatty acid oleic acid (OA, $18:1^{\Delta 9}$) that intercalated into the plasma membrane at a greater rate, had no effect on gramicidin channel formation, suggesting that the effect of DHA was due to changes in bilayer properties, and not due to specific binding (81, 82). Other channels that are modulated by EPA and DHA include inhibiting cardiac Na^+ and L-type Ca^{2+} channels (83, 84), activating TRAAK-1 and TRPV1 channels (85, 86), and increasing desensitization of nAChR and $GABA_a$ channels (87, 88).

1.4.2 n-3 polyunsaturated fatty acids alter the biophysical properties of lipid rafts in the plasma membrane

In the context of plasma membrane lipid rafts, DHA is thought to play a major role in altering the size and/or stability of these mesoscale lipid rafts. As a result of the

highly disordered nature of DHA, one proposed mechanism by which DHA modifies the lateral organization of the plasma membrane is by forming a distinct non-raft DHA domain (89, 90). This DHA domain is distinct from the sphingolipid and cholesterol enriched lipid rafts due to the highly flexible DHA, which is incompatible with the rigidity of sphingolipids and cholesterol. Incorporation of DHA into the plasma membrane results in the distinct non-raft DHA domain inserting itself into lipid rafts, increasing the size of lipid rafts. This mechanism would explain findings using nuclear magnetic resonance (NMR) indicating that both EPA and DHA are incorporated into raft and non-raft domains in a phosphatidylethanolamine/sphingomeylin/cholesterol membrane mixture (91). Similar results have also been observed *in vivo* by analyzing phospholipids of $CD4^+$ T cells after isolating the detergent-resistant and –soluble membrane fractions (68, 78).

An alternative mechanism proposed to explain the effects of n-3 PUFA on lipid raft organization comes from the fact that the flexibility of n-3 PUFA is incompatible with the rigid cholesterol, paradoxically promoting the aggregation of cholesterol in the plasma membrane, resulting in the coalescence of sphingolipid and cholesterol lipid rafts from the bulk membrane (92). Indeed, it has been shown that n-3 PUFA such as EPA and DHA can increase the size of lipid rafts in HEK cells, $CD4^+$ T cells, and B cells (93-95).

1.4.3 Additional biochemical mechanisms by which n-3 polyunsaturated fatty acids modulate cell function

In addition to the effects of n-3 PUFA on the plasma membrane, n-3 PUFA can further exert biological effects by regulating i) eicosanoid metabolism; ii) nuclear transcription factor activation; and iii) activation of G-protein coupled receptors.

Eicosanoids are lipid compounds that act in an autocrine or paracrine fashion that can regulate immune response. Arachidonic acid–derived (AA, $20:4^{\Delta 5,8,11,14}$) eicosanoids such as prostaglandin E_2 are thought to be pro-inflammatory due to their ability to promote $CD4^+$ T_H1 and T_H17 inflammatory subsets (96-99). Indeed, patients with chronic inflammatory diseases such as Crohn's disease and ulcerative colitis have increased levels of AA-derived eicosanoids (100-105). The presence of EPA and DHA in the plasma membrane, however, can impact the levels of AA-derived eicosanoids by first depleting the cell of AA (106), and second by competing for the same enzymes to synthesize alternative ligands (i.e., prostaglandin E_3) that are less potent for signal transduction (107, 108). The recently discovered non-classical eicosanoids such as resolvins and protectins derived from EPA and DHA have been shown to exert potent anti-inflammatory effects on a physiological level, demonstrating another mechanism by which n-3 PUFA can exert anti-inflammatory effects by acting through eicosanoid metabolism (109-112).

The best characterized nuclear receptor that is activated by n-3 PUFA is peroxisome proliferator-activated receptor-γ (PPARγ). $CD4^+$ T cells isolated from PPARγ knockout mice exhibited an increase in IFN-γ secretion and lymphoproliferation

upon activation. In addition, the differentiation of anti-inflammatory Treg cells was also suppressed in PPARγ-null $CD4^+$ T cells, demonstrating that activation of PPARγ can exert anti-inflammatory effects. The crystal structure of PPARγ in complex with 4-oxodocosahexaenoic acid was solved, and shown to be a potent activator of PPARγ (113). The non-oxidized versions of n-3 PUFA themselves have been shown to activate PPARγ, but at a micromolar range (114, 115). In the young adult mouse colonocyte model, DHA was shown to modulate the transactivation of retinoid X receptor-α (RXRα), highlighting the likelihood that other nuclear receptors are also activated by n-3 PUFA (116).

Similar to the mechanism by which n-3 PUFA can act as a ligand itself to activate nuclear receptors, only recently has a G-protein coupled receptor been identified for DHA, GPR120 (117). With sub-micromolar potency, DHA can exert anti-inflammatory effects by activating GPR120 expressed on the surface of macrophages and adipoctyes and alter the gene expression profiles favoring a reduction in inflammation (118). Additionally, DHA can activate GPR120 in macrophages to attenuate NOD-like receptor family, pyrin domain containing 3 (NLRP3) inflammasome activation to prevent metabolic disorder caused by high fat diet (119). Not all beneficial effects of n-3 PUFA are mediated through GPR120, as n-3 PUFA suppressed obesity induced-tumor progression in breast cancer model independent of GPR120, highlighting the pleotropic properties of n-3 PUFA.

1.5 Effects of n-3 polyunsaturated fatty acids on $CD4^+$ T cells

n-3 PUFA have been shown in many clinical studies to attenuate human inflammatory responses (120-125). Although inflammatory responses are orchestrated by a wide spectrum of cells, $CD4^+$ T cells play an important role in the etiology of many chronic inflammatory diseases, such as inflammatory bowel disease (54, 126-128), and obesity (129-131). In light of recent concerns over the safety profiles of non-steroidal anti-inflammatory drugs (NSAIDs), alternatives such as bioactive nutraceuticals are becoming more attractive for the use in medical treatments (132).

In terms of T cell activation, lipid rafts coalesce to form the IS. Importantly, an alteration in the size of rafts can impact IS formation, and thus regulate T cell activation (67, 71). Studies using the immortalized Jurkat T cell line demonstrated that n-3 PUFA displaced many of the signaling proteins necessary for T cell activation, including the Src family kinases Lck and Fyn from detergent-resistant membrane fractions (133), and LAT (134). Additional studies demonstrated that the recruitment and activation of signaling proteins such as PKCθ, LAT, Fas, PLC-γ1, and F-actin were also altered (78, 94). n-3 PUFA, however, did not universally inhibit protein localization; Ly *et al.* observed an enhancement of surface CTLA-4 expression, a negative regulator of T cell activation, in $CD4^+$ T cells isolated from mice fed an EPA-enriched diet (135). It is now appreciated that n-3 PUFA broadly suppress downstream activation signaling, including mitochondrial translocation (136), IL-2 secretion (78, 135, 137-140), and lymphoproliferation (94, 138, 141).

Similar to the dual roles in which lipid rafts play in $CD4^+$ T cell activation and differentiation, n-3 PUFA not only suppress $CD4^+$ T cell activation, but also specific $CD4^+$ T cell differentiation. Early studies examining activation-induced cell death (AICD) demonstrated that only T_H1-like $CD4^+$ T cells exhibited enhanced AICD upon enrichment with n-3 PUFA (142, 143). In addition, $CD4^+$ T cells enriched with n-3 PUFA failed to polarize into T_H1 or T_H17 cells as efficiently when compared to control $CD4^+$ T cells (144-146). One mechanistic possibility by which n-3 PUFA suppress $CD4^+$ T cell polarization into T_H17 $CD4^+$ T cells was recently explored. Allen and colleagues demonstrated the presence of a membrane-targeted alteration in the IL6/gp130/Stat3 pathway (147), corroborating the membrane-specific effects of n-3 PUFA on $CD4^+$ T cell activation and differentiation.

CHAPTER II

n-3 POLYUNSATURATED FATTY ACIDS SUPPRESS PHOSPHATIDYLINOSITOL-(4,5)-BISPHOSPHATE DEPENDENT ACTIN REMODELING DURING $CD4^+$ T CELL ACTIVATION*

2.1 Introduction

One role that the actin cytoskeleton plays is in stabilizing the IS for sustained T cell activation (58-60). The role of actin remodeling is also observed in human disease; for example, Wiskott-Aldrich syndrome, characterized partly by deficient T cell activation (148), is attributed to mutations in the gene encoding the Wiskott-Aldrich syndrome protein (WASP), which regulates *de novo* nucleation of actin filaments (149). Additionally, to emphasize the importance of the actin cytoskeleton to T cell activation, many actin regulating proteins such as ERM proteins, talin, WAVE, and ADF/cofilin, are known to be localized at the IS (59, 150-152). Thus, one mechanism by which n-3 PUFA could suppress $CD4^+$ T cell activation is through inhibition of F-actin remodeling. Indeed, Kim *et al.* has previous demonstrated that the number of $CD4^+$ T cells with F-actin localizing to the IS was decreased when T cells were enriched with n-3 PUFA (94).

Many of the aforementioned actin remodeling proteins, including WASP, are regulated by $PI(4,5)P_2$ (23). Both the magnitude and the kinetics of $PI(4,5)P_2$ metabolism

---

*This research was originally published in Biochemical Journal. Hou TY, Monk JM, Fan YY, Barhoumi R, Chen YQ, Rivera GM, McMurray DN, Chapkin RS. n-3 polyunsaturated fatty acids suppress phosphatidylinositol 4,5-bisphosphate-dependent actin remodelling during CD4+ T-cell activation. *Biochem J.* (2012); **443**(1): 27-37. © the Biochemical Society. Reprinted with permission from Biochemical Society.
*FADS-1 research was originally published in Journal of Lipid Research. Fan YY, Monk JM, Hou TY, Callway E, Vincent L, Weeks B, Yang P, Chapkin RS. Characterization of an arachidonic acid-deficient (Fads1 knockout) mouse model. *J Lipid Res.* (2012); **53**(7): 1287-95. © the American Society for Biochemistry and Molecular Biology. Reprinted with permission from American Society for Biochemistry and Molecular Biology.

are important in actin remodeling, as demonstrated during i) macrophage phagocytosis (153); ii) release of ERM proteins from the plasma membrane of T cells after chemokine stimulation (154); and iii) release and activation of cofilin in carcinoma cells upon EGF stimulation (155). Since $PI(4,5)P_2$ colocalizes in raft domains in T cells (39), and n-3 PUFA such as DHA can increase the size of lipid rafts (93), we tested the hypothesis that $PI(4,5)P_2$ is perturbed by the presence of n-3 PUFA, leading to a suppression of downstream actin remodeling.

2.2 Materials and methods

2.2.1 Animals and $CD4^+$ T cell isolation

All animal protocols have been approved by the Institutional Animal Care and Use Committee at Texas A&M University and follow guidelines approved by the U.S. Public Health Service. The generation, genotyping, and phenotyping of *Fat-1* and FADS-1 transgenic mice on a C57BL/6 background have been described previously [**APPENDIX A**; (78, 94, 116, 136)]. Mice were fed a 10% safflower diet enriched in n-6 PUFA (Research Diets, New Brunswick NJ), provided *ad libitum* in a 12:12 light:dark cycle.

In the diet experiment, 4 to 6 weeks old C57BL/6 mice were fed either an n-6 PUFA enriched 5% corn oil diet or a 4% DHA (n-3 PUFA) triglyceride-enriched diet. Diets differed only in their oil composition, either (control) 5% corn oil by weight or a mixture of 57% pure DHA triglyceride (Martek, Columbia, MD) and corn oil (4:1 w/w). Additional diet components, expressed as g/100 g, were 20 casein, 41.9 sucrose, 22 corn starch, 6 cellulose, 3.5 AIN-76 mineral mix, 1 AIN-76 vitamin mix, 0.3 DL-methionine,

0.2 choline chloride, and 5 dietary oil (68, 78, 142). Mice were fed *ad libitum* for 3 to 4 weeks in a 12:12 light:dark cycle and diet changed daily to prevent the formation of oxidative byproducts.

Spleens were removed aseptically and $CD4^+$ T cells were isolated by positive selection using magnetic CD4 (L3T4) microbeads according to manufacturer's protocol (**APPENDIX B**; Miltenyi Biotec, Auburn, CA). $CD4^+$ T cells were resuspended in complete RPMI media composed of 93% RPMI (contains 25 mM HEPES, Irvine Scientific, Santa Ana, CA), 5% heat-inactivated fetal bovine serum (Irvine Scientific), 1% glutamax (Gibco, Carlsbad, CA), and 1% penicillin-streptomycin (Gibco), henceforth referred to as "complete media", at assay-specific concentrations (5×10^5 cells/mL for basal $PI(4,5)P_2$ measurements using a $PI(4,5)P_2$ mass kit from Echelon Biosciences (Salt Lake City, UT), 5×10^5 cells/100 μL for T cell activation, 3×10^6 cells/mL for immunofluorescence, 1.5×10^7 cells/250 μL for immunoisolation).

2.2.2 $CD4^+$ T cell stimulation time course

Ninety-six well flat-bottom plates containing plate bound anti-CD3 (0.2 μg/mL, eBiosciences, San Diego, CA) and anti-CD28 (1 μg/mL, eBiosciences) were incubated overnight at 4 °C. The wells were washed with PBS and replaced with 200 μL of complete RPMI media. The plates were then placed in 37 °C, 5% CO_2 incubator for at least one h before seeding $CD4^+$ T cells (156). For PMA/ionomycin stimulation, 0.5 μg/mL PMA (Sigma, St Louis, MO) and 500 nM ionomycin (EMD Chemicals, Gibbstown, NJ) in complete media were added into each well and incubated at 37 °C, 5% CO_2, for at least one h before seeding T cells (94). $CD4^+$ T cells were seeded into

each well, stimulated for specified times (0 to 30 min), and then transferred into a low-retention 1.5 mL microcentrifuge tubes and immediately placed on ice to quench cell activation. $CD4^+$ T cells were centrifuged at 4 °C, 4000g for 5 min, and washed in cold PBS before lipid extraction.

2.2.3 Extraction of $PI(4,5)P_2$ for detection using $PI(4,5)P_2$ mass kit or anti-$PI(4,5)P_2$ ELISA

Extraction of $PI(4,5)P_2$ has been previously described, with some modifications [**APPENDIX C**; (157)]. Briefly, after washing with cold PBS, the cells were pelleted at 4000 g, 5 min at 4 °C (described above), supernatant was removed and the pellet was resuspended in 800 µL of 1:1 MeOH:$CHCl_3$. The mixture was vortexed for 1 min, and centrifuged at 7500 g, 5 min at 4 °C. The supernatant was removed, and the pellet was resuspended in 400 µL of 80:40:0.3 MeOH:$CHCl_3$:HCl. The mixture was vortexed for 5 min and subsequently centrifuged at 3000 g for 1 min at 4 °C. An additional 80 µL of 1 N HCl was added to the extract and vortexed for 15 sec before centrifugation at 18000 g for 15 sec at 4 °C. The organic layer was collected and dried under a stream of N_2 gas. The lipid film was dissolved in PBS supplemented with 0.0025% of protein stabilizer (Echelone Biosciences, Salt Lake City, UT) and used for detection of $PI(4,5)P_2$.

2.2.4 Detection of $PI(4,5)P_2$

For basal level $PI(4,5)P_2$ detection, the $PI(4,5)P_2$ mass kit (Echelon Biosciences) was used according to the manufacturer's protocol. Briefly, the mass kit utilizes a $PI(4,5)P_2$ protein detector that is added to a $PI(4,5)P_2$-coated strip for competitive binding. The colorimetric signal is inversely proportional to the amount of $PI(4,5)P_2$.

For determination of the $CD4^+$ T cell stimulation time course, an indirect ELISA was developed to detect the level of $PI(4,5)P_2$ (**APPENDIX D**). $PI(4,5)P_2$ dissolved in PBS supplemented with 0.0025% protein stabilizer was added in duplicate into 96-well flat bottom plates and incubated at room temperature for 2 h. The wells were then washed with PBS 3X, and then blocked in 5% BSA in PBS overnight at 4 °C. The wells were again washed with PBS 3X, and incubated with primary mouse anti-$PI(4,5)P_2$ (Abcam, Cambridge, MA) in blocking solution at a dilution of 1:2500 for 1.5 h at room temperature. The wells were washed with PBS and incubated with secondary goat anti-mouse IgG labeled with horseradish peroxidase (KPL, Gaithersburg, MD) in blocking solution at a dilution of 1:5000 for one h at room temperature, protected from light. The wells were washed with PBS four times, and incubated in TMB high sensitivity substrate solution (BioLegend, San Diego, CA) for 5 min at room temperature, protected from light. The reaction was stopped by the addition of 1 N H_2SO_4, and the absorbance was read at 450 nm. A standard curve was generated with known concentrations of $PI(4,5)P_2$ (Echelon Biosciences), and was used to quantify the $PI(4,5)P_2$ levels. To test the cross-reactivity of the primary antibody, 50 pmol of PI(4)P (Avanti, Alabaster, AL) and $PI(3,4,5)P_3$ (Avanti) were dissolved in PBS supplemented with 0.0025% protein stabilizer, and added into separate wells and subjected to the same ELISA protocol as described. No detectable signals were observed.

2.2.5 Extraction and detection of $PI(4,5)P_2$ using mass spectrometry

Purified splenic $CD4^+$ T cells were isolated and washed as described above. For mass spectrometry, cells from two animals were pooled to increase detection of

PI(4,5)P_2. After washing, purified splenic $CD4^+$ T cells were dissolved in a solvent composed of $CHCl_3$:MeOH:H_2O (32.6:65.3:2.1 v/v/v) and extracted as described previously (158). Dipalmitoyl phosphatidylinositol-4,5-bisphosphate (200 ng) was added into each sample as an internal standard prior to extraction. Lipid extracts were evaporated under argon gas and redissolved in 50 µL of $CHCl_3$:MeOH:H_2O (5:5:1 v/v/v) and analyzed by LC-MS/MS. Mass spectrometry (Thermo TSQ Quantum Discovery Max) operated in the negative ion mode was optimized to detect phosphoinositides as $[M-H]^-$ ions. Using the peak areas, the mass of individual phosphoinositides was estimated and corrected by using the internal standard. Samples were normalized to cell number as determined using a Coulter Counter (Beckman Coulter, Brea, CA).

2.2.6 Immunofluorescence

Immunofluorescence was conducted as previously described [**APPENDIX E**; (78, 94)]. Briefly, 4.0 cm^2 per well chamber cover slides (Nalge, Rochester, NY) were pre-coated with 0.01% poly-L-lysine (Sigma) for 30 min. The solution was removed and the slides were allowed to air dry for one h at room temperature. For T cell stimulation, chamber cover slides were additionally coated with anti-CD3 and anti-CD28 at a concentration of 1 µg/mL and 5 µg/mL, respectively. The unstimulated (control) slides were incubated with PBS overnight. Following $CD4^+$ T cells isolation, 3 x 10^6 cells in complete RPMI media were seeded into chamber slides and incubated for 30 min at 37 °C, 5% CO_2. For bead stimulation, 3 x 10^6 $CD4^+$ T cells were incubated in the presence of Dynabeads Mouse T-activator CD3/CD28 (**APPENDIX F**; Invitrogen,

Carisbad, CA) at a 1:1 ratio for 30 min, at 37 ºC, 5% CO_2. For exogenous PI(4,5)P_2 rescue experiment, 3 x 10^6 *Fat-1* $CD4^+$ T cells were incubated in the presence of exogenous PI(4,5)P_2 at specific concentrations (Echelon Biosciences) for one h, at 37 °C, 5% CO_2, washed one time with warm PBS before stimulation as described above using plated anti-CD3/anti-CD28.

Cells were washed with PBS 3X and immediately fixed in 4% paraformaldehyde for 20 min at room temperature. The chamber slides were washed with PBS, and incubated in 10 mM glycine for 10 min at room temperature, followed by permeabilization using 0.2% Triton X-100 for 5 min at room temperature. The chamber slides were subsequently washed with PBS, followed by overnight incubation at 4 °C in a humid chamber with blocking solution (1% IgG-free BSA, 0.1% NaN_3, 99% PBS). The slides were washed with PBS before the addition of 200 µL of 20 U/mL Alexa 568 conjugated phalloidin (Invitrogen) and incubated for one h in a humid chamber at room temperature, and then washed with PBS 3X, and incubated in 70% ethanol, 95% ethanol, 100% ethanol, and fresh xylene, for 2 min each. ProLong antifade medium (Invitrogen) was applied to each coverglass, and the slides were allowed to dry in the dark overnight at room temperature. Slides were sealed with fingernail polish before examination under microscopy.

For bead-stimulated samples, slides were fixed, washed, treated, and blocked overnight as described above. Two-hundred µL of 20 U/mL Alexa 568 conjugated phalloidin and 4 µg/mL rabbit anti-WASP (Santa Cruz, Santa Cruz, CA) was applied to slides for one h in a humid chamber at room temperature before the slides were washed

with PBS twice. The addition of 6 μg/mL of goat anti-rabbit Alexa 647 (Invitrogen) to slides for one h in a humid chamber at room temperature preceded washes and treatment as described above.

2.2.7 Immunoisolation

Immunoaisolation was conducted as previously described with minor modifications [**APPENDIX G**; (159)]. 1.5 x 10^7 $CD4^+$ T cells were incubated with anti-CD3/anti-CD28 coated Dynabeads (Invitrogen) at a cell-to-bead ratio of 2:1 on ice for 7 min before stimulation at 37 °C for 30 min. Samples were then subjected to nitrogen cavitation at 800 psi for 7 min, transferred to 1.5 mL microcentrifuge tubes, and washed 3X with 1 mL of complete homogenization buffer. Input samples (100 μL) were assayed prior to magnetic bead collection to determine the yield of the cavitation using Western blotting. Samples (12 μL) were analyzed using immunoblotting.

$CD4^+$ T cells were homogenized in ice-cold homogenization buffer composed of 50 mM Tris-HCl, pH 7.2, 250 mM sucrose, 2 mM EDTA, 1 mM EGTA, 50 mM NaF, 100 mM $NaVO_4$, 1% Triton X-100, 40 μL/mL protease cocktail, and 10 mM β-mercaptoethanol, passed through a 27-guage needle twice, incubated on ice for 30 min, and centrifuged at 16000 g for 20 min. The supernatant was collected and protein concentration determined by Commassie Plus Protein assay (Pierce, Rockford, IL). Twenty-five μg of protein was treated with pyronin sample buffer and loaded on a 4-20% Tris-glycine polyacrylamide precast gels (Invitrogen) and separated for 1 h at 4 ºC. Proteins were then transferred onto a polyvinylidene fluoride membrane at 400 mA for 90 min. Membranes were blocked at room temperature for 1 h in 4% nonfat dry milk.

Primary antibodies (Rabbit anti-WASP, Santa Cruz; mouse anti-β-actin, Sigma) were incubated overnight at 4 ºC. Membranes were subsequently washed and incubated with secondary horseradish peroxidase conjugated goat anti-rabbit IgG or horseradish peroxidase conjugated human anti-mouse IgG (KPL) and developed using Pierce SuperSignal West Femto maximum sensitivity substrate. Membranes were then scanned using Fluor-S Max MultiImager system (BioRad, Hercules, CA) and analyzed using QuantityOne (BioRad). Enrichment factor was calculated by dividing the intensity of the band in the IS by the intensity of the band in the input for WASP.

2.2.8 Microscopy and image processing

Slides were examined using a Zeiss 510 META NLO laser scanning microscope equipped with argon laser, LSD software and a 63X objective. Images were exported into TIFF format using AxioVision LE 4.8 and imported into NIS-Elements AR 3.10 (Nikon, Melville, NY). To correct for background, a rectangular region of interest (ROI) was drawn in an area without any cells. This area was used to subtract the background from the image. ROIs were then drawn around cells that were not in contact with other cells, and the mean intensity was recorded. This value was then divided by the number of cells in the field measured to obtain the average mean intensity per cell.

For bead-stimulated samples, slides were examined using a Nikon Ti-E inverted microscope equipped with X-cite 120 fluorescent microscopy illuminator and 60X objective, with 1.5 magnification. Images were captured using a Photometrics Cool-SNAP EZ CCD camera and analyzed in NIS-Elements AR. 2D Fast deconvolution was applied to all captured images. An ROI was drawn around the cell excluding the beads,

and the total intensity was recorded. This value was divided by the area of the cell to obtain the average mean intensity per square micron. For the IS, the ROI was drawn as an oval at the T cell proximal to the bead as previously described (94). The total intensity was recorded and divided by the area of the IS. There were no differences between the size of the cell or the IS between genotypes (data not shown); furthermore, the area of the IS was approximately 10% ± 5% of the whole cell in both genotypes (data not shown).

2.2.9 Chemotaxis assay

After $CD4^+$ T cell isolation, chemotaxis assay was performed as previously described (160). Briefly, cells were resuspended to a final concentration of 1 x 10^6/100 μL RPMI media with 0.5% (w/v) fatty acid-free BSA (Roche Diagnostics). 100 μL of the cell suspension was seeded into a 3.0 μm pore size, 6.5 mm diameter, transwell (Sigma), which was then carefully placed into a 15.6 mm well (24 well plate) containing 600 μL of RPMI media with 0.5% (w/v) fatty acid-free BSA supplemented with 0.25 μg/mL of CCL19 (R&D Systems, Minneapolis, MN). The plate was then incubated for 4 h, at 37 °C. Cells from the lower chamber was collected and counted using a Coulter counter. % migration was calculated by dividing the number of cells collected from the lower chamber to the total number of cells seeded. The assay was repeated in triplicates.

2.2.10 Statistical analysis

Data were expressed as mean ± SEM unless otherwise noted and analyzed using SAS 9.2 for Windows. The time course was tested by two-way ANOVA (main effects: genotype and time). In cases where the interaction between genotype and time was

insignificant, an LSD post-hoc test was conducted. In the cases where the interactions between genotype x time were significant, a Tukey post-hoc test was conducted. Differences between genotypes in single treatment were analyzed by two-tailed Student's t-test. $P < 0.05$ was considered to be statistically significant.

2.3 Results

2.3.1 Basal PI(4,5)P_2 concentration is reduced in Fat-1 CD4$^+$ T cells

Since PI(4,5)P_2 is one of the key mediators of actin remodeling, we determined whether the level of PI(4,5)P_2 is perturbed in *Fat-1* CD4$^+$ T cells. Total lipid analysis revealed enrichment of n-3 PUFA in *Fat-1* CD4$^+$ T cells as compared to wild type (**Figure 2.1**). In addition, we have previously shown that dietary n-3 PUFA were readily incorporated into the plasma membrane of splenic CD4$^+$ T cells (68, 78). We first used mass spectrometry to determine both total PI(4,5)P_2 mass and the acyl species of PI(4,5)P_2 present in purified splenic CD4$^+$ T cells isolated from wild type and *Fat-1* mice. Total PI(4,5)P_2 in purified *Fat-1* splenic CD4$^+$ T cells was decreased by 50% compared to wild type ($P = 0.04$, **Figure 2.2**). In addition, there were significant decreases in the 18:0,20:4 species ($P = 0.02$), and an increase in the 18:1,20:4 species of PI(4,5)P_2 ($P = 0.04$) in *Fat-1* splenic CD4$^+$ T cells (**Figure 2.2**). Using two additional methods (PI(4,5)P_2 mass kit, and indirect anti-PI(4,5)P_2 ELISA), we further validated our observations, demonstrating a decrease in the total PI(4,5)P_2 content in *Fat-1* splenic CD4$^+$ T cells (**Figure 2.3**).

Examination of PIP molecular species revealed a decrease only in the 16:0,20:4 species ($P = 0.03$, **Figure 2.3**). There were no effects on the 18:0,20:4 ($P = 0.09$)

18:1,20:4 PIP (P = 0.53), or the minor species of PIP (P = 0.32) between wild type and *Fat-1* CD4$^+$ T cells (**Figure 2.3**). Furthermore, the total PIP level was not significantly different between genotypes (P = 0.17). Taken together, these results demonstrate that the basal PI(4,5)P_2 concentration is decreased in purified splenic CD4$^+$ T cells isolated from *Fat-1* mice.

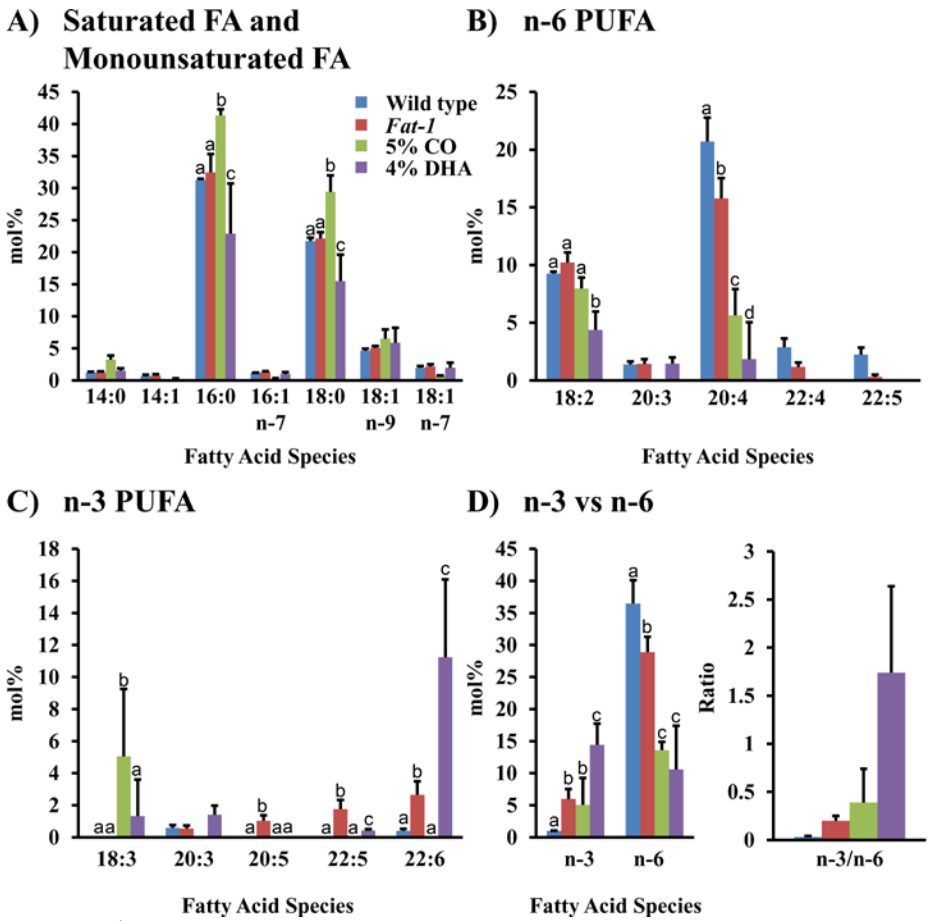

Figure 2.1. Splenic CD4$^+$ T cell total lipid fatty acid composition for A) Saturated and monounsaturated fatty acids; B) n-6 PUFA; C) n-3 PUFA; and D) n-3 vs n-6 PUFA. Isolated cells were extracted from wild type (WT) and *Fat-1* mice fed a 10% safflower diet, or wild type animals fed a 5% corn oil diet (5% CO) or 4% DHA triglyceride-enriched diet plus 1% corn oil diet (4% DHA). Fatty acid composition was analyzed by gas chromatography/mass spectrometry after extraction as previously described (94, 141). Values are expressed as moles of individual fatty acids divided by moles of total fatty acids (mol%), n=3 mice per treatment. Different letters denote a significant difference of P < 0.05.

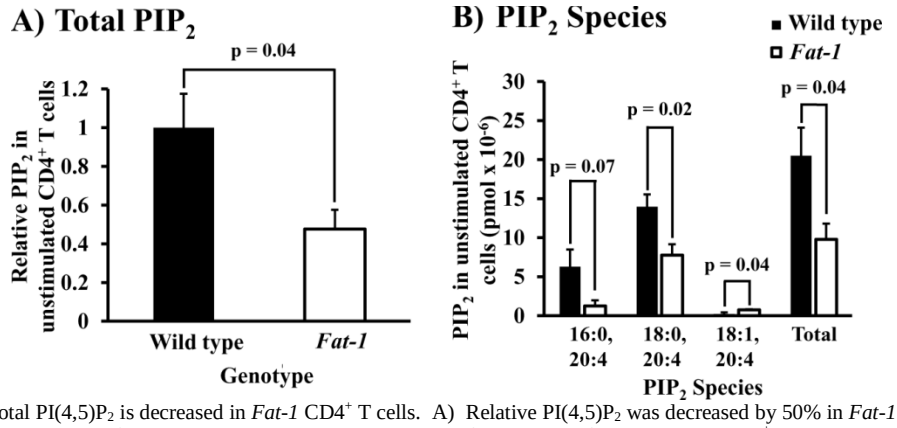

Figure 2.2. Total PI(4,5)P_2 is decreased in *Fat-1* $CD4^+$ T cells. A) Relative PI(4,5)P_2 was decreased by 50% in *Fat-1* $CD4^+$ T cells. $CD4^+$ T cells were isolated from wild type and *Fat-1* spleens (n = 8 for *Fat-1*; 12 for wild type). $CD4^+$ T cell populations from two spleens were pooled for analysis using mass spectrometry as described in the *Methods.* Total PI(4,5)P_2 was quantified following comparison to an internal standard and normalized relative to total $CD4^+$ T cells counted using a Coulter Counter. Relative PI(4,5)P_2 levels were compared by normalizing to wild type PI(4,5)P_2. B) PI(4,5)P_2 molecular species were altered in *Fat-1* $CD4^+$ T cells.

2.3.2 Metabolism of PI(4,5)P_2 upon T cell activation is altered in Fat-1 $CD4^+$ T cells

We have previously demonstrated that *Fat-1* $CD4^+$ T cells have a suppressed activation status, e.g., decreased localization and phosphorylation of PLC-γ1 at the IS (94). Therefore, we examined the metabolism of PI(4,5)P_2 upon T cell activation by anti-CD3/anti-CD28 or PMA/ionomycin in purified splenic *Fat-1* $CD4^+$ T cells. In both stimulation conditions, *Fat-1* $CD4^+$ T cells failed to respond to stimulation (**Figure 2.4**). In contrast, in wild type $CD4^+$ T cells activated with anti-CD3/anti-CD28, the level of PI(4,5)P_2 decreased by 50% in 5 min (P = 0.05), followed by a recovery phase of ~30 min. In addition, *Fat-1* $CD4^+$ T cells showed no change upon activation with anti-CD3/anti-CD28. Similarly, PI(4,5)P_2 levels in wild type $CD4^+$ T cells activated with PMA/ionomycin were decreased by 50% within 5 min of stimulation (P = 0.008). However, PI(4,5)P_2 levels did not recover possibly due to the non-physiological (TCR-independent) activation of the T cells. In contrast, *Fat-1* $CD4^+$ T cells showed no response to PMA/ionomycin.

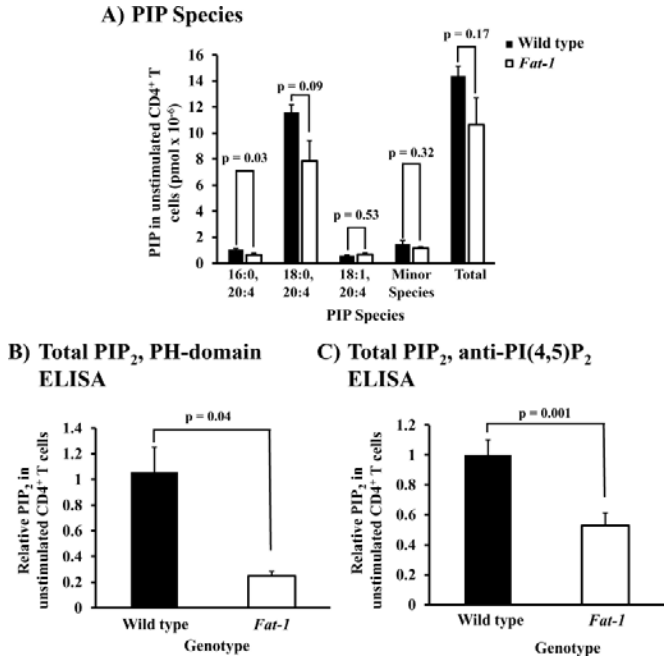

Figure 2.3. PIP is altered in *Fat*-1 $CD4^+$ T cells, and confirmation of $PI(4,5)P_2$ in *Fat-1* $CD4^+$ T cells. A) Relative PIP was moderately altered in *Fat-1* $CD4^+$ T cells. $CD4^+$ T cells were isolated from wild type and *Fat-1* spleens (n = 8 for *Fat-1*; 12 for wild type). $CD4^+$ T cell populations from two spleens were pooled for analysis using mass spectrometry as described in the *Methods.* Minor species included 40:6, 40:5, 40:4, and 42:4. Relative $PI(4,5)P_2$ levels in unstimulated purified splenic $CD4^+$ T cells isolated from wild type and *Fat-1* mice as determined by B) $PI(4,5)P_2$ mass kit (Echelon Biosciences); and C) indirect anti-$PI(4,5)P_2$ ELISA (Abcam).

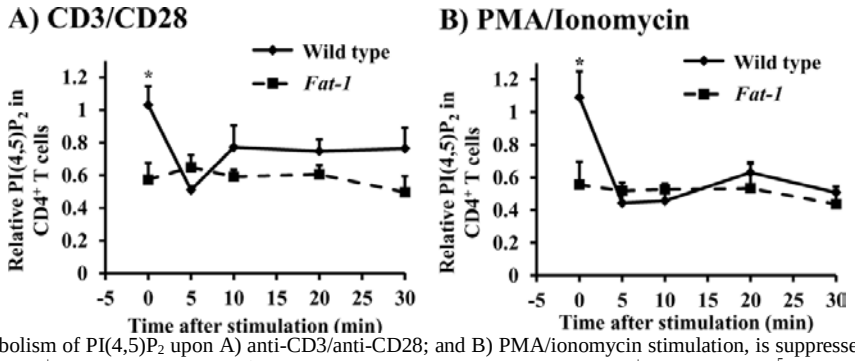

Figure 2.4 Metabolism of $PI(4,5)P_2$ upon A) anti-CD3/anti-CD28; and B) PMA/ionomycin stimulation, is suppressed in *Fat-1* $CD4^+$ T cells. Splenic $CD4^+$ T cells were isolated from wild type and *Fat-1* mice (n = 4). $CD4^+$ T cells (5×10^5) were seeded in 96 well plates containing plated anti-CD3 and anti-CD28 for the indicated times. $PI(4,5)P_2$ was subsequently extracted using acidic organic solvents, dried down under N_2, and dissolved in PBS containing 0.0025% protein stabilizer. $PI(4,5)P_2$ was detected using indirect anti-$PI(4,5)P_2$ ELISA as described in the *Methods*. Absolute values were determined using a standard curve, and normalized relative to wild type $PI(4,5)P_2$. A two-tailed t-test was used to compare individual times points between genotypes (* $P < 0.05$ between genotypes at specific time points).

2.3.3 Actin remodeling following anti-CD3/anti-CD28 stimulation is suppressed in Fat-1 $CD4^+$ T cells

Since we observed both a decrease in the basal concentration of $PI(4,5)P_2$ and a suppression in $PI(4,5)P_2$ metabolism, we subsequently determined whether $PI(4,5)P_2$-mediated actin remodeling was altered in splenic *Fat-1* $CD4^+$ T cells. For this purpose, purified splenic $CD4^+$ T cells were isolated from wild type and *Fat-1* mice and stimulated with anti-CD3/anti-CD28 for 30 min, and actin morphology was examined using alexa-568 phalloidin immunofluorescence (**Figure 2.5**). When compared to unstimulated wild type $CD4^+$ T cells, there was a 2.5-fold increase ($P < 0.05$) in actin fluorescence intensity in anti-CD3/anti-CD28 stimulated wild type $CD4^+$ T cells (**Figure 2.5**). In contrast, there was no difference ($P > 0.05$) between stimulated and unstimulated $CD4^+$ T cells isolated from *Fat-1* mice. These data indicate that actin remodeling is defective in activated splenic $CD4^+$ T cells isolated from *Fat-1* mice.

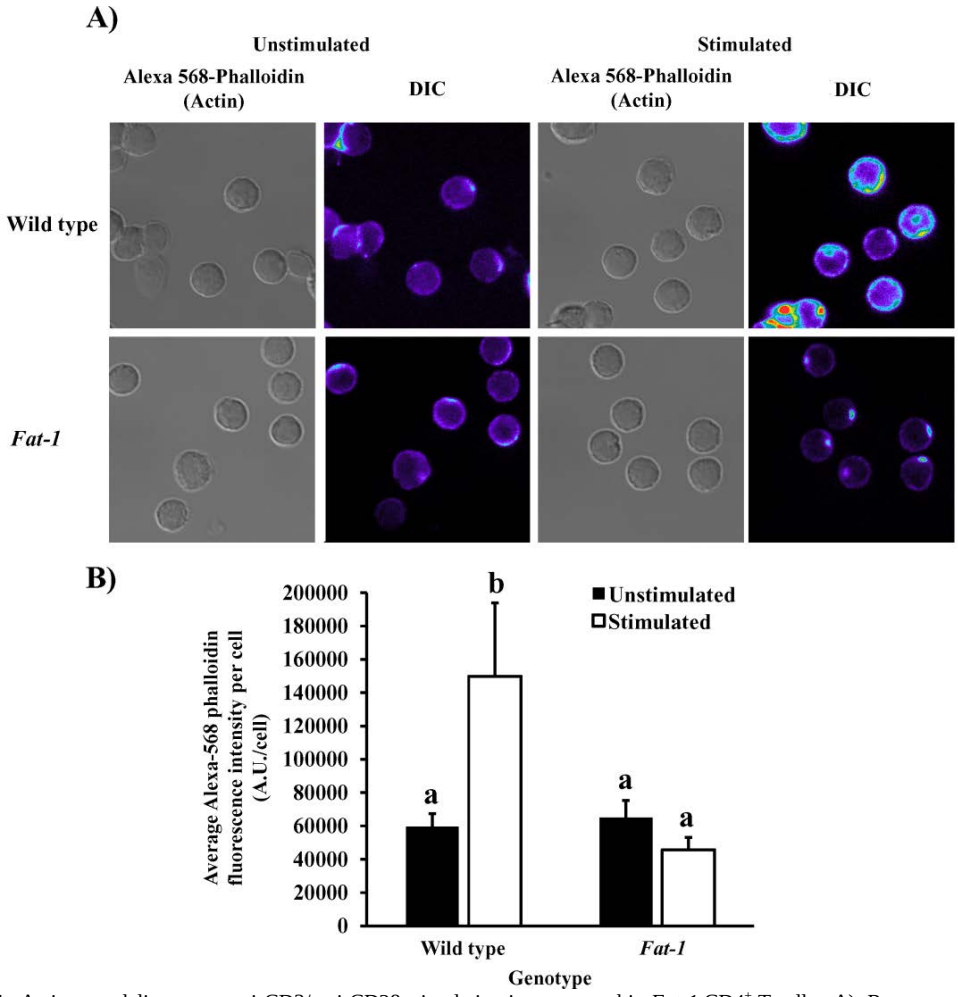

Figure 2.5. Actin remodeling upon anti-CD3/anti-CD28 stimulation is suppressed in *Fat-1* $CD4^+$ T cells. A) Representative alexa-568 phalloidin immunofluorescence images of wild type and *Fat-1* $CD4^+$ T cells seeded on slides containing only poly-L-lysine (unstimulated) or on slides containing anti-CD3/anti-CD28 (stimulated) for 30 min. Images were pseudo-coloured with increasing intensity from blue to red. B) Quantification of actin remodeling as assessed by alexa 568-phalloidin fluorescence. Purified splenic $CD4^+$ T cells (n = 4 per genotype) were seeded, fixed, permeabilized, and labeled as described in the *Methods*. Regions of interest (ROIs) were drawn around individual cells, and background was subtracted by drawing ROIs not occupied by cells. Fluorescence values were divided by the number of cells present in each field. Six fields were obtained per group, with each field containing between 3 and 7 cells. Four independent experiments were conducted. Different letters denote a significant difference of $P < 0.05$.

2.3.4 WASP recruitment to the immunological synapse is suppressed in Fat-1 $CD4^+$ T cells

WASP, a well-characterized actin-regulatory protein, is known to be localized at the IS upon stimulation (161), and to be regulated at the plasma membrane by $PI(4,5)P_2$ (162). Since $PI(4,5)P_2$ metabolism and actin remodeling were both defective in *Fat-1*

$CD4^+$ T cells, we examined whether WASP recruitment to the IS was also decreased in stimulated *Fat-1* $CD4^+$ T cells. Actin recruitment at the IS, as measured by fluorescence intensity per μm^2, was decreased in *Fat-1* $CD4^+$ T cells (**Figure 2.6**), confirming our previous results ((94) and **Figure 2.5**). Under unstimulated conditions, WASP levels were not different between wild type and *Fat-1* $CD4^+$ T cells as assessed by immunoblot (**Figure 2.7**); similarly, whole cell levels of WASP were not different between genotypes upon anti-CD3/anti-CD28 coated bead stimulation (**Figure 2.7**). However, upon measuring the fluorescence intensity at the IS, there was a 2.5 fold decrease in the fluorescence intensity per μm^2, suggesting that the recruitment of WASP to the IS in *Fat-1* $CD4^+$ T cells was impaired (**Figure 2.6**). Colocalization between Alexa 568 (F-actin) and Alexa 647 (WASP) at the IS as determined by Pearson's correlation coefficient showed a decrease in *Fat-1* $CD4^+$ T cells (wild type = 0.45 ± 0.28 ($n = 33$), *Fat-1* = 0.31 ± 0.22 ($n = 35$)**, Figure 2.7**). To further corroborate the impairment of WASP recruitment to the IS in *Fat-1* $CD4^+$ T cells, we isolated IS fractions using immunoisolation (159) to biochemically probe the level of WASP at the IS upon anti-CD3/anti-CD28 stimulation. Examination of the IS fraction revealed that in wild type $CD4^+$ T cells, the enrichment factor between IS versus input was 1.7 ± 0.5 ($n = 3$) while the enrichment factor in *Fat-1* $CD4^+$ T cells was 0.4 ± 0.1 ($n = 4$) (**Figure 2.6**). These results demonstrate that the suppressed actin remodeling in *Fat-1* $CD4^+$ T cells is correlated with decreased WASP recruitment to the IS upon T cell activation.

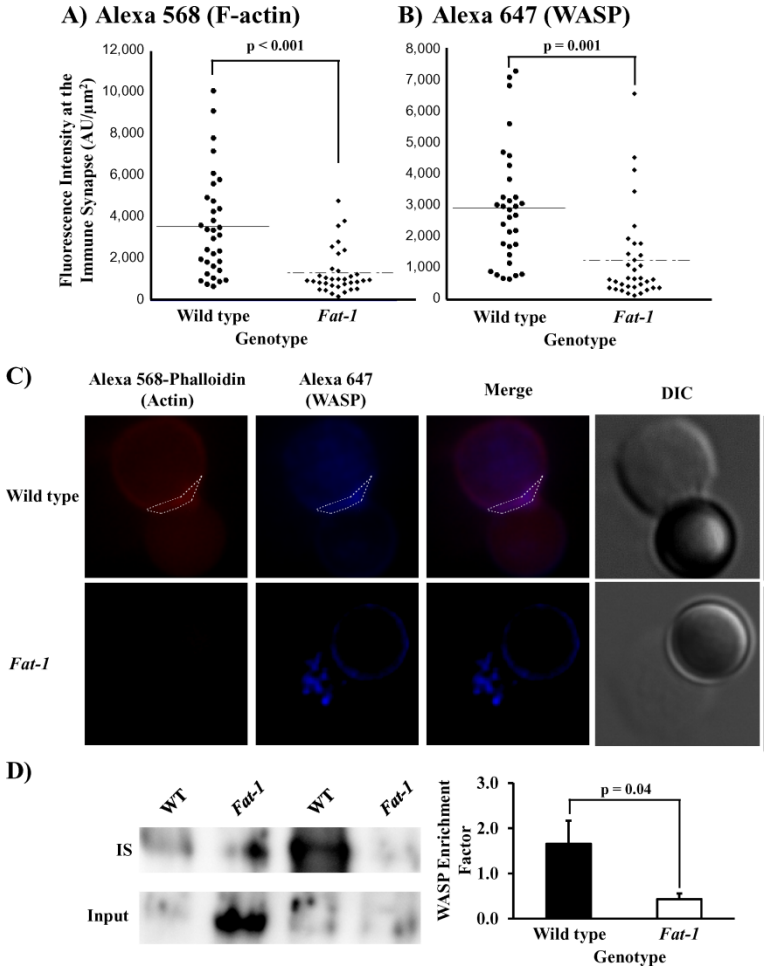

Figure 2.6. WASP localization to the IS and colocalization with actin at the IS are decreased in *Fat-1* CD4$^+$ T cells. A) Actin remodeling at the IS was suppressed in *Fat-1* CD4$^+$ T cells. Purified splenic CD4$^+$ T cells (n = 3 per genotype) were seeded, stimulated with anti-CD3/anti-CD28 coated beads, fixed, permeabilized, and labeled as described in the *Methods.* Regions of interest (ROIs) were drawn and fluorescence values divided by the area of the IS. Ten to 15 cells were analyzed per genotype. Three independent experiments were conducted. A two-tailed t-test was used to compare between genotypes. B) WASP recruitment to the IS was suppressed in *Fat-1* CD4$^+$ T cells. Refer above for experimental details. C) Representative immunofluorescence images of purified splenic CD4$^+$ T cells isolated from wild type and *Fat-1* mice. Cells were seeded onto poly-L-lysine and stimulated with anti-CD3/anti-CD28 coated beads. The ROI was drawn as an oval or polygon (white dashed line) as shown in the wild type panels. D) WASP recruitment to the IS as assessed by immunoisolation. IS fractions from WT (n = 3) and *Fat-1* (n = 4) mice were prepared as described in the *Methods.* WASP (66 kDa) was probed in both the IS and input fractions. Enrichment factor was determined by calculating the ratio of the band intensities from the IS divided by the input. A two-tailed t-test was used to compare between genotypes.

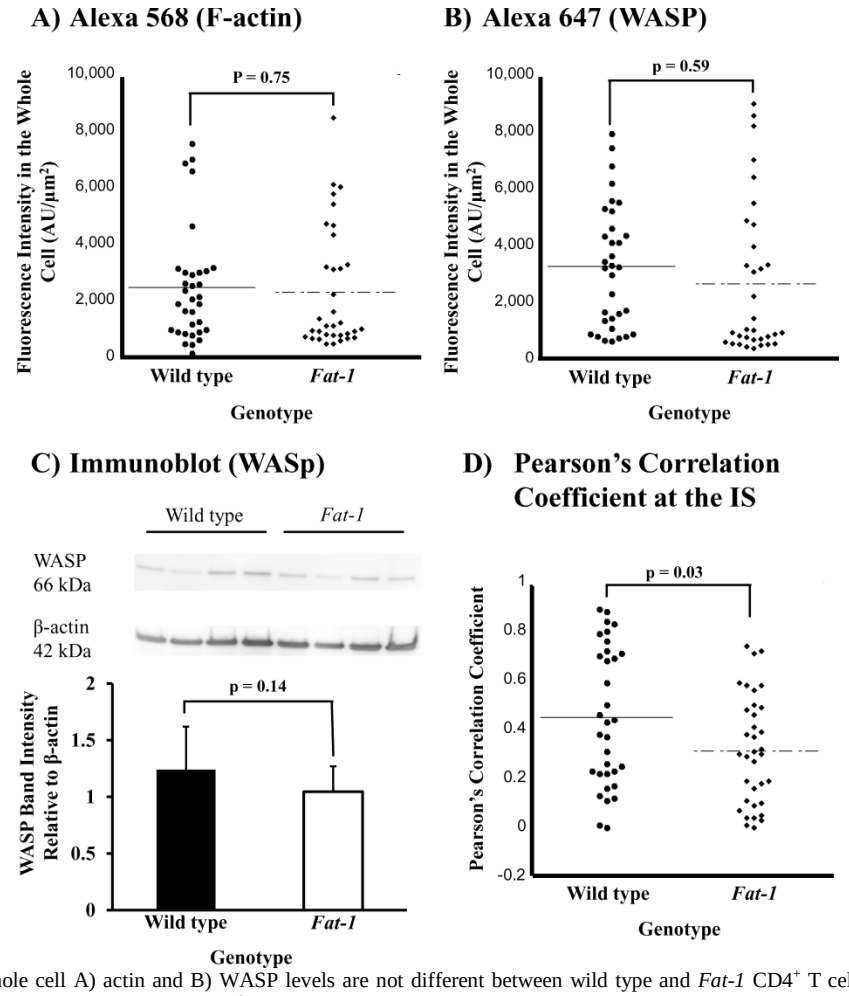

Figure 2.7. Whole cell A) actin and B) WASP levels are not different between wild type and *Fat-1* CD4$^+$ T cells as detected by immunofluorescence. Purified splenic CD4$^+$ T cells (n = 3 per genotype) were seeded, stimulated with anti-CD3/anti-CD28 coated beads, fixed, permeabilized, and labeled as described in the *Methods*. Regions of interest (ROIs) were drawn around the whole cell, excluding the bead, and fluorescence values divided by the area of the ROI. Ten to 15 cells were obtained per genotype. Three independent experiments were conducted. A two-tailed t-test was used to compare between genotypes. C) Whole cell WASP levels were not different in wild type and *Fat-1* CD4$^+$ T cells as detected by immunoblotting. Whole cell lysates were prepared and detected as described in *Supplemental Methods*. Levels of WASP were normalized to β-actin. A two-tailed t-test was used to compare between genotypes. D) Dot plot of Pearson's correlation coefficients at the IS between wild type and *Fat-1* CD4$^+$ T cells. A two-tailed t-test was used to compare between genotypes.

2.3.5 Defects in actin remodeling following anti-CD3/anti-CD28 stimulation are rescued by incubation with exogenous PI(4,5)P$_2$ in Fat-1 CD4$^+$ T cells

Since *Fat-1* CD4$^+$ T cells exhibited decreased basal PI(4,5)P$_2$ (**Figure 2.3**), we determined whether preincubation of *Fat-1* CD4$^+$ T cells with exogenous PI(4,5)P$_2$ would "rescue" the defects in actin remodeling (**Figure 2.5**). Treatment of *Fat-1* CD4$^+$

T cells with exogenous PI(4,5)P_2 at increasing concentrations showed a dose-dependent rescue of actin remodeling following stimulation with anti-CD3/anti-CD28 (**Figure 2.8**). Significantly, incubation of *Fat-1* $CD4^+$ T cells with 1.25 and 2.5 µM of exogenous PI(4,5)P_2 restored actin remodeling to the level seen in wild type $CD4^+$ T cells (**Figure 2.8**). These results not only demonstrate the direct role of PI(4,5)P_2 in regulating actin remodeling upon $CD4^+$ T cell activation, but also show that defects in *Fat-1* $CD4^+$ T cell actin remodeling can be rescued using exogenous PI(4,5)P_2.

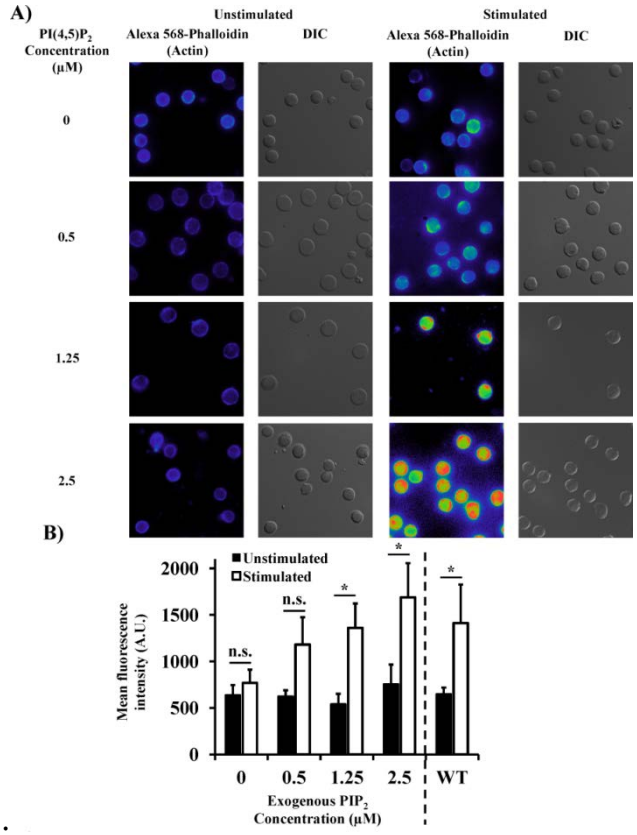

Figure 2.8. Incubation of *Fat-1* $CD4^+$ T cells with exogenous PI(4,5)P_2 can rescue defects in actin remodeling following anti-CD3/anti-CD28 stimulation. *Fat-1* $CD4^+$ T cells were isolated and incubated with PI(4,5)P_2 at various concentrations (0.5, 1.25, 2.5 µM) or PBS (0 µM) for one h prior to stimulation with plated anti-CD3/anti-CD28 for 30 min. Cells were analyzed as described in Figure 3. Images were pseudo-coloured with increasing intensity from blue to red. A two-tailed t-test was used to compare stimulation within specific concentrations (* $P < 0.05$ at specific concentrations of PI(4,5)P_2).

2.3.6 $CD4^+$ T cells isolated from mice fed a DHA triglyceride-enriched diet exhibit a phenotype similar to Fat-1 $CD4^+$ T cells

The effect of exogenous (dietary) DHA on PI(4,5)P_2-dependent actin remodeling was also examined. For this purpose, mice were fed a 4% DHA triglyceride-enriched diet in an attempt to mimic the phenotype observed in *Fat-1* $CD4^+$ T cells. No difference was observed between the body weights of animals fed a 5% CO diet (control, contains no n-3 PUFA) or the 4% DHA triglyceride-enriched diet (data not shown)**.** Total lipid analysis was carried out to verify that DHA was incorporated into $CD4^+$ T cells (**Figure 2.1**). In unstimulated $CD4^+$ T cells, there was a 25% decrease in the amount of PI(4,5)P_2 detected in $CD4^+$ T cells isolated from mice fed a 4% DHA-enriched diet (**Figure 2.9A**, $P = 0.04$) compared to control. Furthermore, there was a suppression of PI(4,5)P_2 metabolism following anti-CD3/anti-CD28 stimulation and PMA/ionomycin stimulation in purified splenic $CD4^+$ T cells from mice fed 4% DHA (**Figure 2.9B & C**, $P = 0.005$ and 0.01, respectively) compared to the control diet, as revealed by two-way ANOVA. Interestingly, actin morphology remained unchanged in splenic $CD4^+$ T cells isolated from animals fed a DHA-enriched diet, while splenic $CD4^+$ T cells isolated from animals fed the control diet showed a significant increase upon anti-CD3/anti-CD28 stimulation ($P < 0.05$, **Figure 2.9**). These results indicate that $CD4^+$ T cells isolated from *Fat-1* mice or animals fed a 4% DHA triglyceride-enriched diet exhibit similar phenotypes with regard to PI(4,5)P_2 metabolism and actin remodeling.

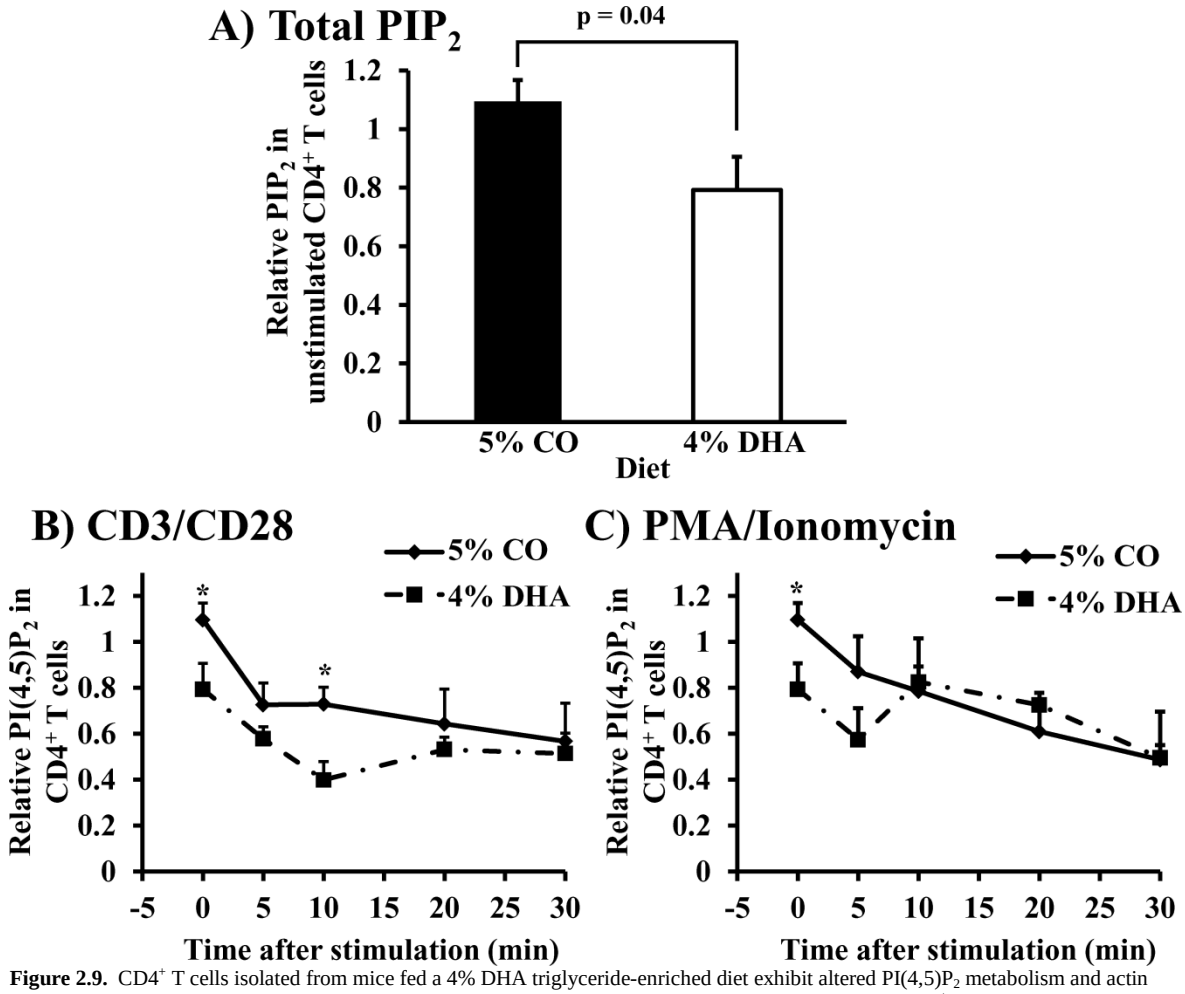

Figure 2.9. $CD4^+$ T cells isolated from mice fed a 4% DHA triglyceride-enriched diet exhibit altered $PI(4,5)P_2$ metabolism and actin remodeling upon anti-CD3/anti-CD28 stimulation. A) Relative $PI(4,5)P_2$ levels in unstimulated splenic $CD4^+$ T cells isolated from mice fed a 5% corn oil diet (control, n = 7) or 4% DHA triglyceride-enriched (n=8) diet were determined by indirect anti-$PI(4,5)P_2$ ELISA as described in *Methods*. Relative $PI(4,5)P_2$ levels were compared by normalizing to wild type $PI(4,5)P_2$. B) $PI(4,5)P_2$ levels upon anti-CD3/anti-CD28 stimulation in $CD4^+$ T cells isolated from mice fed a 5% CO or 4% DHA triglyceride-enriched diets. $CD4^+$ T cells were seeded in 96 well plates with plate bound anti-CD3 and anti-CD28 as described in the *Methods.* A two-way ANOVA indicated statistical significance between two diet groups (P = 0.005). C) $PI(4,5)P_2$ levels upon PMA/ionomycin stimulation in $CD4^+$ T cells isolated from mice fed a 5% CO or 4% DHA triglyceride-enriched diet. A two-way ANOVA indicated statistical significance between the diet groups (P = 0.01). A two-tailed t-test was used to compare individual times points between treatment groups (* $P < 0.05$ at specific time points).

2.3.7 Basal $PI(4,5)P_2$ concentration is reduced in FADS-1 null $CD4^+$ T cells

Since the acyl backbone is predominantly the stearate (C18:0) at the *sn-1*, and arachidonate ($C20:4^{\Delta 5,8,11,14}$) at the *sn-2* position, we wanted to examine whether the depletion of arachidonic acid affects the PI(4,5)P2 concentration in $CD4^+$ T cells. To

test the hypothesis that depleting arachidonic acid would decrease $PI(4,5)P_2$, we isolated $CD4^+$ T cells from FADS-1 null mice, in which the enzyme responsible for desaturating the n-6 carbon (delta-5 desaturase) is deleted. Using an indirect ELISA method, we show that the basal level of $PI(4,5)P_2$ is decreased by approximately 24% in the *FADS-1* null $CD4^+$ T cells (**Figure 2.10**).

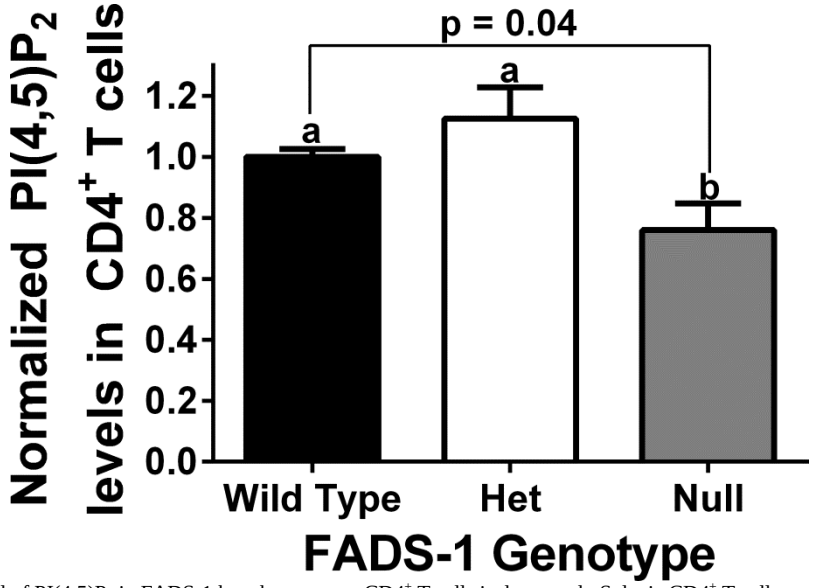

Figure 2.10. Level of $PI(4,5)P_2$ in FADS-1 knockout mouse $CD4^+$ T cells is decreased. Splenic $CD4^+$ T cells were isolated and $PI(4,5)P_2$ was quantified using an indirect ELISA method. Data were normalized to wild type level (n = 4 – 6 per genotype, mean ± sem). Values not sharing the same letter indicate significant differences using one way ANOVA.

2.3.8 n-3 PUFA do not inhibit chemotactic response to CCL19 in $CD4^+$ T cells

We reasoned that since n-3 PUFA perturbed $PI(4,5)P_2$-dependent actin remodeling in $CD4^+$ T cells by n-3 PUFA, additional cellular processes that require actin remodeling, such as chemotaxis, would also be affected. To test this hypothesis, we determined the chemotactic response of wild type and *Fat-1* $CD4^+$ T cells to the chemokine CCL19 (**Figure 2.11**), which is an important chemokine to attract naïve

$CD4^+$ T cells (160). Based on the results, although n-3 PUFA suppressed $PI(4,5)P_2$-dependent actin remodeling, n-3 PUFA had no effect on chemokine-induced actin remodeling, as assessed by the chemotactic ability of $CD4^+$ T cells to migrate towards CCL19.

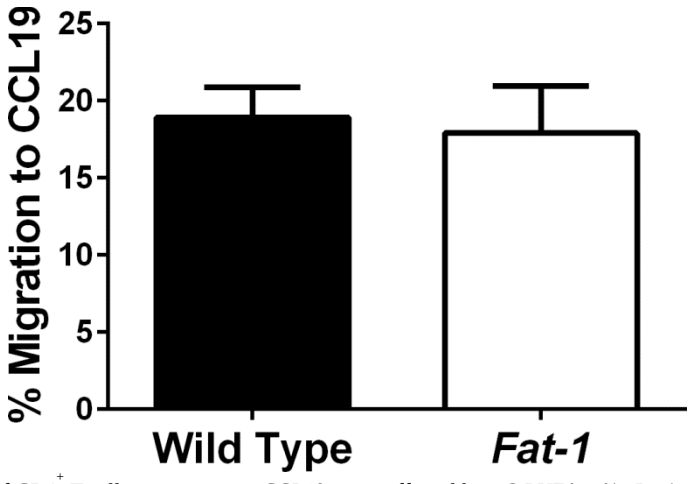

Figure 2.11. Migration of $CD4^+$ T cells in response to CCL19 is not affected by n-3 PUFA. A) *In vitro* chemotaxis assay set-up. B) Splenic $CD4^+$ T cells were isolated from wild type and *Fat-1* mice and assayed for their chemotactic response to CCL19 (0.25 µg/mL, naïve T cells). % migration was determined by dividing the number of cells collected from the lower chamber to the total number of cells seeded. Experiments were performed in triplicates with n = 5. Values represent mean ± sem.

2.4 Discussion

In the current study, we have shown that n-3 PUFA i.e., DHA, critically regulate $PI(4,5)P_2$-dependent actin remodeling in $CD4^+$ T cells. This novel effect was associated with decreased levels of $PI(4,5)P_2$ in unstimulated $CD4^+$ T cells, and suppressed metabolism of $PI(4,5)P_2$ upon anti-CD3/anti-CD28 or PMA/ionomycin stimulation.

$PI(4,5)P_2$ can be synthesized via two pathways: i) the *de novo* pathway (Kennedy pathway); and ii) the remodeling pathway (Lands' cycle). Since the incorporation of polyunsaturated fatty acids at the *sn-2* position of $PI(4,5)P_2$ is predominantly driven by

the Lands' cycle rather than the Kennedy cycle (163, 164), the phospholipid composition of the membrane can potentially influence the acyl composition of phosphoinositides (165). Indeed, it has been shown that platelet 1-acyl-glycero-3-phosphoinositol acyltransferase, which catalyzes the condensation between fatty acyl Co-A and lysophospholipid, prefers n-6 PUFA over n-3 PUFA (166). Our results support this model as the presence of n-3 PUFA decreased the 16:0,20:4 and 18:0,20:4 species of $PI(4,5)P_2$, while concomitantly increasing the 18:1,20:4 species of $PI(4,5)P_2$ (**Figure 2.2**). To target the *sn-2* position of $PI(4,5)P_2$, we also utilized the FADS-1 knockout mouse model, in which levels of arachidonic acid were depleted by deleting the delta-5 desaturase (167). Similar to the presence of n-3 PUFA acting as a competitive inhibitor for the remodeling of $PI(4,5)P_2$, depleting the remodeling enzyme's preferred substrate also led to a decrease in the amount of $PI(4,5)P_2$ in $CD4^+$ T cells (**Figure 2.10**), demonstrating how attacking the *sn-2* position of $PI(4,5)P_2$ can decrease its level in $CD4^+$ T cells.

With regard to $PI(4,5)P_2$ metabolic turnover plots (**Figure 2.3**), wild type data are similar to previously published work (47). Furthermore, $PI(4,5)P_2$ metabolism in *Fat-1* and 4% DHA $CD4^+$ T cells are consistent with published results showing that porcine cardiac myocytes incubated with DHA exhibited no change in IP_3 generation after stimulation by an α_1-adrenoreceptor agonist (168). Similarly, we have previously shown that diacylglycerol production in purified murine T lymphocytes isolated from mice fed dietary EPA and DHA is suppressed upon stimulation (137). The $PI(4,5)P_2$ metabolic

profile in *Fat-1* $CD4^+$ T cells also corroborates our previous data that PLC-γ1 and phosphorylated PLC-γ1 are down-regulated in T cells at the IS (94).

The magnitude and kinetics of $PI(4,5)P_2$ metabolism are important for actin remodeling, as demonstrated in various cell types and physiological processes (153-155). For example, the overexpression of PIP5K, which increases the availability of $PI(4,5)P_2$, perturbs stress actin fibers and membrane ruffling, indicative of defects in actin reorganization (169). Our data reveal that the distortion of $PI(4,5)P_2$ levels is associated with the suppression of actin remodeling in *Fat-1* and 4% DHA derived $CD4^+$ T cells (**Figures 2.4 and 2.9**). We also demonstrate that the defects in actin remodeling observed in *Fat-1* CD^+ T cells can be rescued by the introduction of exogenous $PI(4,5)P_2$ (**Figure 2.8**). It is interesting to note that mitochondrial translocation in $CD4^+$ T cells is inhibited by latrunculin, a drug that sequesters actin monomers, preventing actin polymerization (170). We have previously shown that mitochondrial translocation after stimulation in *Fat-1* $CD4^+$ T cells is suppressed (136), thus our results that actin remodeling is suppressed in *Fat-1* $CD4^+$ T cells may partially explain the lack of mitochondrial translocation upon $CD4^+$ T cell stimulation.

It is interesting to note that not all actin remodeling processes are perturbed by n-3 PUFA. For example, chemotaxis of $CD4^+$ T cells, which utilizes actin cytoskeleton, is not affected by n-3 PUFA (**Figure 2.11**). This may be due to the fact that chemotaxis involves other, compensatory signals that may be able to overcome the inhibition exerted by n-3 PUFA (171). It is interesting to note that chemotaxis of the immortalized young

adult mouse colonoytes treated with EPA or DHA was suppressed, as assessed by the wounding assay (172).

WASP, an actin regulatory protein, is activated by $PI(4,5)P_2$ though interaction between the basic domain of WASP and the acidic $PI(4,5)P_2$ to release WASP from its autoinhibitory conformation (149, 162). Interestingly, activation of N-WASP, a member of the WASP family, is dependent upon PIP_2 density, i.e., increased PIP_2 density leads to hyperactivation of N-WASP *in vitro* (22). Furthermore, depletion of the PIP_2 fraction in the raft pool resulted in decreased T cell capping upon T cell activation (39). One can speculate, therefore, that $PI(4,5)P_2$ metabolism upon activation of $CD4^+$ T cell leads to a local increase in $PI(4,5)P_2$ density, which results in the recruitment and activation of WASP at the IS and subsequent actin remodeling. In the presence of n-3 PUFA, not only is basal $PI(4,5)P_2$ decreased, but $PI(4,5)P_2$ fails to metabolize upon activation, leading to suppressed WASP recruitment to the IS and actin remodeling (**Figure 2.6**). Further experiments are required to test this hypothesis.

In the 4% DHA triglyceride-enriched diet, DHA contributed approximately 5% toward the total energy (kcals) intake. In a typical Greenland Inuit diet, n-3 PUFA constitutes approximately 2.7 – 6.3% of daily energy (173-175). Thus, our 4% DHA diet is within the physiological range achievable though diet. In humans, comparable intakes could also be achieved through the ingestion of DHA supplements. At this level, we did not observe any adverse effects, as food intake and changes in body weight were similar between the dietary groups (data not shown).

In summary, our results demonstrate the novel effects of n-3 PUFA on critical mechanisms of early T cell activation (**Figure 2.12**). We have previously demonstrated that n-3 PUFA can suppress T cell activation, in part, by affecting recruitment and activation of signaling proteins such as PLC-γ1, PKCθ, and F-actin, as well as mitochondrial translocation necessary to sustain Ca^{2+} signaling for nuclear NF-κB and AP-1 activation and IL-2 secretion (78, 94, 136). We extend this model by demonstrating that n-3 PUFA, such as DHA, can also affect $PI(4,5)P_2$-dependent actin remodeling by decreasing steady-state $PI(4,5)P_2$ levels, suppressing $PI(4,5)P_2$ metabolism upon stimulation, and inhibiting $PI(4,5)P_2$-dependent actin remodeling. In addition, a mechanism by which n-3 PUFA suppress $PI(4,5)P_2$-dependent actin remodeling is through decreased WASP recruitment to the IS. In contrast to commonly used pharmacological perturbations, our *in vivo* genetic and dietary intervention studies carry significant biological relevance. Overall, our findings highlight a novel modality by which n-3 PUFA influence membrane microorganization, thereby modulating biological responses.

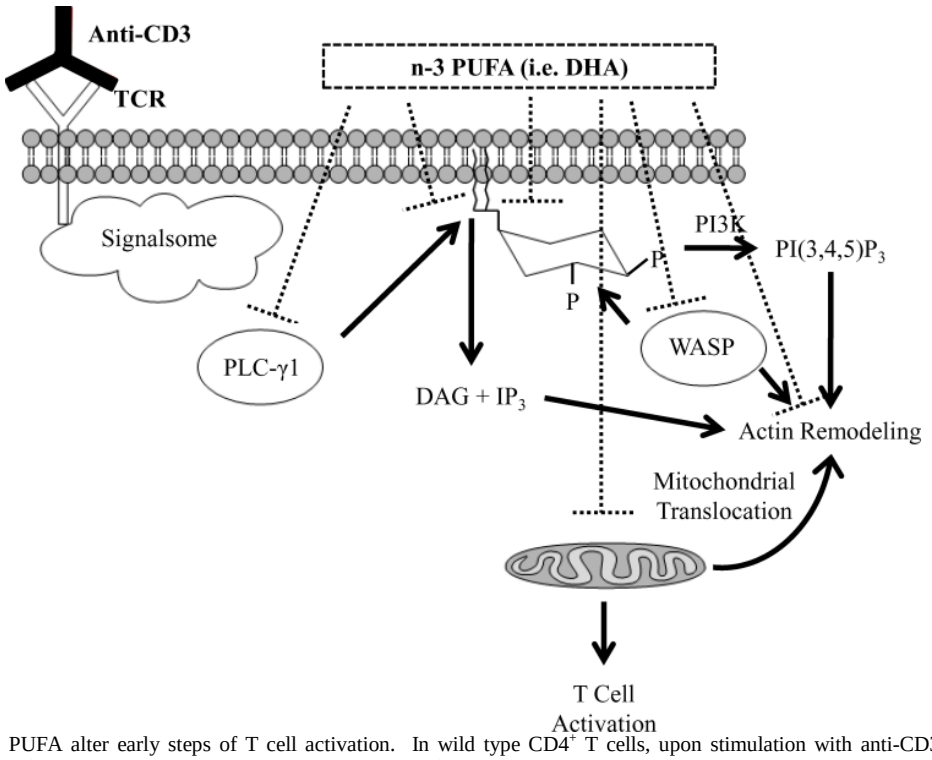

Figure 2.12. n-3 PUFA alter early steps of T cell activation. In wild type $CD4^+$ T cells, upon stimulation with anti-CD3 (and costimulatory signal from CD28), the TCR signalsome composed of Lck, ZAP70, LAT, GADS, SLP76, NCK, ITK, VAV1, PAK, and PLC-γ1 is formed, recruiting additional proteins such as PLC-γ1. PLC-γ1 hydrolyzes the lipid mediator $PI(4,5)P_2$ to DAG and IP_3, leading to induction of Ca^{2+} signaling and the PKCθ signaling pathway. The hydrolysis of $PI(4,5)P_2$ is also important for actin remodeling by releasing actin regulating proteins localized at the plasma membrane. Additionally, $PI(4,5)P_2$ is phosphorylated by class I PI3K to generate $PI(3,4,5)P_3$ which also triggers actin remodeling. WASP is recruited to the plasma membrane and activated by $PI(4,5)P_2$ to regulate actin remodeling. These pathways synergistically regulate actin remodeling at the plasma membrane for mitochondrial translocation and T cell activation. We have previously shown that n-3 PUFA suppress total and phosphorylated PLC-γ1 translocation to the IS (dotted hammerheads signify suppression) (94); and mitochondrial translocation to the IS (136). We now show that n-3 PUFA such as DHA can suppress i) the basal level of $PI(4,5)P_2$ in unstimulated $CD4^+$ T cells; ii) the metabolism of $PI(4,5)P_2$ upon anti-CD3/anti-CD28 or PMA/ionomycin stimulation; iii) WASP recruitment to the IS; and iv) actin remodeling upon anti-CD3/anti-CD28 stimulation. The suppression of these early immediate events in T cell activation leads to inhibition of T cell function, and thus may suppress inflammatory responses.

CHAPTER III

n-3 POLYUNSATURATED FATTY ACIDS UNIQUELY ALTER PHOSPHOTIDYLINOSITOL-(4,5)-BISPHOSPHATE ORGANIZATION AND REGULATE THE $CD4^+$ T CELL PROLIFERATIVE RESPONSE, AS REVEALED BY IMAGING PLASMA MEMBRANE LIPID DOMAINS

3.1 Introduction

Previous published data and data from the last chapter demonstrated using the transgenic *Fat-1* mouse model, which generates n-3 PUFA *de novo* and enriches the membrane with n-3 PUFA (176), that early signaling events critical to T cell activation are suppressed, including $PI(4,5)P_2$-dependent actin remodeling, signaling protein and mitochondrial translocation to the IS, and calcium signaling (78, 94, 136, 177). Complementary studies have shown that incorporation of EPA or 7-ketocholesterol into the plasma membrane of Jurkat T cells can not only change the biophysical properties of the plasma membrane, but also suppress T cell activation (67, 71), demonstrating the intricate link between the biophysical properties of the plasma membrane and T cell signaling.

Since the plasma membrane plays a critical role in T cell signaling, and we have previously demonstrated that n-3 PUFA can increase its lipid order (93, 94, 178), we hypothesized that n-3 PUFA suppress T cell signaling and function, in part, by modifying the membrane topography and spatial organization of $PI(4,5)P_2$ in the plasma membrane. By using a variety of fluorescence resonance energy transfer (FRET) probes, we demonstrate, for the first time, that dietary bioactive molecules such as EPA

and DHA can not only modify the biophysics of the plasma membrane, but also alter the spatial organization of $PI(4,5)P_2$, a critical phospholipid that regulates the spatiotemporal properties of plasma membrane mesodomains. We demonstrate that these effects result in the suppression of clonal expansion upon activation of primary $CD4^+$ T cells. These data highlight the intrinsic effects of n-3 PUFA on the proximal events immediately following engagement of the TCR on the $CD4^+$ T cell surface. Modulation of these events results in a suppression of T cell proliferation and contributes to an overall anti-inflammatory environment that may be beneficial for human subjects suffering from chronic inflammatory diseases or patients undergoing medical surgeries requiring total parenteral nutrition (TPN) (179).

3.2 Materials and methods

3.2.1 Plasmids

ECFP, and YPet were synthesized by Integrated DNA Technologies (Coralville, Iowa) into pIDTSMART and subcloned into pLenti vector using BamHI and NotI (**APPENDIX H**; New England Biolabs, Ipswich, MA). An NheI site was included immediately downstream of BamHI for insertion of additional fragments. cDNA containing the first 10 amino acids of Lck [Lck(N10)], the first 15 amino acids of Src [Src(N15)], the transmembrane domain of linker for activation of T cells [LAT(TM)], and the PH domain of phospholipase-δ [PH(PLC-δ)], were synthesized and subcloned into pLenti using BamHI and NheI restriction sites, upstream and in-frame to ECFP or YPet. All plasmids were verified by sequencing (Eton Bioscience, San Diego, CA), and

expressed as fusion probes in 293T cells followed by examination under microscopy and Western blotting.

3.2.2 Generation of lentivirus

Lentivirus was generated as previously described with minor modifications for lentivirus (180, 181). Individual pLenti constructs were co-transfected with pLP-1, pLP-2, and pVSV-G (Life Technologies, Grand Island, NY) into HEK293T/17 (ATCC CRL-11268) using calcium phosphate precipitation (**APPENDIX I** and **J**). Medium containing the virus was harvested 3X within 72 h of transfection. Lentivirus was then concentrated using a concentrator (Clontech, Mountain View, CA), resuspended in RPMI media (Irvine Scientific, Santa Ana, CA) containing 5% fetal bovine serum, 1% glutamax (Life Technologies), and 1% penicillin-streptomycin (Life Technologies), and stored at -80 °C until the time of the transduction.

3.2.3 Animal husbandry and $CD4^+$ T cell isolation

Animal protocols have been approved by the Institutional Animal Care and Use Committee at Texas A&M University and follow the U.S. Public Health Service guidelines. *Fat-1* transgenic mice on a C57BL/6 background, generously provided by Dr. Jing X. Kang (Department of Medicine, Harvard University), were bred, genotyped, and phenotyped as previously described [**APPENDIX A**; (94, 136, 177)]. Wild type and *Fat-1* litter-mate controls were fed a 10% safflower diet *ad libitum* in a 12:12 light:dark cycle. $CD4^+$ T cells were purified by removing the spleen aseptically and labeling with magnetic CD4 (L3T4) microbeads according to manufacturer's protocol (**APPENDIX B**; Miltenyi Biotec, Auburn, CA). $CD4^+$ T cells were cultured in complete RPMI

media, 20 ng/mL rIL-2 (eBioscience, San Diego, CA), and 20 μM 2-mercaptoethanol (Sigma Aldrich, St Louis, MO), until the start of the downstream assay (within h). For rescue experiments using exogenous $PI(4,5)P_2$, cells were treated after lentiviral transduction with $PI(4,5)P_2$ dissolved in PBS supplemented with 0.0025% of protein stabilizer (Echelon Biosciences, Salt Lake City, UT) for one hr, at 37 °C, 5% CO_2, collected, and washed, before FRET experiments.

In the diet experiment, 4 to 6 weeks old C57BL/6 mice were fed either an n-6 PUFA enriched 5% corn oil diet, 0.95% DHA (low n-3 PUFA) or 4% DHA (high n-3 PUFA) triglyceride-enriched diet. Diets differed only in their oil composition, either (control) 5% corn oil by weight or a mixture of 57% pure DHA triglyceride (Martek, Columbia, MD) and corn oil (0.95:4.05 or 4:1 w/w). Additional diet components, expressed as g/100 g, were 20 casein, 41.9 sucrose, 22 corn starch, 6 cellulose, 3.5 AIN-76 mineral mix, 1 AIN-76 vitamin mix, 0.3 DL-methionine, 0.2 choline chloride, and 5 dietary oil (68, 78, 142). Mice were fed *ad libitum* for 3 to 4 weeks in a 12:12 light:dark cycle and diet changed daily to prevent the formation of oxidative byproducts.

3.2.4 Lentiviral transduction

$CD4^+$ T cells were resuspended to a final concentration of 7.5×10^6 cells/mL, seeded into a 24 well plate and incubated with lentivirus for 48 h before imaging in the presence of 2 μg/mL polybrene (**APPENDIX K**). Typically ECFP-containg lentivirus was added 8 h prior to YPet lentivirus to optimize the level of the fluorophores for imaging. After 48 h of incubation, $CD4^+$ T cells were collected, washed, resuspended in

300 μL of Leibovitz's media, and seeded onto poly-L-lysine coated 35 mm glass bottom dishes (MatTek, Ashland, MA) for imaging.

3.2.5 Microscopy and image analysis

FRET experiments were conducted using the Zeiss LSM 510 META laser scanning confocal microscope with an excitation at 458 nm for ECFP, and 514 nm for YPet by the equipped argon laser. Emissions were detected between 480 – 520 nm for ECFP, and between 535 – 590 nm for YPet. Samples were imaged with a 63X oil objective with a numerical aperture of 1.2, and recorded in 8-bit mode. Images were processed using the accompanying software and values were exported and analyzed in Microsoft Excel.

FRET was analyzed by acceptor photobleaching to detect the increase in ECFP signal. A region of interest was drawn around the plasma membrane, and photobleaching was conducted by illuminating the region of interest for 200 iterations with the laser. For each cell, four images were recorded: i) YFP_{PRE}, YPet fluorescence before photobleaching; ii) CFP_{Pre}, ECFP fluorescence before photobleaching; iii) YFP_{Post}, YPet fluorescence after photobleaching; and iv) CFP_{Post}, ECFP fluorescence after photobleaching. Corrections to the fluorescence intensities were also made by conducting acceptor photobleaching cells expressing only the ECFP and YPet probes to determine the bleaching of ECFP during photobleaching (CFP_{Bleach}), and the bleed-through of YPet into the CFP channel (CFP_{YFP}). Corrections to the CFP intensities before and after photobleaching were calculated as follows:

$$CFP_{Pre,\ Corrected} = CFP_{Pre} - CFP_{YFP\ Bleed} \quad \text{(Eq.1)}$$

$$CFP_{Post,\ Corrected} = (CFP_{Post} - CFP_{YFP}) + CFP_{Bleach} \quad \text{(Eq. 2)}$$

To determine the FRET efficiency (E%), the corrected CFP values were used in the following equation:

$$E\% = \frac{CFP_{Post,\ Corrected} - CFP_{Pre,\ Corrected}}{CFP_{Post,\ Corrected}} X100 \qquad \text{(Eq. 3)}$$

To determine FRAP, the following equation was used to analyze cells expressing only the YPet probe where F(t) is fluorescence intensity at time (t), F(∞) is the fluorescence intensity after recovery, F(0) is the initial fluorescence intensity, and k is the rate of fluorescence intensity recovery after photobleaching:

$$F(t) = [F(\infty) - F(0)] \times [1 - \exp(-kt)] + F(0) \qquad \text{(Eq. 4)}$$

3.2.6 CFSE assay

After $CD4^+$ T cell isolation, cells were labeled with CFSE as previously described [**APPENDIX M**; (94, 141)]. In brief, 5 mM of CFSE (Life Technologies) in dimethyl sulfoxide (DMSO, Sigma Aldrich) was added into 1 x 10^6 cells/mL in PBS (Life Technologies) containing 0.1% BSA (Roche Diagnostics), incubated at 37 °C for 30 min, before rapid chilling by adding excess of ice-cold complete RPMI and incubated for 5 min on ice. Cells were then collected, washed with PBS, and resuspended to a final cell concentration of 2 x 10^6 cells/mL. Cells were then cultured in 96 well plates either unstimulated, or stimulated with plated anti-CD3 (Clone 145-2C11, 0.2 µg/mL, eBiosciences) and suspended anti-CD28 (Clone 37.51, 1 µg/mL, eBiosciences) for 72 h, at 37 °C. On the day of analysis, cells were collected, washed with PBS, and then resuspended in staining buffer (eBioscience) containing 1 µg/mL of PI (Miltenyi Biotec). Samples were then processed using a BD Accuri C6 flow cytometer (BD Bioscience, San Joe, CA).

3.2.7 Statistical analysis

All experiments were conducted with at least four animals, and data were expressed as mean ± sem unless otherwise noted. Using GraphPad Prism (La Jolla, CA), data were analyzed by two-tailed Student's t-test between genotypes with a single treatment, one-way ANOVA between multiple groups, or by two-way ANOVA between genotypes and treatments. In cases where the F statistic was significant ($P < 0.05$) in ANOVA, a Tukey post-hoc test was conducted. $P < 0.05$ was considered to be statistically significant.

3.3 Results

3.3.1 Using raft and non-raft markers to probe the effects of n-3 PUFA on plasma membrane mesodomains

We have previously shown that n-3 PUFA perturb the membrane lipid bilayer by increasing the liquid order of plasma membrane mesodomains in $CD4^+$ T cells genetically enriched with n-3 PUFA (94), and in $CD4^+$ T cells isolated from mice fed a diet enriched in n-3 PUFA, e.g., DHA (178). To further probe the effects of n-3 PUFA on the plasma membrane mesodomains, in a series of FRET experiments, we utilized the raft markers Lck(N10) and LAT(TM), in which the 10 N-terminal amino acids of Lck and the transmembrane domain LAT are fused to fluorescent reporters. For comparative purposes, we also investigated the properties of the non-raft marker Src(N15), which contains the 15 N-terminal amino acids of c-Src (182).

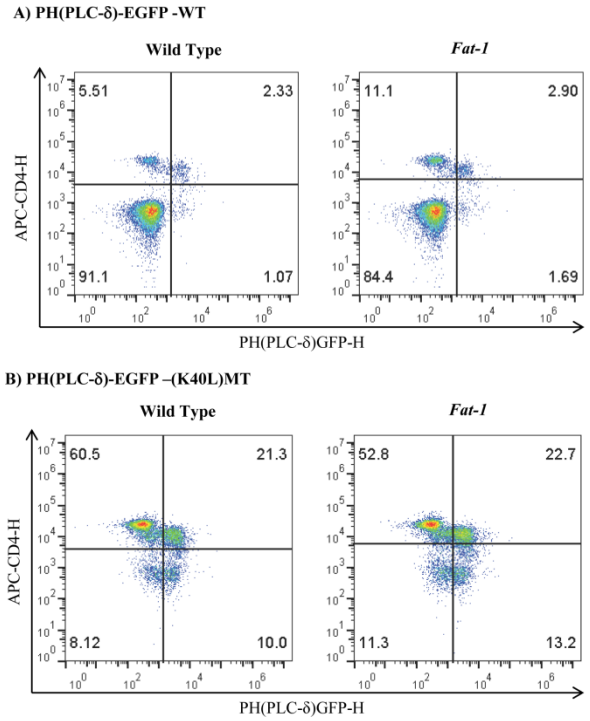

Figure 3.1. Expression of (A) wild type; and (B) K40L mutant PH(PLC-δ)-EGFP constructs in $CD4^+$ T cells isolated from wild type and *Fat-1* transgenic mice. $CD4^+$ T cells were isolated using positive selection and cultured in the presence of 10 μM 2-mercaptoethanol and 40 ng/μL recombinant IL-2 for 1 hr at 37 °C, 5% CO_2, prior to lentiviral transduction of the PH(PLC-δ)-EGFP construct (n = 3 per genotype). $CD4^+$ T cells were then further cultured for 48 h at 37 °C, 5% CO_2 before labeling with APC-CD4 for flow cytometry analysis. Percentages of wild type and *Fat-1* $CD4^+$ T cells transduced with wild type (2.73 ± 1.29 and 2.58 ± 0.82 for wild type and *Fat-1*, respectively) and K40L mutant (15.34 ± 6.72 and 11.21 ± 6.19 for wild type and *Fat-1*, respectively) constructs.

Mammals are unable to convert n-6 PUFA into n-3 PUFA, thus we utilized the *Fat-1* transgenic mouse model, in which the plasma membrane is enriched with n-3 PUFA upon feeding a diet high in n-6 PUFA (141, 176). We hypothesized that the presence of n-3 PUFA in the plasma membrane would increase the FRET efficiency between the lipid raft markers, since increased liquid order would favor an increase in the coalescence of lipid raft mesodomains. We utilized a lentivirus system to transduce the reporter plasmids in order to avoid activating the $CD4^+$ T cells with antibodies or chemicals (183, 184). Using this system, the presence of n-3 PUFA did not affect the lentiviral transduction efficiency (**Figure 3.1**). We verified our FRET approach by

performing a series of control experiments (**Figure 3.2**). We first expressed the FRET standards C5V, C32V, and Cerulean in 293T cells and calculated the FRET efficiencies using Eq. 3 to determine the FRET efficiencies using our microscope system and conditions [**Figure 3.2**; (185)]. We then determined the FRET efficiencies of the Lck(N10)/Lck(N10) FRET pair in 293T cells and primary $CD4^+$ T cells to evaluate the change between photobleaching the whole cell versus a region of interest, where we saw no statistical difference between the two approaches (**Figure 3.2B**). This is important to ensure that the diffusion of YPet outside of the region of interest is slow enough to accurately measure FRET efficiency immediately after photobleaching. We then optimized the iterations of photobleaching in order to ensure maximum photobleaching without prolonged laser exposure to minimize effects on cell viability (**Figure 3.2C**).

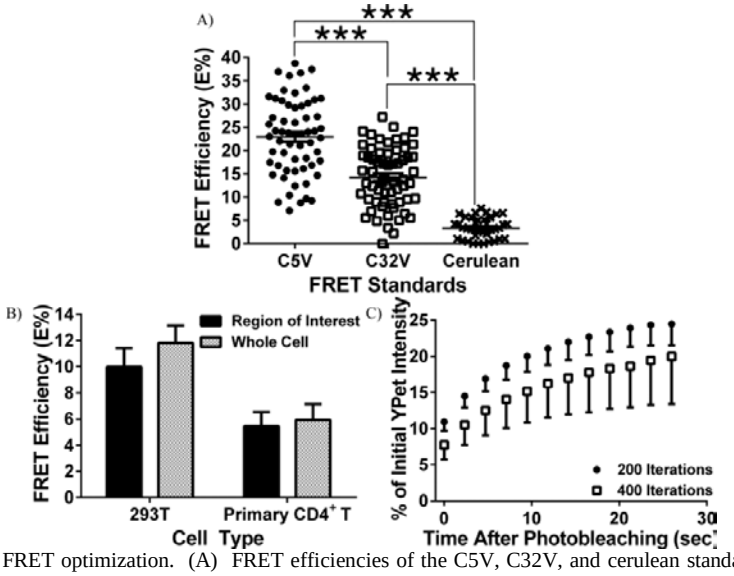

Figure 3.2. Experimental FRET optimization. (A) FRET efficiencies of the C5V, C32V, and cerulean standards measured using acceptor photobleaching. C5V, C32V, and cerulean generated by S.S. Vogel and described previously(185), were obtained from Addgene (#26394 for C5V, #26396 for C32V, and #27795 for cerulean). 293T cells were transfected with C5V and C32V plasmids, and acceptor photobleaching was determined using a Zeiss 510 LSM microscope. FRET efficiency (E%) was determined by comparing the CFP intensity before and after acceptor photobleaching. Published values for C5V is 45.1% ± 4.42%, C32V is 25.6 ± 4.89%(186). (B) Comparison between FRET efficiencies of Lck(N10)/Lck(N10) obtained from acceptor photobleaching of the region of interest versus whole cell in 293T cells and primary $CD4^+$ T cells. (C) Relative intensities of PH(PLC-δ)-YPet in the YFP channel monitored throughout the photobleaching scheme in primary $CD4^+$ T cells using 200 and 400 iterations for photobleaching.

After performing these control experiments, we measured the FRET efficiency between the various raft and non-raft markers (**Figures 3.3**). As predicted based on our previous data showing that n-3 PUFA increase the liquid order of the plasma membrane, the incorporation of n-3 PUFA into the plasma membrane increased the FRET efficiencies of the lipid raft markers Lck(N10)/Lck(N10), and Lck(N10)/LAT(ΔCP), compared to the non-interacting markers Lck(N10)/Src(N15) (**Figure 3.3D & E**). Since the diffusion of membrane proteins can be influenced by whether they are localized in lipid raft mesodomains (187), we also determined the rate of fluorescence recovery after photobleaching (FRAP) of the raft markers Lck(N10) and LAT(ΔCP). FRAP of Lck(N10) in $CD4^+$ T cells enriched with n-3 PUFA exhibited a 20% decrease relative to the FRAP of Lck(N10) expressed in wild type $CD4^+$ T cells (**Figure 3.3G**). We did not observe a difference in the FRAP of LAT(ΔCP) between genotypes, perhaps due to the slow rate of recovery exhibited by LAT(ΔCP) (**Figure 3.3H**). Collectively, the results from the FRET and FRAP experiments indicate that n-3 PUFA alter the dynamics of the lipid raft mesodomains in the plasma membrane.

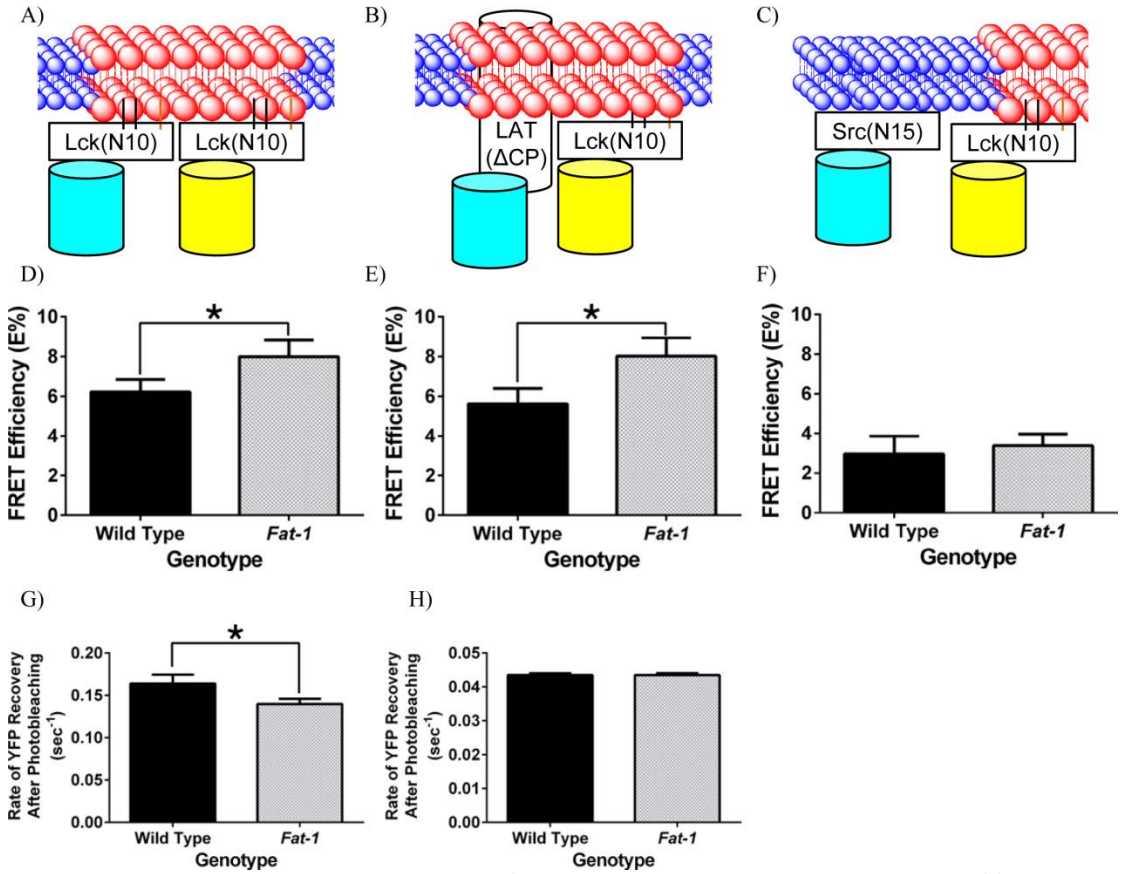

Figure 3.3. n-3 PUFA perturb the biophysical properties of the plasma membrane by increasing the interaction of fluorescent lipid raft markers Lck(N10)/Lck(N10), and Lck(N10)/LAT(ΔCP) detected using FRET, and decreasing the rate of FRAP of the lipid raft marker Lck(N10). (A, B, and C) Schematic diagrams of the interaction between neighboring fluorescent probes targeted to the raft or the non-raft membrane fraction of the plasma membrane. Lck(N10) and Src(N15) consist of the first 10 and 15 N-terminal amino acids of Lck and Src, respectively. LAT(ΔCP) consists of the first 36 amino acids, representing the extracellular, transmembrane, and the membrane anchoring portions of LAT. Splenic $CD4^+$ T cells were incubated with lentivirus containing (D) Lck(N10)/Lck(N10), (E) Lck(N10)/LAT(ΔCP), or (F) Lck(N10)/Src(N15) before FRET by acceptor photobleaching (n = 4 per genotype). FRET efficiency (E%) was determined by comparing the CFP intensity before and after acceptor photobleaching, and normalized to the FRET efficiency obtained from the C5V standard (*$P < 0.05$ between genotypes). The rate of recovery after photobleaching was also determined for $CD4^+$ T cells expressing (G) Lck(N10)-YPet and (H) LAT(ΔCP)-YPet (*$P < 0.05$ between genotypes).

3.3.2 Incorporation of n-3 PUFA into the plasma membrane decreases the non-raft pool of PI(4,5)P_2

Since we have shown that the lipid raft mesodomains in the plasma membrane are perturbed by the presence of n-3 PUFA, and PI(4,5)P_2 couples the mesoscale raft domains with membrane cytoskeleton compartments (14, 188, 189), we hypothesized

that incorporation of n-3 PUFA into the plasma membrane alters the spatial organization of $PI(4,5)P_2$ relative to raft and non-raft mesodomains. Utilizing the raft markers [Lck(N10) and LAT(ΔCP)] and the non-raft marker [Src(N15)] in combination with the $PI(4,5)P_2$ reporter PH(PLC-δ) (**Figure 3.4**), we tested our hypothesis in a series of FRET experiments. Although n-3 PUFA increased the FRET efficiencies between lipid raft markers (**Figure 3.3**), the FRET efficiency between PH(PLC-δ) and either Lck(N10) or LAT(ΔCP) was not affected in $CD4^+$ T cells enriched with n-3 PUFA (**Figures 3.4D & E**). This was corroborated by measuring the co-localization between GM1, a well-characterized lipid raft marker (190, 191), and PH(PLC-δ), which showed no difference in the presence of n-3 PUFA (**APPENDIX L**; **Figure 3.5**). The FRET efficiency between PH(PLC-δ) and the non-raft marker Src(N15), however, was decreased by 20% in $CD4^+$ T cells enriched with n-3 PUFA (**Figure 3.4F**). These results suggest that the incorporation of n-3 PUFA into the plasma membrane not only influences the biophysical properties of the phospholipid bilayer, but also alters the spatial organization of $PI(4,5)P_2$ by depleting the non-raft pool of $PI(4,5)P_2$.

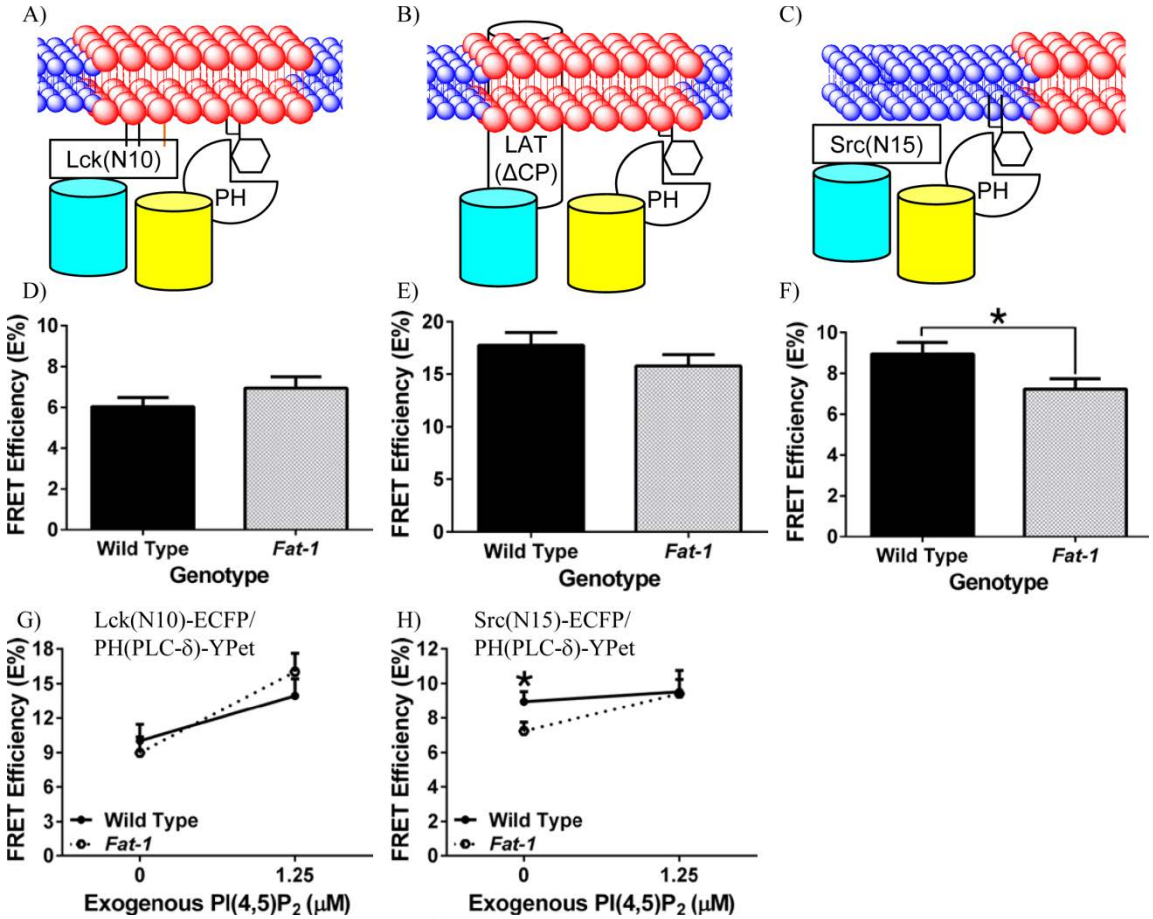

Figure 3.4. n-3 PUFA decrease the interaction of fluorescent non-raft and $PI(4,5)P_2$ markers as detected using FRET, and exogenous $PI(4,5)P_2$ can rescue the non-raft population of $PI(4,5)P_2$ in *Fat-1* $CD4^+$ T cells. (A, B, and C) Schematic diagrams of the interaction between neighboring fluorescent probes targeted to the raft or the non-raft membrane fraction of the plasma membrane, and PH(PLC-δ), a $PI(4,5)P_2$ reporter. $CD4^+$ T cells were incubated with lentivirus containing (D) Lck(N10)/PH(PLC-δ), (E) LAT(ΔCP)/ PH(PLC-δ), or (F) Src(N15)/PH(PLC-δ) before FRET by acceptor photobleaching (n = 4 per genotype). FRET efficiency (E%) was determined as described in Figure 1 (*$P < 0.05$ between genotypes). *Fat-1* $CD4^+$ T cells were isolated and transduced with (G) Lck-ECFP and PH-YPet; or (H) Src-ECFP and PH-YPet for 48 h before they were incubated with 1.25 μM $PI(4,5)P_2$ or PBS (0 μM) for one hr. Cells were analyzed as described in Figure 3.3. A two-tailed t-test was used to compare FRET efficiencies within specific concentrations (* $P < 0.05$ at specific concentrations of $PI(4,5)P_2$).

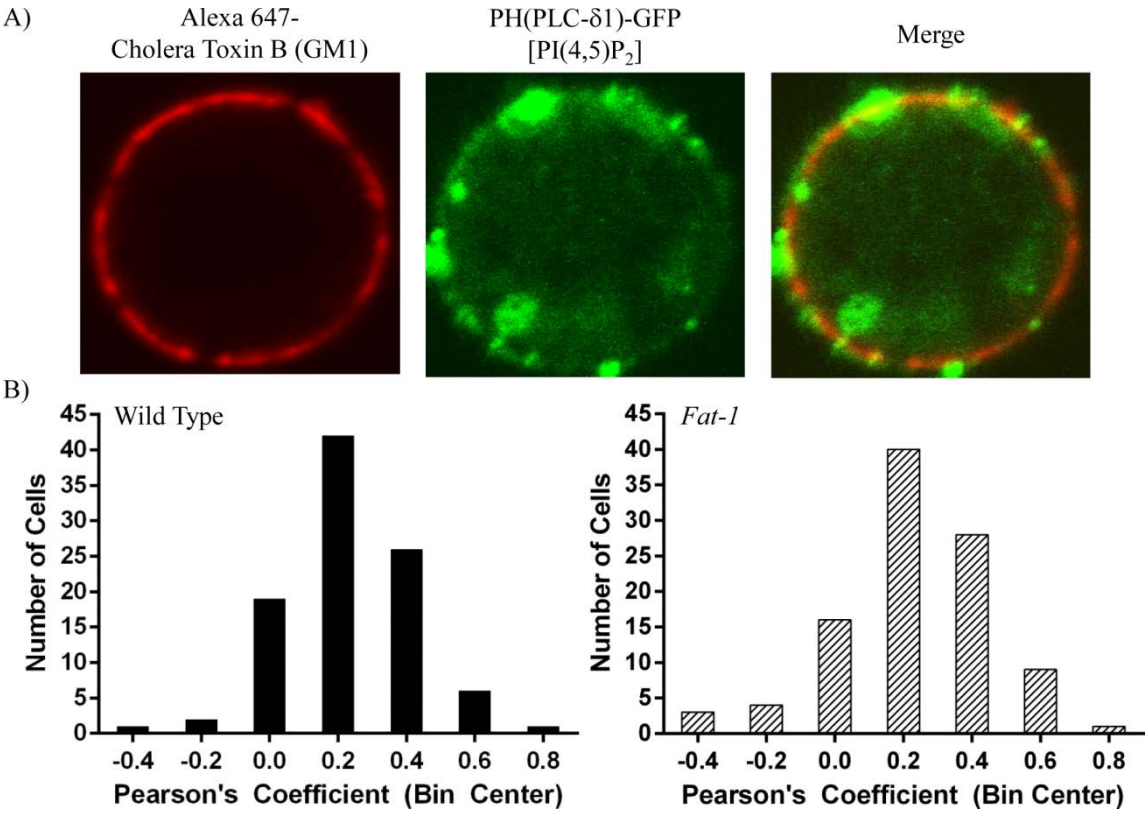

Figure 3.5 – Colocalization between the lipid raft marker GM1 and PI(4,5)P_2 is not altered in the presence of n-3 PUFA. Splenic $CD4^+$ T cells were positively selected and incubated with lentivirus containing pLenti-PH(PLC-δ)-GFP for 48 h (n = 4 per genotype). Cells were collected, washed, labeled with Alexa 647 Cholera Toxin B (final concentration 10 μg/mL) and crosslinked with anti-Cholera Toxin B [Vybrant Lipid Raft Labeling Kit (Life Technologies)] according to manufacturer's protocol (**APPENDIX L**). (**A**) Cells were imaged using a Zeiss 510 META confocal microscope. (**B**) The plasma membrane region of the cell was drawn and Pearson's coefficient was determined using NIS-Element (Nikon).

We have previously demonstrated that the incorporation of n-3 PUFA into the plasma membrane of $CD4^+$ T cells decreases the amount of overall PI(4,5)P_2 by 50%, resulting in suppressed actin remodeling upon anti-CD3/anti-CD28 stimulation (177). The suppression of PI(4,5)P_2-dependent actin remodeling, however, was recovered by incubation with exogenous PI(4,5)P_2. However, recent studies have suggested that different pools of PI(4,5)P_2 are responsible for various signaling pathways, such as calcium signaling and actin remodeling (42-44). Therefore, we hypothesized that exogenous incubation of PI(4,5)P_2 with $CD4^+$ T cells enriched in n-3 PUFA would

rescue the non-raft pool of PI(4,5)P_2. Using the lipid raft marker Lck(N10) and PI(4,5)P_2 marker PH(PLC-δ), the FRET efficiency before and after incubation with exogenous PI(4,5)P_2 did not differ between wild type and $CD4^+$ T cells enriched with n-3 PUFA (**Figure 3.4G**). In contrast, using the non-raft marker Src(N15) and PH(PLC-δ), the FRET efficiency of $CD4^+$ T cells enriched with n-3 PUFA increased to the level of wild type $CD4^+$ T cells (**Figure 3.4H**). These data indicate that exogenous PI(4,5)P_2 increases the non-raft pool of PI(4,5)P_2 in $CD4^+$ T cells enriched with n-3 PUFA to a level comparable to wild type cells.

3.3.3 Exogenous PI(4,5)P_2 rescues the suppression of T cell proliferation in $CD4^+$ T cells enriched with n-3 PUFA

We have previously shown that $CD4^+$ T cells enriched with n-3 PUFA exhibit suppressed T cell proliferation following anti-CD3/anti-CD28 stimulation (78, 94). Since exogenous PI(4,5)P_2 restores the non-raft pool of PI(4,5)P_2 (**Figure 3.4H**), and can rescue PI(4,5)P_2-dependent actin remodeling (177), we hypothesized that exogenous PI(4,5)P_2 would also reverse the suppressed proliferative phenotype in $CD4^+$ T cells enriched with n-3 PUFA. Using carboxyfluorescein succinimidyl ester (CFSE) fluorescence as a marker of T cell proliferation, and propidium iodide (PI) fluorescence as a marker of cell viability, cell division was determined based on the number of distinct CFSE fluorescence intensity peaks (**Figure 3.6).** The proliferation index of each population was determined using the generational data, providing an indicator of the proliferation capacity of the population. $CD4^+$ T cells enriched with n-3 PUFA exhibited a suppressed (~20% lower) T cell proliferative capacity compared to wild type

(**Figure 3.6D**). Importantly, the n-3 PUFA suppressed phenotype was rescued to wild type levels upon pre-treatment with exogenous PI(4,5)P_2. These findings demonstrate that i) incorporation of n-3 PUFA into the plasma membrane of $CD4^+$ T cells not only alters the spatial organization of PI(4,5)P_2 by decreasing the non-raft pool of PI(4,5)P_2, but also suppresses T cell proliferation; and ii) replenishment of the non-raft pool of PI(4,5)P_2 (**Figure 3.4**) and rescue of PI(4,5)P_2-dependent actin remodeling in $CD4^+$ T cells enriched with n-3 PUFA (177), restore full proliferation capacity.

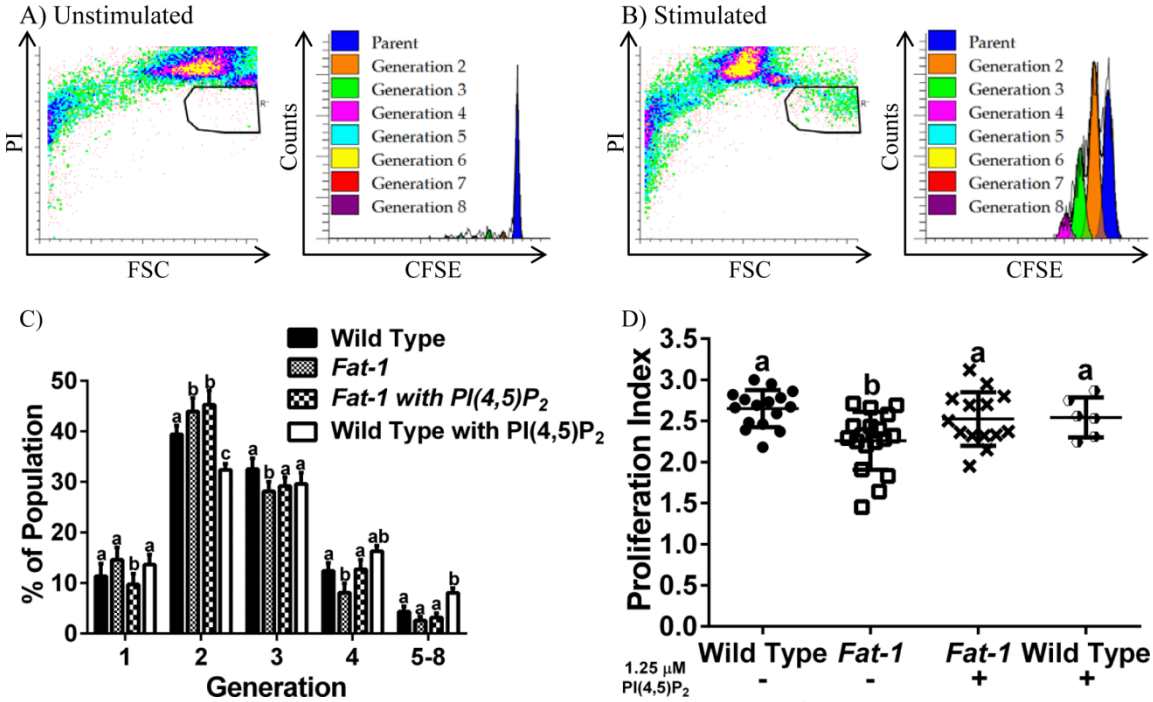

Figure 3.6. Exogenous PI(4,5)P_2 rescues the n-3 PUFA-induced suppression of T cell proliferation. Representative scatterplots and CFSE profiles of (A) unstimulated, and (B) anti-CD3/anti-CD28 stimulated $CD4^+$ T cell cultures. Splenic $CD4^+$ T cells were stained with CFSE, then cultured (n = 4 per genotype) either in unstimulated or stimulated conditions for 72 h in triplicate. Cells were collected and gated by propidium iodide staining to exclude dead cells. (C) Cell proliferation was analyzed using the Proliferation Wizard in ModFitLT3.2 to determine the percent population at each generation. Different letters represent statistically significant differences between the groups ($P < 0.05$). (D) Proliferation Index, the amount of total cells divided by theoretical parental population, was calculated using ModFitLT 3.2 (192).

3.3.4 CD4$^+$ T cells isolated from mice fed a 4% DHA triglyceride-enriched diet exhibit decreased raft PI(4,5)P_2, non-raft PI(4,5)P_2, and lymphoproliferation that was rescued by exogenous PI(4,5)P_2

In order to determine whether dietary n-3 PUFA such as DHA could recapitulate the phenotypes seen in *Fat-1* CD4$^+$ T cells, C56BL/6 mice were fed 5% corn oil (CO)-enriched (control), 0.95% DHA-triglyceride-enriched, or 4% DHA-triglyceride-enriched diet. Using the raft and non-raft probes of Lck(N10) and Src(N15), respectively, in conjunction with the PI(4,5)P_2 probe PH(PLC-δ), we detected decreased FRET efficiencies between CD4$^+$ T cells isolated from mice fed the control diet, and 4% DHA-triglyceride-enriched diet using the combination of Lck(N10)/PH(PLC-δ) and Src(N15)/PH(PLC-δ), suggesting that both the lipid raft and non-raft pools of PI(4,5)P_2 are perturbed (**Figure 3.7C & D**). Decreased PI(4,5)P_2 was also correlated with suppressed lymphoproliferation, as seen in *Fat-1* CD4$^+$ T cells (**Figure 3.7E)**. Importantly, incubating CD4$^+$ T cells with exogenous PI(4,5)P_2 reversed the DHA-mediated suppression of lymphoproliferation caused by decreased PI(4,5)P_2, demonstrating that decreased status of PI(4,5)P_2 directly suppresses lymphoproliferation.

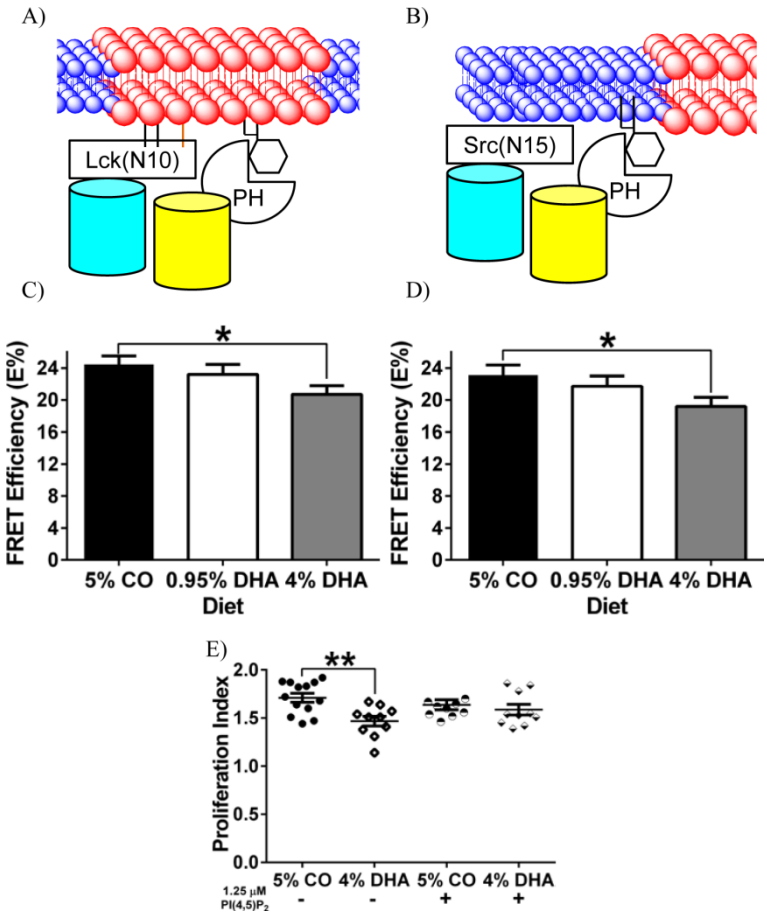

Figure 3.7. DHA decreases the interaction of fluorescent raft and non-raft probes with PI(4,5)P_2 marker detected using FRET, resulting in suppressed lymphproliferation that can be rescued by exogenous PI(4,5)P_2 in $CD4^+$ T cells. (A and B) Schematic diagrams of the interaction between neighboring fluorescent probes targeted to the raft or the non-raft membrane fraction of the plasma membrane, and PH(PLC-δ), a PI(4,5)P_2 reporter. $CD4^+$ T cells were incubated with lentivirus containing (C) Lck(N10)/PH(PLC-δ), or (D) Src(N15)/PH(PLC-δ) before FRET by acceptor photobleaching (n = 4 per genotype). FRET efficiency (E%) was determined as described in Figure 3.3 (*$P < 0.05$ between genotypes). (E) Splenic $CD4^+$ T cells were stained with CFSE, then cultured (n = 6 per diet) either in unstimulated or stimulated conditions for 72 h in triplicate. Cells were collected and gated by propidium iodide staining to exclude dead cells. Proliferation Index was calculated using ModFitLT 3.2 (192). **$P < 0.01$ as determined by one-way ANOVA followed by post-hoc test.

3.4 Discussion

The use of fish oils, containing bioactive EPA and DHA, for their anti-inflammatory properties is growing exponentially. It is, therefore, important to elucidate the mechanisms by which n-3 PUFA exert their anti-inflammatory properties. Previous studies have examined the extrinsic effects of n-3 PUFA (i.e. generation of novel

metabolites to act upon receptors and enzymes) (118, 119, 193, 194), as well as the effects of n-3 PUFA downstream of TCR engagement with MHCII antigen presentation (78, 94, 136, 177). Since lipid raft mesodomains in the plasma membrane play a critical role in initiating T cell activation (67, 71), and n-3 PUFA are incorporated into the plasma membrane, we hypothesized that n-3 PUFA suppress T cell activation by altering i) the biophysical properties of lipid raft mesodomains; and ii) the spatial organization of $PI(4,5)P_2$ relative to lipid raft and non-raft mesodomains. By using lipid raft and non-raft markers in a series of FRET experiments, we demonstrate for the first time in primary $CD4^+$ T cells that n-3 PUFA alter the topology of the lipid raft mesodomains. The increase in FRET efficiency between the lipid raft markers observed in $CD4^+$ T cells enriched in n-3 PUFA can be interpreted either as an increase in the size of the lipid raft mesodomains, or an increase in the stability of the lipid raft mesodomains. In both cases, the enhancement of lipid raft mesodomains would be expected to decrease the average diffusion of the lipid raft marker, since it has been shown that an association with lipid raft mesodomains retards the diffusion rate of these markers (195, 196). This is consistent with the FRAP data reported in **Figure 3.3**. From an immunological perspective, this perturbation in the plasma membrane biophysics results in a suppression of T cell proliferation [**Figure 3.6**; (94, 141)]. Interestingly, other forms of perturbation to the plasma membrane topology can change the threshold for T cell activation. For example, incubation of Jurkat T cells with 7-ketocholesterol decreased the membrane order and resulted in a suppression of downstream T cell signaling (71). In addition, some human autoimmune diseases can be attributed to changes in the lipids

associated with lipid raft mesodomains (197). For example, $CD4^+$ T cells isolated from patients with systemic lupus erythematosus exhibit elevated levels of glycosphingolipids associated with lipid rafts, and this alteration was correlated with hyperaction of T cells. By correcting glycosphingolipid metabolism in $CD4^+$ T cells isolated from systemic lupus erythematosus patients, normal T cell function was restored, demonstrating the direct relationship between lipid raft mesodomains and T cell function (76, 198). In fact, the lipid order of the plasma membrane can influence the differentiation of naïve $CD4^+$ T cells into effector $CD4^+$ T cells, highlighting the importance of lipid raft mesodomains in dictating the function of $CD4^+$ T cells (73, 75, 77).

Since the organization of lipid raft mesodomains is closely linked with the actin cytoskeleton, and the actin cytoskeleton is regulated by $PI(4,5)P_2$ (23), we hypothesized that the incorporation of n-3 PUFA into the plasma membrane of $CD4^+$ T cells alters the spatial organization of $PI(4,5)P_2$. Indeed, we have previously shown that n-3 PUFA in $CD4^+$ T cells reduced the amount of total $PI(4,5)P_2$ by 50%, and this reduction was correlated with a suppression of $PI(4,5)P_2$-dependent actin remodeling necessary for proper T cell activation (177). Surprisingly, the increase in FRET efficiency between lipid raft markers in the presence of n-3 PUFA did not correlate with a change in the lipid raft pool of $PI(4,5)P_2$; rather, the non-raft pool of $PI(4,5)P_2$ was decreased (**Figure 3.4**). In the context of $PI(4,5)P_2$-dependent actin remodeling, this may not be surprising, as this remodeling has been shown in other cell types to be regulated by a specific PIP5K isoform (PIP5Kγ) which is capable of synthesizing the non-raft pool of $PI(4,5)P_2$ (42-44). Furthermore, perturbations in the raft and non-raft pools of $PI(4,5)P_2$ using

targeted phosphatase in Jurkat T cells produced different actin-dependent phenotypes (39). These studies demonstrate the compartmentalization of $PI(4,5)P_2$ in the plasma membrane (raft and non-raft), and the importance of non-raft $PI(4,5)P_2$ in regulating actin remodeling. It is also noteworthy, that incubation with exogenous $PI(4,5)P_2$ increased $PI(4,5)P_2$ mass back to wild type levels (**Figure 3.4**), which is consistent with the rescue of $PI(4,5)P_2$-dependent actin remodeling upon stimulation (177).

We have previously demonstrated that incorporation of n-3 PUFA into the T cell plasma membrane suppresses lymphoproliferation upon stimulation (94, 141). Thus, we hypothesized that the rescue of the non-raft pool of $PI(4,5)P_2$ would also reverse the suppression of T cell proliferation, linking the biochemistry and cellular biology of the T cell membrane with a highly relevant immunological end point. Using the CFSE assay to measure T cell proliferation, we demonstrated that rescue of the non-raft pool of $PI(4,5)P_2$ in $CD4^+$ T cells enriched with n-3 PUFA also restored T cell proliferation back to wild type levels.

It is interesting to note that in our dietary model, only $CD4^+$ T cells isolated from animals fed a 4% DHA-triglyceride-enriched diet exhibited decreased $PI(4,5)P_2$ in both lipid raft and non-raft pools (**Figure 3.7**). This may highlight the difference in n-3 PUFA dose between the genetic *Fat-1* model, and the dietary 4% DHA model; indeed, examining the fatty acid profiles of the two models highlight the fact that $CD4^+$ T cells isolated from animals fed a 4% DHA-triglyceride-enriched diet exhibited 3 – 4 times more incorporation of n-3 PUFA, compared to *Fat-1* $CD4^+$ T cells (**Figure 2.1**). These data also suggest that there is a dose-dependent dietary intake of n-3 PUFA that is

required for physiological phenotype, as $CD4^+$ T cells isolated from 0.95% DHA-triglyceride-enriched diet exhibited no change in $PI(4,5)P_2$. Therefore, more experiments involving dose of n-3 PUFA will be required to clarify the dose-dependent response of $CD4^+$ T cells.

To put the FRET efficiencies into biological perspective, previous studies demonstrated that a 3 to 4% change in FRET efficiency correlated to a significant decrease in Lck phosphorylation, and suppression of subsequent T cell activation (199). Thus the changes demonstrated in this study have biological relevance.

In conclusion, this study highlights how n-3 PUFA, found in dietary fish oil, directly affect the lipid-lipid interactions fundamental to the formation of lipid raft mesodomains in the plasma membrane, thereby perturbing downstream signals required for T cell proliferation (**Figure 3.8**). Thus, our data further support the concept that n-3 PUFA can be used rationally for the treatment of chronic inflammatory diseases in which T cells are inappropriately activated.

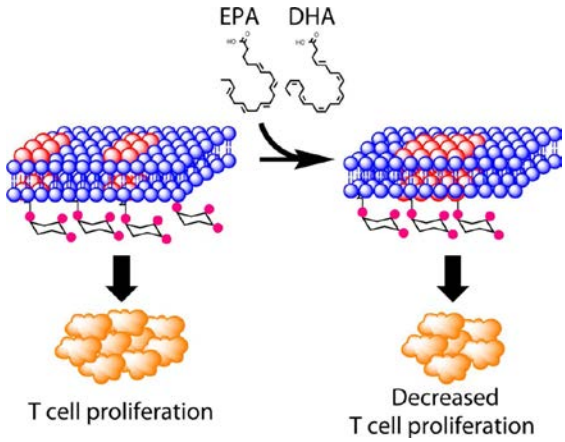

Figure 3.8 – Incorporation of n-3 PUFA such as EPA and DHA into the plasma membrane alters its topology by increasing the size and/or stability of lipid raft mesodomains (represented by the red headgroup) and by decreasing the non-raft pool of $PI(4,5)P_2$. Because the incorporation of n-3 PUFA affects proximal signaling events upon ligation of the TCR with antigen presented in the context of the MHCII, this study demonstrates the intrinsic membrane effect of bioactive n-3 PUFA and their potential therapeutic use in decreasing T cell proliferation upon activation.

CHAPTER IV

n-3 POLYUNSATURATED FATTY ACIDS DO NOT ALTER THE POST-TRANSLATIONAL LIPIDATION STATUS OF $CD4^+$ T CELL

4.1 Introduction

To explore an alternative hypothesis regarding the effects of n-3 PUFA on T cell activation, the post-translational modification of signaling proteins was examined. Post-translational modification of proteins by lipids is an important regulator of protein function due to the ability of the lipids to change the localization, the activation, and/or the binding partner of the specific protein (200). Three prevalent lipidation processes occur in eukaryotes, and they include fatty acids, isoprenoids, and glycosylphosphatidylinositols. We therefore opted to focus on the post-translational modifications of proteins by fatty acids since many of the signaling proteins involved in T cell activation are post-translationally modified by fatty acids (i.e. LCK, LAT, FYN) (200). In addition, EPA and DHA have been shown to alter the fatty acyl composition of cells (68), which could lead to a perturbation in the post-translational modification of signaling proteins, and/or the localization of these modified proteins.

In N-myristoylation, a myristate group (14 carbon fatty acid chain) is irreversibly added to the N-terminal glycine residue via an amide linkage. This reaction is catalyzed by N-myristoyltransferase (NMT) that recognizes the consensus sequence M**G**XXXS/T where the underlined glycine is the site of myristoylation, and the first methionine is commonly removed (201). To date, two N-myristoyltransferases have been identified in humans, NMT1 and NMT2. In contrast, S-acylation, specifically palmitoylation,

commonly involves the reversible attachment of a palmitic acid (16 carbon fatty acid chain) to the cysteine residue via a thioester bond, although other palmitoylation modifications do occur (i.e. N-palmitoylation, O-palmitoylation) (201). Unlike N-myristoylation, there are no known consensus sequences for the site of palmitoylation; moreover, there are more than 20 palmitoyl acyltransferases identified in mammalian genome (202). By adding fatty acids to a protein, the modification provides a hydrophobic interface to allow for membrane association. For example, palmitoylation can be used to regulate the association between a protein and the raft phase for integral raft proteins (203).

Not surprisingly, receptors and kinases involved in T cell activation are post-translationally modified. CD4, the marker of $CD4^+$ T cells, is palmitoylated at cysteines 394 and 397 (204). LCK is myristoylated at glycine 2 and palmitoylated at cysteine 3 and cysteine 5; all three sites are required for stable membrane insertion and association (200). Similarly, LAT is palmitoylated at cysteines 26 and 29, and these palmitoylation events are essential for optimal localization of LAT to detergent-resistant membranes, and subsequent recruitment and activation of the signalsome (205). Finally, FYN, a Src family kinase that has been implicated to play a role in T cell activation, is also myristoylated at glycine 2 and palmitoylated at cysteines 3 and 6 (206). Post-translational modifications of LCK, LAT, and FYN are necessary for the localization to lipid rafts and downstream function for T cell activation (200). Therefore, an alternative hypothesis, that n-3 PUFA alter the post-translational modification of signaling proteins such as LCK, LAT, and FYN in $CD4^+$ T cells, will be pursued.

4.2 Materials and methods

4.2.1 CD4$^+$ T cell isolation

All animal procedures were approved by the Institutional Animal Care and Use Committee at Texas A&M University and followed the U.S. Public Health Service guidelines. Wild type and *Fat-1 1* transgenic mice on a C57BL/6 background, generously provided by Dr. Jing X. Kang (Department of Medicine, Harvard University), were fed a 10% safflower diet *ad libitum* in a 12:12 light:dark cycle [**APPENDIX A**; (94, 136, 177)]. CD4$^+$ T cells were enriched by removing the spleen aseptically and labeling with magnetic CD4 (L3T4) microbeads according to manufacturer's protocol (**APPENDIX B**; Miltenyi Biotec, Auburn, CA). CD4$^+$ T cells were cultured in complete RPMI media, supplemented with 20 ng/mL rIL-2 (eBioscience, San Diego, CA). 15 x 10^6 cells in 4 mL were seeded in 35 mm plate and incubated for 1 hr before loading with 15-azidopentadecanoic acid (**APPENDIX N**).

4.2.2 Treatment of CD4$^+$ T cell with 15-azidopentadecanoic acid

15-azidopentadecanoic acid (Life Technologies, Grand Island, NY) dissolved in DMSO (50 mM) was added to each cell culture to a final concentration of 50 µM, and incubated for 24 h. Cells were then collected, washed, and homogenized in homogenization buffer composed of 50 mM Tris-HCl, pH = 8, 1% SDS (w/v), 100 µM of sodium orthovanadate, 1X sigma protease cocktail, and 250 units of benzonase nuclease. Protein lysates from two cell cultures were pooled and concentrated using centrifugal concentrator (3 kDa cut-off, Millipore, Billerica, MA). Protein concentration

was then determined using the bicinchoninic acid assay (Thermo Scientific, Rockford, IL) and protein concentration was adjusted to 4 µg/µL for Click chemistry.

4.2.3 Click chemistry

Click chemistry was performed using the Click-iT kit (Life Technologies) according to the manufacturer's protocol. Briefly, 200 µg of cellular protein was combined with 100 µL of Click-iT reaction buffer containing PEG4 carboxamide-propargyl biotin (Life Technologies), 10 µL of ddH_2O, vortexed for 5 sec, before addition of $CuSO_4$ and component C. The reaction was vortexed for 5 sec, and incubated for 3 min at 23 °C for 3 min. Finally, component D was added to the reaction and incubated for 30 min at 23 °C for 30 min, protected from light. After the reaction, protein was precipitated according to the manufacturer's protocol. Briefly, 400 µL of MeOH was added to the reaction first, followed by 150 µL of $CHCl_3$ and 400 µL of ddH_2O. Phase separation was conducted by centrifuging the mixture for 5 min at 18,000 g. Most of the upper aqueous phase was removed, retaining the interface and lower phase. Protein was pelleted by an addition of 450 µL of MeOH, followed by centrifugation for 5 min at 18,000 g. The supernatant was removed, and the protein pellet was washed with an additional 450 µL of MeOH. Protein was pelleted again with centrifugation for 5 min at 18,000 g, followed by the removal of the supernatant. The pellet was air dried for 10 min before it was resuspended in a homogenization buffer containing 50 mM Tris-HCl, pH = 7.5, 15 mM EGTA, pH = 7.5, 100 mM NaCl, 0.1% Triton X-100, 500 µM of sodium orthovanadate, 1X Sigma protease cocktail, and 10

mM β-mercaptoethanol. The protein concentration was determined by the Commassie Plus Protein assay (Pierce, Rockford, IL).

4.2.4 Immunoprecipitation using protein G Dynabeads

100 µg of protein was combined with rabbit polyclonal IgG anti-Lck (Millipore) for 90 min at 4 °C before addition of Protein G Dynabeads for overnight incubation at 4 °C. The next day, the protein-antibody complex was collected using DynaMagnet, and boiled in the presence of 2X pyronin. Samples were then loaded on 4-20% Tris-glycine polyacrylamide precast gel (Invitrogen) and separated for 2.5 h at 4 ºC. Proteins were then transferred onto polyvinylidene fluoride membranes at 400 mA for 90 min. Membranes were blocked at room temperature for 1 h in 4% nonfat dry milk. Primary antibody against biotin (mouse anti-biotin, Jackson ImmunoResearch, West Grove, PA) was incubated overnight at 4 ºC. Membranes were subsequently washed and incubated with secondary horseradish peroxidase conjugated rabbit anti-mouse IgG (KPL) and developed using Pierce SuperSignal West Femto maximum sensitivity substrate. Membranes were then scanned using Fluor-S Max MultiImager system (BioRad, Hercules, CA) and analyzed using QuantityOne (BioRad).

4.3 Results

4.3.1 Incorporation of azido-palmitic acid is superior to the alkynyl-palmitic acid probe in Jurkat T cells

In order to probe the post-tranlsational lipidation of signaling proteins in $CD4^+$ T cells, we employed the highly sensitive Click chemistry using labeled palmitic acid and biotin (201, 207). Click chemistry involves the Huisgen cycloaddition of an azide and

an alkyne in the presence of copper as a catalyst at room temperature (208), thus we determined whether azido- or alkynyl-palmitic acid was better for detecting the palmitoylation of proteins in $CD4^+$ T cells. By using Jurkat T cells as a proxy, we determined that incubating T cells with azido-palmitic acid yielded better signal when detecting palmitoylation in proteins using immunoblotting (**Figure 4.1**). For subsequent experiments, azido-palmitic acid was used to detect palmitoylation in $CD4^+$ T cells.

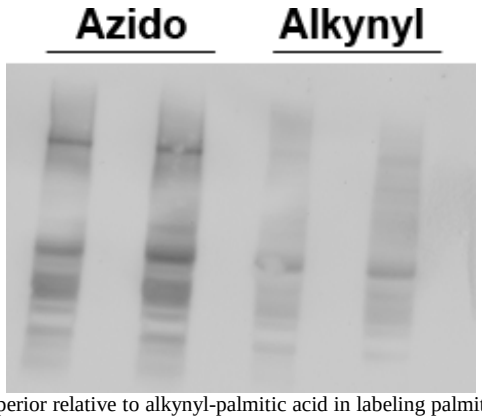

Figure 4.1. Azido-palmitic acid is superior relative to alkynyl-palmitic acid in labeling palmitoylated proteins in Jurkat T cells. 1 x 10^7 Jurkat T cells were seeded in a 35 mm culture dish with 3 mL of RPMI media supplemented with 2% FBS overnight at 37 ºC, 5% CO_2. Cells were treated as indicated and 100 µg of protein lysate was used for Click chemistry. Subsequently, 60 µg of protein lysate was used for Western blotting after protein precipitation subsequent to the chemistry reaction and detected by immunoblotting.

4.3.2 Global palmitoylation is not affected by n-3 PUFA in unstimulated primary $CD4^+$ T cells

$CD4^+$ T cells were isolated from wildtype and *Fat-1* mice, and subsequently incubated the azido-palmitic acid, followed by Click chemistry. Contrary to previous results suggesting that n-3 PUFA altered the palmitoylation of signaling proteins, global palmitoylation status was not affected in *Fat-1* $CD4^+$ T cells (**Figure 4.2A**). To examine whether palmitoylation was affected in specific proteins, we chose to perform immunoprecipitation of LCK in order to isolate and detect its specific palmitoylation.

Similar to our observation for global palmitoylation, n-3 PUFA did not affect the palmitoylation of LCK in $CD4^+$ T cells (**Figure 4.2B**).

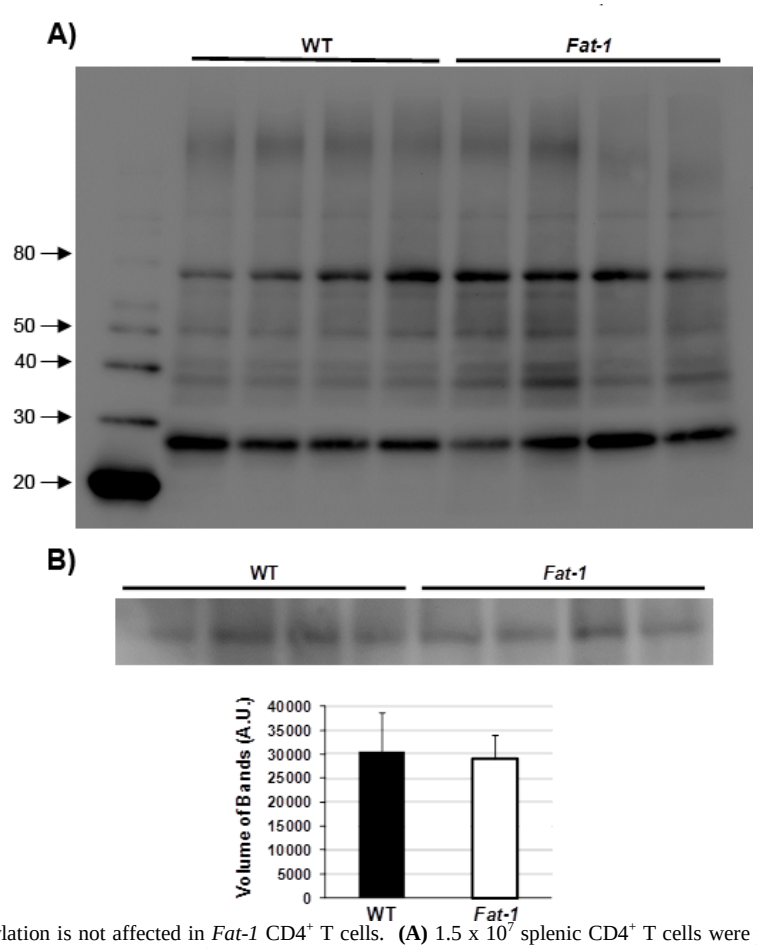

Figure 4.2. Palmitoylation is not affected in *Fat-1* $CD4^+$ T cells. **(A)** 1.5 x 10^7 splenic $CD4^+$ T cells were positively selected and seeded in a 35 mm culture dish with 4 mL of RPMI media supplemented with 2% FBS and rIL-2 overnight overnight. Cells were treated with 50 μM of azido-palmitic acid for 24 h and 2 wells were pooled to create 1 sample. Subsequently, 100 μg of protein lysate was used for Click chemistry and palmitoylation was detected by immunoblotting. Numbers on the side represent molecular weights of the marker. **(B)** Palmitoylation of Lck is not affected in *Fat-1* $CD4^+$ T cells. Cells were selected and processed as in **(A)**, and was subsequently immunoprecipitated (IP) using polyclonal rabbit IgG anti-Lck. Palmitoylated Lck was detected by immunoblotting, and quantified.

4.4 Discussion

Contrary to previously published reports, which observed that palmitoylation of signaling proteins in $CD4^+$ T cells were decreased in the presence of n-3 PUFA such as

EPA (209, 210), our data indicate that palmitoylation of LCK was not impacted by the presence of n-3 PUFA. There are two possibilities for these apparent differences. First, different methods of palmitoylation detection were used in each experiment. In the previously published reports, palmitoylation was detected by radiolabeled 16-[^{125}I]iodohexanoic acid, compared to the use of azido-palmitic acid. A second possibility is that the cell type was different, immortalized human Jurkat T cells versus primary mouse $CD4^+$ T cells. Because malignant transformed Jurkat T cells are continuously growing, it may be possible that effect of n-3 PUFA on palmitoylation is only observed under rapid post-translational turnover when $CD4^+$ T cells are activated.

If palmitoylation of signaling proteins is not altered by the presence of n-3 PUFA, then the displacement of signaling proteins at the IS is not due to inhibition of enzymatic palmitoyltransferase activity, but rather, due to the unique biophysical properties of n-3 PUFA that allow these fatty acids to alter the size and/or stability of mesoscale lipid rafts, thus altering the localization of proteins at the plasma membrane. It would be interesting to test whether the localization of palmitoylated proteins at the IS is altered by n-3 PUFA. It could be possible that even if the signaling proteins are palmitoylated, the localization of these proteins are altered at the plasma membrane.

To date, there are no structural data on palmitoyl acyltransferases, and substrate specificity for these enzymes has focused on their target proteins. It would be interesting to examine whether n-3 PUFA can bind to the palmitic acid binding pocket of these acyltransferases and act as a substrate inhibitor, or whether these palmitoyl acyltransferases are not affected enzymatically by n-3 PUFA. Based on our data, one

would speculate that n-3 PUFA do not affect the enzyme activity of these palmitoyl acyltransferases.

CHAPTER V

SUMMARY AND CONCLUSIONS

5.1 Summary

Epidemiological studies have suggested that high intake of EPA and DHA derived from diets rich in fish is correlated with decreased incidence of chronic inflammatory diseases (211, 212). This is especially important given the fact that chronic inflammation is associated with a plethora of diseases, such as cardiovascular diseases (213, 214), ulcerative colitis (54, 123, 211, 215), rheumatoid arthritis (216, 217), neurological disorders (218, 219), metabolic disorders (220, 221), and cancer (222-224). It has only been recently appreciated that obesity can be considered as low-grade chronic inflammation that drives changes in not only adipose tissues, but immune cells as well, leading to systemic inflammation (225-228). This is especially relevant since the Centers for Disease Control and Prevention reported in 2013 that 69% of the U.S. population is overweight or obese (229). One could only imagine the burden this health risk will put on the health care system in the United States. In the absence of obesity, there is a balance between adipocytes and the various immune cells such as M2-like macrophages, T_H2 and T_{reg} cells, and eosinophils, contributing to an anti-inflammatory environment. With the development of obesity, however, there is a switch in cell types associated with the adipose tissue; there is an increase in pro-inflammatory immune cells such as M1-like macrophages, $CD4^+$ T_H1 cells, $CD8^+$ effector T cells, and mast cells. Concomitantly, there is a decrease in immune cells such as eosinophils, T_H2 cells, and anti-inflammatory T_{reg} cells. Pro-inflammatory adipokines such as MCP-1 and LTB_4 are

released, along with the pro-inflammatory cytokines such as TNF-α and IL-1β, creating a pathophysiological, inflammatory environment (230). Thus, research on innocuous bioactive compounds such as EPA and DHA found in fish oil is urgently needed to combat the inflammation epidemic. More critically, examining the biochemical and biophysical mechanisms by which n-3 PUFA such as EPA and DHA exert their beneficial, anti-inflammatory effects can potentially lead to the identification of common mechanisms by which signaling cascades can be modulated at the plasma membrane level.

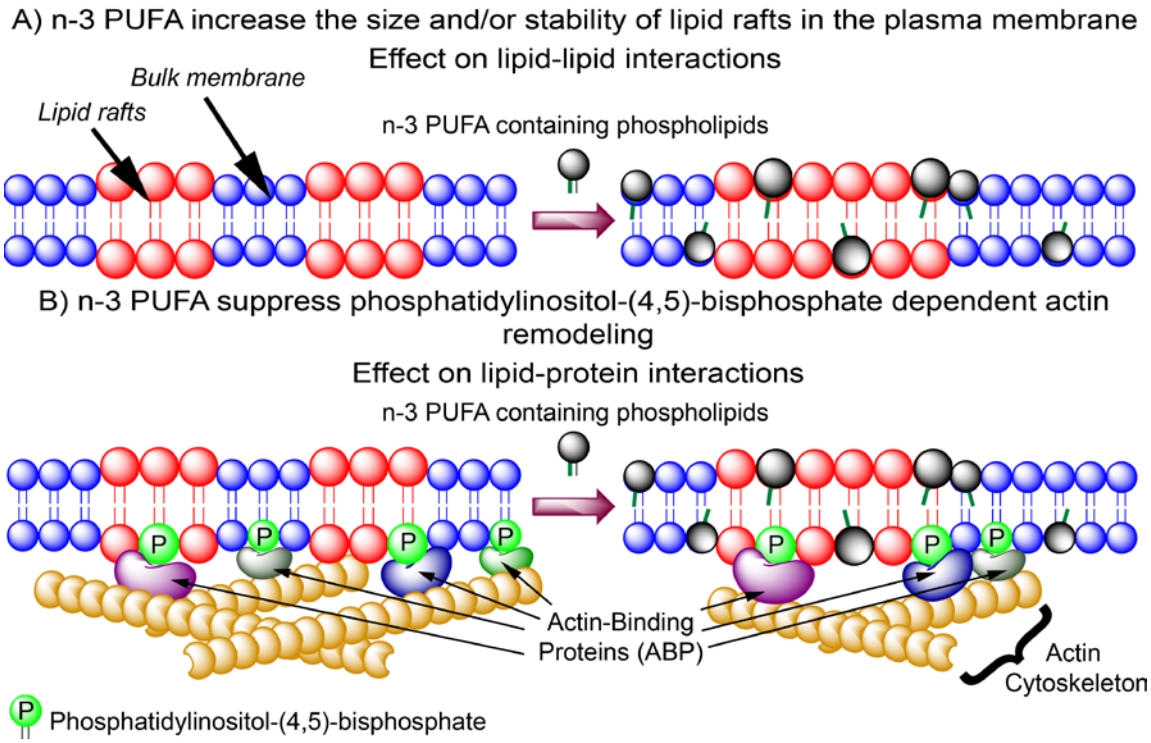

Figure 5.1. Effects of n-3 PUFA on lipid-lipid interactions and lipid-protein interactions. Data from our lab, and this work, suggest that upon incorporation of n-3 PUFA into the plasma membrane increase the size and/or stability of the mesoscale lipid rafts. In addition, n-3 PUFA also decrease the level of PI(4,5)P2 in the plasma membrane, resulting in reduced actin cytoskeleton and the dysregulation of the mesoscale lipid rafts. Physiologically, this translated into decreased lymphoproliferation upon activation.

As highlighted in the obesity example, inflammation is orchestrated by many cell types (54, 72, 130). The focus of this body of work is on the $CD4^+$ T cell population due to its ability to differentiate into additional T cell subsets that are involved in both pro- and anti-inflammatory responses. Previous studies have shed light on how n-3 PUFA such as EPA and DHA exert their anti-inflammatory effects, but the phenotypes observed were associated with later events during the inflammation process (68, 78, 94, 133-147, 167, 231). To identify the nexus where n-3 PUFA exert their effects, the studie reported herein examined the events before and proximal (within minutes) after T cell activation. Data presented herein clearly demonstrate that the incorporation of n-3 PUFA into the plasma membrane increased the interaction between lipid raft probes, consistent with previous data that n-3 PUFA increase the size of lipid rafts in HeLa cells as measured by clustering analysis of a cholesterol-dependent H-Ras probe (93), and in $CD4^+$ T cells as determined by the generalized polarization value of Laurdan, a lipophilic probe that is sensitive to its lipid environment [**Figure 5.1A**, (94)]. The effects of n-3 PUFA on plasma membrane microdomains may be cell-specific. Although B cells isolated from mice fed a fish oil-enriched diet exhibited a similar increase in membrane order (95), treatment of immortalized Jurkat T cells with EPA or DHA exhibited an opposite trend (67, 232). This may be due to intrinsic differences in the cell types, but also highlights the need to examine each cell specifically, since incorporation of n-3 PUFA into the plasma membrane may have cell-specific effects. Additionally, not all n-3 PUFA are effective at perturbing plasma membrane lipid rafts. Phenotypes are not interchangeable when cells are treated with EPA or DHA (172, 233),

and biophysical studies have demonstrated that EPA and DHA do not disrupt lipid rafts with equal efficiency (91). Adding to the complication, 1-palmitoyl-2-docosahexaenoylphosphatidylethanolamine preferentially segregates into the non-raft plasma membrane, while 1-palmitoyl-2-docosahexaenoylphosphatidylcholine prefers the mesoscale raft domains of the plasma membrane (89), demonstrating that the headgroups of the phospholipids can also shape the mechanism by which these n-3 PUFA modulate plasma membrane properties. Clearly, more biophysical, biochemical, and molecular studies are needed to understand how these n-3 PUFA affect the plasma membrane to modulate downstream signaling and impact physiology.

In addition to altering the biophysical properties of the $CD4^+$ T cell plasma membrane (**Figure 5.1A**), the concentration of $PI(4,5)P_2$ was decreased, and non-raft pool of $PI(4,5)P_2$ was also altered, even before T cell activation commenced. As a result, $PI(4,5)P_2$ metabolism (within minutes) was blunted, and actin remodeling (within 30 minutes) was also suppressed (**Figure 5.1B**). Since actin remodeling was suppressed, the stabilization of lipid rafts necessary for the formation of the IS would also be affected. One possible mechanism by which actin remodeling was suppressed was the failure of WASP to be recruited to the IS. On a physiological level, enrichment of the plasma membrane with n-3 PUFA resulted in suppressed lymphoproliferation, as previously reported (94, 138, 141). Importantly, these defects, including i) altered non-raft pool of $PI(4,5)P_2$; ii) suppressed actin remodeling upon stimulation; and iii) suppressed lymphoproliferation could be rescued by incubation with exogenous

$PI(4,5)P_2$, demonstrating that the modulation of $PI(4,5)P_2$ by n-3 PUFA directly influences T cell biochemistry and function.

In order to recapitulate phenotypes seen in the genetically modified *Fat-1* mouse model, $CD4^+$ T cells were also isolated from mice fed a 4% DHA-triglyceride enriched diet, and parallel experiments were conducted. Phenotypes such as i) decreased basal $PI(4,5)P_2$; ii) altered non-raft pool of $PI(4,5)P_2$; iii) repressed actin remodeling upon stimulation; and iv) suppressed lymphoproliferation, were all consistent with effects seen in the genetic *Fat-1* $CD4^+$ T cells. As mentioned previously, the 4% DHA-triglyceride-enriched diet provides approximately 5% DHA as total energy (kcals). On an energy intake basis, this is within the physiological range achievable though diet (173-175). Although in this body of work, there were no adverse effects related to the intake of DHA at this high level, some concerns have been raised. Since n-3 PUFA exert anti-inflammatory effects, high doses of these bioactive compounds may be, in fact, immune-suppressive. Studies have demonstrated that n-3 PUFA reduced resistance to *Mycobacterium tuberculosis* infection in guinea pigs by altering T cell function (234), and in mice by suppressing macrophage function (235). In addition, dietary fish oil exacerbated an infection model of colitis by altering T cell populations (236), illustrating the need for additional research on not only the mechanisms of how n-3 PUFA exert their anti-inflammatory effects, but also the optimal dose.

The described work is also one of the few examples of linking biochemical mechanisms (i.e., perturbations at the plasma membrane) to cellular consequences (i.e., suppression of lymphoproliferation). Although both biochemical and physiological

studies are important in determining how n-3 PUFA operate on a molecular or physiological level, the work presented in this dissertation connects the molecular mechanisms of n-3 PUFA, to a physiological phenotype. This is important because small changes on the biochemical level can have a profound impact at the physiological level, and this is often underappreciated. For example, incubation of Jurkat T cells with a 2:1 ratio of cholesterol:7-ketocholesterol, which would affect the packing of mesoscale lipid rafts, only changed the generalized polarization of Laurdan by 0.12, yet IL-2 secretion was decreased by 40% (71). Similarly, a 3 to 4% change in FRET efficiency correlated to a significant decrease in Lck phosphorylation, and suppression of subsequent T cell activation (199). These highlight how small biochemical changes can have big physiological impact.

5.2 Future directions

5.2.1 T cell receptor and mechanotransduction

Mechanotransduction is the ability of the cell to sense mechanical force, and transmit the mechanical cue as cellular signaling (237). This process is important for many physiological processes, including the ability to hear (238), and to touch (239). Mechanotransduction is becoming more important, because it has been recently recognized that cells can sense extracellular matrices and distinguish rigidity, density, and topography of the extracellular matrix in order to modulate focal adhesions (240, 241). Cancer cells, however, show abnormal focal adhesions, suggesting a dysregulation in mechanosensory function (242-244). In the context of $CD4^+$ T cell activation, the T cell receptor itself has been recently identified as an anisotropic mechanosensor, where T

cell activation occurred when force is applied in a perpendicular fashion (245). TCR acting as a mechanosensor was further verified by using micromanipulation of T cells bound to artificial antigen presenting cells (246), by imaging the pushing and pulling phases of T cell activation (247), and by using atomic force microscopy (248). One way T cells can sense the mechanical force may be the rigidity of the substrate, as IL-2 secretion is correlated to the elasticity that is presented to the T cell (249). The rigidity of the antigen has also been shown to influence peripheral blood T cell activation and secretion of IL-2, demonstrating the relevance to human health and disease (250). Not surprisingly, the ability to sense the mechanical force is intricately regulated by actin cytoskeleton (251, 252), and mechanosensing by T cell receptors requires actin cytoskeleton, as demonstrated by imaging actin dynamics (247), and by treating cells with blebbistatin, an inhibitor of actin contraction (249).

Fundamental to mechanosensing is the force-from-lipid principle (253, 254), in which mechanosensing transmembrane proteins can sense force applied by the bilayer mismatch of tension, bending, and membrane curvature of the bilayers (255). Since the incorporation of n-3 PUFA into the plasma membrane has been shown to affect the elasticity of the plasma membrane (81, 82), and the present study has demonstrated the effects of n-3 PUFA on the actin cytoskeleton upon T cell activation, one would hypothesize that the incorporation of n-3 PUFA into the plasma membrane of the $CD4^+$ T cells will affect the mechanotransduction of the T cell receptor at the i) lipid-lipid level; and ii) lipid-protein (cytoskeletal) level. In order to test this hypothesis, the cell stiffness can be probed by using atomic force microcopy, as demonstrated previously

with regard to the role of Nck, RhoA, and Src in regulating cytoskeletal dynamics (180, 256). Additionally, by varying the rigidity of the substrate (249), it is possible to determine whether $CD4^+$ T cells enriched with n-3 PUFA require higher force threshold to become activated, as measured by Ca^{2+} and IL-2 secretion. To determine whether the actin cytoskeleton plays a role related to the effect of n-3 PUFA on mechanotransduction, exogenous $PI(4,5)P_2$ can be introduced to see whether rescuing $PI(4,5)P_2$-dependent actin remodeling is effective at also rescuing mechanotransduction.

5.2.2 Effects of n-3 PUFA on the TCR and LAT interaction upon T cell activation

Once a cognate antigen presented in the major histocompatibility class II engages the $CD4^+$ T cell receptor, tyrosine kinases Lck and ZAP70 are activated and subsequently phosphorylate the adaptor protein linker for activation of T cells (LAT), leading to the assembly of the signalsome for downstream signaling. Although segregated clusters of TCR^+ and LAT^+ islands may form before T cell activation, precisely where the LAT^+ protein islands are located is still controversial (257). One proposed model (membrane island model) suggests that while TCR^+ protein islands exist in the bulk membrane as higher-ordered protein structure, LAT^+ protein islands exist in lipid rafts of the plasma membrane. Upon TCR-MHCII engagement, additional TCR^+ protein islands coalesce, and LAT^+ protein islands concatenate with TCR^+ protein islands without mixing. This allows LAT^+ proteins to be phosphorylated to propagate downstream signaling (65). In the alternative model (sub-synaptic vesicles model), LAT is localized to vesicles that come into contact with activated TCR clusters to allow for LAT phosphorylation without LAT transport into the plasma membrane (activation of

LAT in *trans*) (258, 259). In either case, since n-3 PUFA perturb the spatial organization of the plasma membrane (membrane island model), and previous data from this laboratory has shown that n-3 PUFA alter the trafficking of proteins to the plasma membrane [sub-synaptic vesicles model, (260)], one would hypothesize that the incorporation of n-3 PUFA into the plasma membrane of the $CD4^+$ T cells affects the interaction between activated TCR and LAT at the plasma membrane level (membrane island model) or the plasma membrane, sub-synaptic vesicle level (sub-synaptic vesicles model). In order to test this hypothesis, the localization of TCR and LAT at the plasma membrane can be detected using super-resolution microscopy. Super-resolution microscopy can also be used to determine the localization of LAT vesicles, and whether n-3 PUFA affect this population of signaling proteins. In addition, FRET probes for TCR and LAT can be generated and used in order to probe how n-3 PUFA influence the engagement of these two signaling proteins for sustained downstream signaling (7, 260).

5.3 Conclusions

This body of work demonstrates, using both genetic and dietary models, that n-3 PUFA such as DHA can suppress $CD4^+$ T cells, in part, by modulating the biophysical properties of the plasma membrane. n-3 PUFA increase the size of lipid rafts in the plasma membrane, and suppress $CD4^+$ T cell activation by decreasing the basal level and altering the spatial organization of $PI(4,5)P_2$, resulting in perturbations to $PI(4,5)P_2$ metabolism, suppression of actin remodeling, and a decrease in lymphoproliferation upon T cell activation. One potential mechanism by which n-3 PUFA suppress actin remodeling is through the inhibition of WASP recruitment to the IS, which is regulated

by $PI(4,5)P_2$. By adding exogenous $PI(4,5)P_2$ back to $CD4^+$ T cells enriched with n-3 PUFA, phenotypes such as i) decreased $PI(4,5)P_2$; ii) altered $PI(4,5)P_2$ localization; iii) inhibited actin remodeling; and iv) suppressed lymphoproliferation, are reverted back to wild type levels, demonstrating the direct link between the regulation of $PI(4,5)P_2$ and n-3 PUFA.

The alternative hypothesis, that n-3 PUFA suppressed post-translational lipidation of signaling proteins in $CD4^+$ T cells, was also tested, albeit in a preliminary fashion. The data indicate that n-3 PUFA do not affect the post-translational lipidation of one signaling protein, LCK, in $CD4^+$ T cells, suggesting that the effects of n-3 PUFA on $CD4^+$ T cells are exerted at the plasma membrane, by perturbing the size of lipid rafts, and $PI(4,5)P_2$-dependent actin remodeling. The possibility that other central signaling proteins undergo altered post-translational modification in $CD4^+$ T cells enriched with n-3 PUFA remains to be investigated.

REFERENCES

1. Singer SJ, Nicolson GL. The fluid mosaic model of the structure of cell membranes. *Science*. (1972); **175**(4023): 720-31.

2. Fahy E, Subramaniam S, Murphy RC, Nishijima M, Raetz CR, Shimizu T, et al. Update of the LIPID MAPS comprehensive classification system for lipids. *J Lipid Res*. (2009); **50 Suppl**: S9-14.

3. Nicolau DV, Jr., Burrage K, Parton RG, Hancock JF. Identifying optimal lipid raft characteristics required to promote nanoscale protein-protein interactions on the plasma membrane. *Mol Cell Biol*. (2006); **26**(1): 313-23.

4. Zidovetzki R, Levitan I. Use of cyclodextrins to manipulate plasma membrane cholesterol content: evidence, misconceptions and control strategies. *Biochim Biophys Acta*. (2007); **1768**(6): 1311-24.

5. Toulmay A, Prinz WA. Direct imaging reveals stable, micrometer-scale lipid domains that segregate proteins in live cells. *J Cell Biol*. (2013); **202**(1): 35-44.

6. Pike LJ, Han X, Gross RW. Epidermal growth factor receptors are localized to lipid rafts that contain a balance of inner and outer leaflet lipids: a shotgun lipidomics study. *J Biol Chem*. (2005); **280**(29): 26796-804.

7. Turk HF, Barhoumi R, Chapkin RS. Alteration of EGFR spatiotemporal dynamics suppresses signal transduction. *PLoS One*. (2012); **7**(6): e39682.

8. Muppidi JR, Siegel RM. Ligand-independent redistribution of Fas (CD95) into lipid rafts mediates clonotypic T cell death. *Nat Immunol*. (2004); **5**(2): 182-9.

9. Wang L, Yang JK, Kabaleeswaran V, Rice AJ, Cruz AC, Park AY, et al. The Fas-FADD death domain complex structure reveals the basis of DISC assembly and disease mutations. *Nat Struct Mol Biol*. (2010); **17**(11): 1324-9.

10. Frisz JF, Klitzing HA, Lou K, Hutcheon ID, Weber PK, Zimmerberg J, et al. Sphingolipid domains in the plasma membranes of fibroblasts are not enriched with cholesterol. *J Biol Chem*. (2013); **288**(23): 16855-61.

11. Frisz JF, Lou K, Klitzing HA, Hanafin WP, Lizunov V, Wilson RL, et al. Direct chemical evidence for sphingolipid domains in the plasma membranes of fibroblasts. *Proc Natl Acad Sci U S A*. (2013); **110**(8): E613-22.

12. Mizuno H, Abe M, Dedecker P, Makino A, Rocha S, Ohno-Iwashita Y, et al. Fluorescent probes for superresolution imaging of lipid domains on the plasma membrane. *Chemical Science*. (2011); **2**(8): 1548-53.

13. Luna EJ, Hitt AL. Cytoskeleton--plasma membrane interactions. *Science*. (1992); **258**(5084): 955-64.

14. Kusumi A, Fujiwara TK, Chadda R, Xie M, Tsunoyama TA, Kalay Z, et al. Dynamic organizing principles of the plasma membrane that regulate signal transduction: commemorating the fortieth anniversary of Singer and Nicolson's fluid-mosaic model. *Annu Rev Cell Dev Biol*. (2012); **28**: 215-50.

15. Lee GM, Zhang F, Ishihara A, McNeil CL, Jacobson KA. Unconfined lateral diffusion and an estimate of pericellular matrix viscosity revealed by measuring the mobility of gold-tagged lipids. *J Cell Biol*. (1993); **120**(1): 25-35.

16. Swaisgood M, Schindler M. Lateral diffusion of lectin receptors in fibroblast membranes as a function of cell shape. *Exp Cell Res*. (1989); **180**(2): 515-28.

17. Ladha S, Mackie AR, Harvey LJ, Clark DC, Lea EJ, Brullemans M, et al. Lateral diffusion in planar lipid bilayers: a fluorescence recovery after photobleaching investigation of its modulation by lipid composition, cholesterol, or alamethicin content and divalent cations. *Biophys J*. (1996); **71**(3): 1364-73.

18. Sonnleitner A, Schutz GJ, Schmidt T. Free Brownian motion of individual lipid molecules in biomembranes. *Biophys J*. (1999); **77**(5): 2638-42.

19. Fujiwara T, Ritchie K, Murakoshi H, Jacobson K, Kusumi A. Phospholipids undergo hop diffusion in compartmentalized cell membrane. *J Cell Biol*. (2002); **157**(6): 1071-81.

20. Kwiatkowska K. One lipid, multiple functions: how various pools of PI(4,5)P(2) are created in the plasma membrane. *Cell Mol Life Sci*. (2010); **67**(23): 3927-46.

21. Hansen SB, Tao X, MacKinnon R. Structural basis of PIP2 activation of the classical inward rectifier K+ channel Kir2.2. *Nature*. (2011); **477**(7365): 495-8.

22. Padrick SB, Cheng HC, Ismail AM, Panchal SC, Doolittle LK, Kim S, et al. Hierarchical regulation of WASP/WAVE proteins. *Mol Cell*. (2008); **32**(3): 426-38.

23. Saarikangas J, Zhao H, Lappalainen P. Regulation of the actin cytoskeleton-plasma membrane interplay by phosphoinositides. *Physiol Rev*. (2010); **90**(1): 259-89.

24. Ferguson KM, Lemmon MA, Schlessinger J, Sigler PB. Structure of the high affinity complex of inositol trisphosphate with a phospholipase C pleckstrin homology domain. *Cell*. (1995); **83**(6): 1037-46.

25. Lemmon MA, Ferguson KM, O'Brien R, Sigler PB, Schlessinger J. Specific and high-affinity binding of inositol phosphates to an isolated pleckstrin homology domain. *Proc Natl Acad Sci U S A*. (1995); **92**(23): 10472-6.

26. Korzeniowski MK, Popovic MA, Szentpetery Z, Varnai P, Stojilkovic SS, Balla T. Dependence of STIM1/Orai1-mediated calcium entry on plasma membrane phosphoinositides. *J Biol Chem*. (2009); **284**(31): 21027-35.

27. Walsh CM, Chvanov M, Haynes LP, Petersen OH, Tepikin AV, Burgoyne RD. Role of phosphoinositides in STIM1 dynamics and store-operated calcium entry. *Biochem J*. (2010); **425**(1): 159-68.

28. Kusumi A, Suzuki KG, Kasai RS, Ritchie K, Fujiwara TK. Hierarchical mesoscale domain organization of the plasma membrane. *Trends Biochem Sci*. (2011); **36**(11): 604-15.

29. Simons K, Sampaio JL. Membrane organization and lipid rafts. *Cold Spring Harb Perspect Biol*. (2011); **3**(10): a004697.

30. Turk HF, Chapkin RS. Membrane lipid raft organization is uniquely modified by n-3 polyunsaturated fatty acids. *Prostaglandins Leukot Essent Fatty Acids*. (2013); **88**(1): 43-7.

31. Wilson NS, Dixit V, Ashkenazi A. Death receptor signal transducers: nodes of coordination in immune signaling networks. *Nat Immunol*. (2009); **10**(4): 348-55.

32. Sasaki T, Takasuga S, Sasaki J, Kofuji S, Eguchi S, Yamazaki M, et al. Mammalian phosphoinositide kinases and phosphatases. *Prog Lipid Res*. (2009); **48**(6): 307-43.

33. Mellman DL, Gonzales ML, Song C, Barlow CA, Wang P, Kendziorski C, et al. A PtdIns4,5P2-regulated nuclear poly(A) polymerase controls expression of select mRNAs. *Nature*. (2008); **451**(7181): 1013-7.

34. Balla A, Vereb G, Gulkan H, Gehrmann T, Gergely P, Heilmeyer LM, Jr., et al. Immunohistochemical localisation of two phosphatidylinositol 4-kinase isoforms, PI4K230 and PI4K92, in the central nervous system of rats. *Exp Brain Res*. (2000); **134**(3): 279-88.

35. Kakuk A, Friedlander E, Vereb G, Jr., Kasa A, Balla A, Balla T, et al. Nucleolar localization of phosphatidylinositol 4-kinase PI4K230 in various mammalian cells. *Cytometry A*. (2006); **69**(12): 1174-83.

36. de Graaf P, Klapisz EE, Schulz TK, Cremers AF, Verkleij AJ, van Bergen en Henegouwen PM. Nuclear localization of phosphatidylinositol 4-kinase beta. *J Cell Sci*. (2002); **115**(Pt 8): 1769-75.

37. Weixel KM, Blumental-Perry A, Watkins SC, Aridor M, Weisz OA. Distinct Golgi populations of phosphatidylinositol 4-phosphate regulated by phosphatidylinositol 4-kinases. *J Biol Chem*. (2005); **280**(11): 10501-8.

38. Hollander MC, Blumenthal GM, Dennis PA. PTEN loss in the continuum of common cancers, rare syndromes and mouse models. *Nat Rev Cancer*. (2011); **11**(4): 289-301.

39. Johnson CM, Chichili GR, Rodgers W. Compartmentalization of phosphatidylinositol 4,5-bisphosphate signaling evidenced using targeted phosphatases. *J Biol Chem*. (2008); **283**(44): 29920-8.

40. Sezgin E, Kaiser HJ, Baumgart T, Schwille P, Simons K, Levental I. Elucidating membrane structure and protein behavior using giant plasma membrane vesicles. *Nat Protoc*. (2012); **7**(6): 1042-51.

41. Charras GT, Hu CK, Coughlin M, Mitchison TJ. Reassembly of contractile actin cortex in cell blebs. *J Cell Biol*. (2006); **175**(3): 477-90.

42. Calloway N, Owens T, Corwith K, Rodgers W, Holowka D, Baird B. Stimulated association of STIM1 and Orai1 is regulated by the balance of PtdIns(4,5)P(2) between distinct membrane pools. *J Cell Sci*. (2011); **124**(Pt 15): 2602-10.

43. Wang Y, Litvinov RI, Chen X, Bach TL, Lian L, Petrich BG, et al. Loss of PIP5KIgamma, unlike other PIP5KI isoforms, impairs the integrity of the membrane cytoskeleton in murine megakaryocytes. *J Clin Invest*. (2008); **118**(2): 812-9.

44. Wang Y, Zhao L, Suzuki A, Lian L, Min SH, Wang Z, et al. Platelets lacking PIP5KIgamma have normal integrin activation but impaired cytoskeletal-membrane integrity and adhesion. *Blood*. (2013); **121**(14): 2743-52.

45. Golebiewska U, Nyako M, Woturski W, Zaitseva I, McLaughlin S. Diffusion coefficient of fluorescent phosphatidylinositol 4,5-bisphosphate in the plasma membrane of cells. *Mol Biol Cell*. (2008); **19**(4): 1663-9.

46. Cho H, Kim YA, Ho WK. Phosphate number and acyl chain length determine the subcellular location and lateral mobility of phosphoinositides. *Mol Cells*. (2006); **22**(1): 97-103.

47. Pike LJ, Casey L. Localization and turnover of phosphatidylinositol 4,5-bisphosphate in caveolin-enriched membrane domains. *J Biol Chem*. (1996); **271**(43): 26453-6.

48. Liu Y, Casey L, Pike LJ. Compartmentalization of phosphatidylinositol 4,5-bisphosphate in low-density membrane domains in the absence of caveolin. *Biochem Biophys Res Commun*. (1998); **245**(3): 684-90.

49. McLaughlin S, Wang J, Gambhir A, Murray D. PIP(2) and proteins: interactions, organization, and information flow. *Annu Rev Biophys Biomol Struct*. (2002); **31**: 151-75.

50. Watt SA, Kular G, Fleming IN, Downes CP, Lucocq JM. Subcellular localization of phosphatidylinositol 4,5-bisphosphate using the pleckstrin homology domain of phospholipase C delta1. *Biochem J*. (2002); **363**(Pt 3): 657-66.

51. Barlow CA, Laishram RS, Anderson RA. Nuclear phosphoinositides: a signaling enigma wrapped in a compartmental conundrum. *Trends Cell Biol*. (2010); **20**(1): 25-35.

52. Rando OJ, Zhao K, Janmey P, Crabtree GR. Phosphatidylinositol-dependent actin filament binding by the SWI/SNF-like BAF chromatin remodeling complex. *Proc Natl Acad Sci U S A*. (2002); **99**(5): 2824-9.

53. Boronenkov IV, Loijens JC, Umeda M, Anderson RA. Phosphoinositide signaling pathways in nuclei are associated with nuclear speckles containing pre-mRNA processing factors. *Mol Biol Cell*. (1998); **9**(12): 3547-60.

54. Zenewicz LA, Antov A, Flavell RA. CD4 T-cell differentiation and inflammatory bowel disease. *Trends Mol Med*. (2009); **15**(5): 199-207.

55. Lee KH, Dinner AR, Tu C, Campi G, Raychaudhuri S, Varma R, et al. The immunological synapse balances T cell receptor signaling and degradation. *Science*. (2003); **302**(5648): 1218-22.

56. Monks CR, Freiberg BA, Kupfer H, Sciaky N, Kupfer A. Three-dimensional segregation of supramolecular activation clusters in T cells. *Nature*. (1998); **395**(6697): 82-6.

57. Tybulewicz VL, Henderson RB. Rho family GTPases and their regulators in lymphocytes. *Nat Rev Immunol*. (2009); **9**(9): 630-44.

58. Gomez TS, Billadeau DD. T cell activation and the cytoskeleton: you can't have one without the other. *Adv Immunol*. (2008); **97**: 1-64.

59. Huang Y, Burkhardt JK. T-cell-receptor-dependent actin regulatory mechanisms. *J Cell Sci*. (2007); **120**(Pt 5): 723-30.

60. Meiri KF. Lipid rafts and regulation of the cytoskeleton during T cell activation. *Philos Trans R Soc Lond B Biol Sci*. (2005); **360**(1461): 1663-72.

61. Campi G, Varma R, Dustin ML. Actin and agonist MHC-peptide complex-dependent T cell receptor microclusters as scaffolds for signaling. *J Exp Med*. (2005); **202**(8): 1031-6.

62. DeMond AL, Mossman KD, Starr T, Dustin ML, Groves JT. T cell receptor microcluster transport through molecular mazes reveals mechanism of translocation. *Biophys J*. (2008); **94**(8): 3286-92.

63. Yokosuka T, Sakata-Sogawa K, Kobayashi W, Hiroshima M, Hashimoto-Tane A, Tokunaga M, et al. Newly generated T cell receptor microclusters initiate and sustain

T cell activation by recruitment of Zap70 and SLP-76. *Nat Immunol*. (2005); **6**(12): 1253-62.

64. Kaizuka Y, Douglass AD, Varma R, Dustin ML, Vale RD. Mechanisms for segregating T cell receptor and adhesion molecules during immunological synapse formation in Jurkat T cells. *Proc Natl Acad Sci U S A.* (2007); **104**(51): 20296-301.

65. Lillemeier BF, Mortelmaier MA, Forstner MB, Huppa JB, Groves JT, Davis MM. TCR and Lat are expressed on separate protein islands on T cell membranes and concatenate during activation. *Nat Immunol*. (2010); **11**(1): 90-6.

66. Jury EC, Flores-Borja F, Kabouridis PS. Lipid rafts in T cell signalling and disease. *Semin Cell Dev Biol*. (2007); **18**(5): 608-15.

67. Zech T, Ejsing CS, Gaus K, de Wet B, Shevchenko A, Simons K, et al. Accumulation of raft lipids in T-cell plasma membrane domains engaged in TCR signalling. *EMBO J*. (2009); **28**(5): 466-76.

68. Fan YY, McMurray DN, Ly LH, Chapkin RS. Dietary (n-3) polyunsaturated fatty acids remodel mouse T-cell lipid rafts. *J Nutr*. (2003); **133**(6): 1913-20.

69. Burack WR, Lee KH, Holdorf AD, Dustin ML, Shaw AS. Cutting edge: quantitative imaging of raft accumulation in the immunological synapse. *J Immunol*. (2002); **169**(6): 2837-41.

70. Xavier R, Brennan T, Li Q, McCormack C, Seed B. Membrane compartmentation is required for efficient T cell activation. *Immunity*. (1998); **8**(6): 723-32.

71. Rentero C, Zech T, Quinn CM, Engelhardt K, Williamson D, Grewal T, et al. Functional implications of plasma membrane condensation for T cell activation. *PLoS One*. (2008); **3**(5): e2262.

72. Zhu J, Yamane H, Paul WE. Differentiation of effector CD4 T cell populations. *Annu Rev Immunol*. (2010); **28**: 445-89.

73. Balamuth F, Leitenberg D, Unternaehrer J, Mellman I, Bottomly K. Distinct patterns of membrane microdomain partitioning in Th1 and th2 cells. *Immunity*. (2001); **15**(5): 729-38.

74. Thauland TJ, Koguchi Y, Wetzel SA, Dustin ML, Parker DC. Th1 and Th2 cells form morphologically distinct immunological synapses. *J Immunol*. (2008); **181**(1): 393-9.

75. Miguel L, Owen DM, Lim C, Liebig C, Evans J, Magee AI, et al. Primary human CD4+ T cells have diverse levels of membrane lipid order that correlate with their function. *J Immunol*. (2011); **186**(6): 3505-16.

76. McDonald G, Deepak S, Miguel L, Hall CJ, Isenberg DA, Magee AI, et al. Normalizing glycosphingolipids restores function in CD4+ T cells from lupus patients. *J Clin Invest*. (2014); **124**(2): 712-24.

77. Zhu Y, Gumlaw N, Karman J, Zhao H, Zhang J, Jiang JL, et al. Lowering glycosphingolipid levels in CD4+ T cells attenuates T cell receptor signaling, cytokine production, and differentiation to the Th17 lineage. *J Biol Chem*. (2011); **286**(17): 14787-94.

78. Fan YY, Ly LH, Barhoumi R, McMurray DN, Chapkin RS. Dietary docosahexaenoic acid suppresses T cell protein kinase C theta lipid raft recruitment and IL-2 production. *J Immunol*. (2004); **173**(10): 6151-60.

79. Gawrisch K, Soubias O. Structure and dynamics of polyunsaturated hydrocarbon chains in lipid bilayers-significance for GPCR function. *Chem Phys Lipids*. (2008); **153**(1): 64-75.

80. Soubias O, Gawrisch K. Docosahexaenoyl chains isomerize on the sub-nanosecond time scale. *J Am Chem Soc*. (2007); **129**(21): 6678-9.

81. Bruno MJ, Koeppe RE, 2nd, Andersen OS. Docosahexaenoic acid alters bilayer elastic properties. *Proc Natl Acad Sci U S A*. (2007); **104**(23): 9638-43.

82. Bruno MJ, Rusinova R, Gleason NJ, Koeppe RE, 2nd, Andersen OS. Interactions of drugs and amphiphiles with membranes: modulation of lipid bilayer elastic properties by changes in acyl chain unsaturation and protonation. *Faraday Discuss*. (2013); **161**: 461-80; discussion 563-89.

83. Xiao YF, Kang JX, Morgan JP, Leaf A. Blocking effects of polyunsaturated fatty acids on Na+ channels of neonatal rat ventricular myocytes. *Proc Natl Acad Sci U S A*. (1995); **92**(24): 11000-4.

84. Xiao YF, Gomez AM, Morgan JP, Lederer WJ, Leaf A. Suppression of voltage-gated L-type Ca2+ currents by polyunsaturated fatty acids in adult and neonatal rat ventricular myocytes. *Proc Natl Acad Sci U S A*. (1997); **94**(8): 4182-7.

85. Fink M, Lesage F, Duprat F, Heurteaux C, Reyes R, Fosset M, et al. A neuronal two P domain K+ channel stimulated by arachidonic acid and polyunsaturated fatty acids. *EMBO J*. (1998); **17**(12): 3297-308.

86. Matta JA, Miyares RL, Ahern GP. TRPV1 is a novel target for omega-3 polyunsaturated fatty acids. *J Physiol*. (2007); **578**(Pt 2): 397-411.

87. Bouzat CB, Barrantes FJ. Effects of long-chain fatty acids on the channel activity of the nicotinic acetylcholine receptor. *Receptors Channels*. (1993); **1**(3): 251-8.

88. Nabekura J, Noguchi K, Witt MR, Nielsen M, Akaike N. Functional modulation of human recombinant gamma-aminobutyric acid type A receptor by docosahexaenoic acid. *J Biol Chem*. (1998); **273**(18): 11056-61.

89. Shaikh SR, Kinnun JJ, Leng X, Williams JA, Wassall SR. How polyunsaturated fatty acids modify molecular organization in membranes: Insight from NMR studies of model systems. *Biochim Biophys Acta*. (2014).

90. Wassall SR, Stillwell W. Docosahexaenoic acid domains: the ultimate non-raft membrane domain. *Chem Phys Lipids*. (2008); **153**(1): 57-63.

91. Williams JA, Batten SE, Harris M, Rockett BD, Shaikh SR, Stillwell W, et al. Docosahexaenoic and eicosapentaenoic acids segregate differently between raft and nonraft domains. *Biophys J*. (2012); **103**(2): 228-37.

92. Wassall SR, Stillwell W. Polyunsaturated fatty acid-cholesterol interactions: domain formation in membranes. *Biochim Biophys Acta*. (2009); **1788**(1): 24-32.

93. Chapkin RS, Wang N, Fan YY, Lupton JR, Prior IA. Docosahexaenoic acid alters the size and distribution of cell surface microdomains. *Biochim Biophys Acta*. (2008); **1778**(2): 466-71.

94. Kim W, Fan YY, Barhoumi R, Smith R, McMurray DN, Chapkin RS. n-3 polyunsaturated fatty acids suppress the localization and activation of signaling proteins at the immunological synapse in murine CD4+ T cells by affecting lipid raft formation. *J Immunol*. (2008); **181**(9): 6236-43.

95. Rockett BD, Teague H, Harris M, Melton M, Williams J, Wassall SR, et al. Fish oil increases raft size and membrane order of B cells accompanied by differential effects on function. *J Lipid Res*. (2012); **53**(4): 674-85.

96. Yao C, Sakata D, Esaki Y, Li Y, Matsuoka T, Kuroiwa K, et al. Prostaglandin E2-EP4 signaling promotes immune inflammation through Th1 cell differentiation and Th17 cell expansion. *Nat Med*. (2009); **15**(6): 633-40.

97. Boniface K, Bak-Jensen KS, Li Y, Blumenschein WM, McGeachy MJ, McClanahan TK, et al. Prostaglandin E2 regulates Th17 cell differentiation and function through cyclic AMP and EP2/EP4 receptor signaling. *J Exp Med*. (2009); **206**(3): 535-48.

98. Chizzolini C, Chicheportiche R, Alvarez M, de Rham C, Roux-Lombard P, Ferrari-Lacraz S, et al. Prostaglandin E2 synergistically with interleukin-23 favors human Th17 expansion. *Blood*. (2008); **112**(9): 3696-703.

99. Napolitani G, Acosta-Rodriguez EV, Lanzavecchia A, Sallusto F. Prostaglandin E2 enhances Th17 responses via modulation of IL-17 and IFN-gamma production by memory CD4+ T cells. *Eur J Immunol*. (2009); **39**(5): 1301-12.

100. Ahrenstedt O, Hallgren R, Knutson L. Jejunal release of prostaglandin E2 in Crohn's disease: relation to disease activity and first-degree relatives. *J Gastroenterol Hepatol*. (1994); **9**(6): 539-43.

101. Ligumsky M, Karmeli F, Sharon P, Zor U, Cohen F, Rachmilewitz D. Enhanced thromboxane A2 and prostacyclin production by cultured rectal mucosa in ulcerative colitis and its inhibition by steroids and sulfasalazine. *Gastroenterology*. (1981); **81**(3): 444-9.

102. Rampton DS, Sladen GE, Youlten LJ. Rectal mucosal prostaglandin E2 release and its relation to disease activity, electrical potential difference, and treatment in ulcerative colitis. *Gut*. (1980); **21**(7): 591-6.

103. Sharon P, Ligumsky M, Rachmilewitz D, Zor U. Role of prostaglandins in ulcerative colitis. Enhanced production during active disease and inhibition by sulfasalazine. *Gastroenterology*. (1978); **75**(4): 638-40.

104. Sharon P, Stenson WF. Enhanced synthesis of leukotriene B4 by colonic mucosa in inflammatory bowel disease. *Gastroenterology*. (1984); **86**(3): 453-60.

105. Wiercinska-Drapalo A, Flisiak R, Prokopowicz D. Mucosal and plasma prostaglandin E2 in ulcerative colitis. *Hepatogastroenterology*. (1999); **46**(28): 2338-42.

106. Lands WE, Libelt B, Morris A, Kramer NC, Prewitt TE, Bowen P, et al. Maintenance of lower proportions of (n - 6) eicosanoid precursors in phospholipids of

human plasma in response to added dietary (n - 3) fatty acids. *Biochim Biophys Acta*. (1992); **1180**(2): 147-62.

107. Culp BR, Titus BG, Lands WE. Inhibition of prostaglandin biosynthesis by eicosapentaenoic acid. *Prostaglandins Med*. (1979); **3**(5): 269-78.

108. Bagga D, Wang L, Farias-Eisner R, Glaspy JA, Reddy ST. Differential effects of prostaglandin derived from omega-6 and omega-3 polyunsaturated fatty acids on COX-2 expression and IL-6 secretion. *Proc Natl Acad Sci U S A*. (2003); **100**(4): 1751-6.

109. Lawrence T, Willoughby DA, Gilroy DW. Anti-inflammatory lipid mediators and insights into the resolution of inflammation. *Nat Rev Immunol*. (2002); **2**(10): 787-95.

110. Arita M, Yoshida M, Hong S, Tjonahen E, Glickman JN, Petasis NA, et al. Resolvin E1, an endogenous lipid mediator derived from omega-3 eicosapentaenoic acid, protects against 2,4,6-trinitrobenzene sulfonic acid-induced colitis. *Proc Natl Acad Sci U S A*. (2005); **102**(21): 7671-6.

111. Flower RJ, Perretti M. Controlling inflammation: a fat chance? *J Exp Med*. (2005); **201**(5): 671-4.

112. Spite M, Claria J, Serhan CN. Resolvins, specialized proresolving lipid mediators, and their potential roles in metabolic diseases. *Cell Metab*. (2014); **19**(1): 21-36.

113. Itoh T, Fairall L, Amin K, Inaba Y, Szanto A, Balint BL, et al. Structural basis for the activation of PPARgamma by oxidized fatty acids. *Nat Struct Mol Biol*. (2008); **15**(9): 924-31.

114. Xu HE, Lambert MH, Montana VG, Parks DJ, Blanchard SG, Brown PJ, et al. Molecular recognition of fatty acids by peroxisome proliferator-activated receptors. *Mol Cell*. (1999); **3**(3): 397-403.

115. Kliewer SA, Sundseth SS, Jones SA, Brown PJ, Wisely GB, Koble CS, et al. Fatty acids and eicosanoids regulate gene expression through direct interactions with peroxisome proliferator-activated receptors alpha and gamma. *Proc Natl Acad Sci U S A*. (1997); **94**(9): 4318-23.

116. Fan YY, Spencer TE, Wang N, Moyer MP, Chapkin RS. Chemopreventive n-3 fatty acids activate RXRalpha in colonocytes. *Carcinogenesis*. (2003); **24**(9): 1541-8.

117. Hirasawa A, Tsumaya K, Awaji T, Katsuma S, Adachi T, Yamada M, et al. Free fatty acids regulate gut incretin glucagon-like peptide-1 secretion through GPR120. *Nat Med*. (2005); **11**(1): 90-4.

118. Oh DY, Talukdar S, Bae EJ, Imamura T, Morinaga H, Fan W, et al. GPR120 is an omega-3 fatty acid receptor mediating potent anti-inflammatory and insulin-sensitizing effects. *Cell*. (2010); **142**(5): 687-98.

119. Yan Y, Jiang W, Spinetti T, Tardivel A, Castillo R, Bourquin C, et al. Omega-3 fatty acids prevent inflammation and metabolic disorder through inhibition of NLRP3 inflammasome activation. *Immunity*. (2013); **38**(6): 1154-63.

120. Belluzzi A, Brignola C, Campieri M, Pera A, Boschi S, Miglioli M. Effect of an enteric-coated fish-oil preparation on relapses in Crohn's disease. *N Engl J Med*. (1996); **334**(24): 1557-60.

121. Bouwens M, van de Rest O, Dellschaft N, Bromhaar MG, de Groot LC, Geleijnse JM, et al. Fish-oil supplementation induces antiinflammatory gene expression profiles in human blood mononuclear cells. *Am J Clin Nutr*. (2009); **90**(2): 415-24.

122. Farzaneh-Far R, Harris WS, Garg S, Na B, Whooley MA. Inverse association of erythrocyte n-3 fatty acid levels with inflammatory biomarkers in patients with stable coronary artery disease: The Heart and Soul Study. *Atherosclerosis*. (2009); **205**(2): 538-43.

123. Uchiyama K, Nakamura M, Odahara S, Koido S, Katahira K, Shiraishi H, et al. N-3 polyunsaturated fatty acid diet therapy for patients with inflammatory bowel disease. *Inflamm Bowel Dis*. (2010); **16**(10): 1696-707.

124. Vedin I, Cederholm T, Freund Levi Y, Basun H, Garlind A, Faxen Irving G, et al. Effects of docosahexaenoic acid-rich n-3 fatty acid supplementation on cytokine release from blood mononuclear leukocytes: the OmegAD study. *Am J Clin Nutr*. (2008); **87**(6): 1616-22.

125. Weaver KL, Ivester P, Seeds M, Case LD, Arm JP, Chilton FH. Effect of dietary fatty acids on inflammatory gene expression in healthy humans. *J Biol Chem*. (2009); **284**(23): 15400-7.

126. Feng T, Qin H, Wang L, Benveniste EN, Elson CO, Cong Y. Th17 cells induce colitis and promote Th1 cell responses through IL-17 induction of innate IL-12 and IL-23 production. *J Immunol*. (2011); **186**(11): 6313-8.

127. Yen D, Cheung J, Scheerens H, Poulet F, McClanahan T, McKenzie B, et al. IL-23 is essential for T cell-mediated colitis and promotes inflammation via IL-17 and IL-6. *J Clin Invest*. (2006); **116**(5): 1310-6.

128. Zhang Z, Zheng M, Bindas J, Schwarzenberger P, Kolls JK. Critical role of IL-17 receptor signaling in acute TNBS-induced colitis. *Inflamm Bowel Dis*. (2006); **12**(5): 382-8.

129. Winer S, Paltser G, Chan Y, Tsui H, Engleman E, Winer D, et al. Obesity predisposes to Th17 bias. *Eur J Immunol*. (2009); **39**(9): 2629-35.

130. Lumeng CN, Maillard I, Saltiel AR. T-ing up inflammation in fat. *Nat Med*. (2009); **15**(8): 846-7.

131. Bertola A, Ciucci T, Rousseau D, Bourlier V, Duffaut C, Bonnafous S, et al. Identification of adipose tissue dendritic cells correlated with obesity-associated insulin-resistance and inducing Th17 responses in mice and patients. *Diabetes*. (2012); **61**(9): 2238-47.

132. Chan SS, Luben R, Bergmann MM, Boeing H, Olsen A, Tjonneland A, et al. Aspirin in the aetiology of Crohn's disease and ulcerative colitis: a European prospective cohort study. *Aliment Pharmacol Ther*. (2011); **34**(6): 649-55.

133. Stulnig TM, Berger M, Sigmund T, Raederstorff D, Stockinger H, Waldhausl W. Polyunsaturated fatty acids inhibit T cell signal transduction by modification of detergent-insoluble membrane domains. *J Cell Biol*. (1998); **143**(3): 637-44.

134. Stulnig TM, Huber J, Leitinger N, Imre EM, Angelisova P, Nowotny P, et al. Polyunsaturated eicosapentaenoic acid displaces proteins from membrane rafts by altering raft lipid composition. *J Biol Chem*. (2001); **276**(40): 37335-40.

135. Ly LH, Smith R, Switzer KC, Chapkin RS, McMurray DN. Dietary eicosapentaenoic acid modulates CTLA-4 expression in murine CD4+ T-cells. *Prostaglandins Leukot Essent Fatty Acids*. (2006); **74**(1): 29-37.

136. Yog R, Barhoumi R, McMurray DN, Chapkin RS. n-3 polyunsaturated fatty acids suppress mitochondrial translocation to the immunologic synapse and modulate calcium signaling in T cells. *J Immunol*. (2010); **184**(10): 5865-73.

137. Jolly CA, Jiang YH, Chapkin RS, McMurray DN. Dietary (n-3) polyunsaturated fatty acids suppress murine lymphoproliferation, interleukin-2 secretion, and the formation of diacylglycerol and ceramide. *J Nutr*. (1997); **127**(1): 37-43.

138. McMurray DN, Jolly CA, Chapkin RS. Effects of dietary n-3 fatty acids on T cell activation and T cell receptor-mediated signaling in a murine model. *J Infect Dis*. (2000); **182 Suppl 1**: S103-7.

139. Arrington JL, McMurray DN, Switzer KC, Fan YY, Chapkin RS. Docosahexaenoic acid suppresses function of the CD28 costimulatory membrane receptor in primary murine and Jurkat T cells. *J Nutr*. (2001); **131**(4): 1147-53.

140. Chapkin RS, Arrington JL, Apanasovich TV, Carroll RJ, McMurray DN. Dietary n-3 PUFA affect TcR-mediated activation of purified murine T cells and accessory cell function in co-cultures. *Clin Exp Immunol*. (2002); **130**(1): 12-8.

141. Fan YY, Kim W, Callaway E, Smith R, Jia Q, Zhou L, et al. fat-1 transgene expression prevents cell culture-induced loss of membrane n-3 fatty acids in activated CD4+ T-cells. *Prostaglandins Leukot Essent Fatty Acids*. (2008); **79**(6): 209-14.

142. Switzer KC, Fan YY, Wang N, McMurray DN, Chapkin RS. Dietary n-3 polyunsaturated fatty acids promote activation-induced cell death in Th1-polarized murine CD4+ T-cells. *J Lipid Res*. (2004); **45**(8): 1482-92.

143. Switzer KC, McMurray DN, Morris JS, Chapkin RS. (n-3) Polyunsaturated fatty acids promote activation-induced cell death in murine T lymphocytes. *J Nutr*. (2003); **133**(2): 496-503.

144. Zhang P, Smith R, Chapkin RS, McMurray DN. Dietary (n-3) polyunsaturated fatty acids modulate murine Th1/Th2 balance toward the Th2 pole by suppression of Th1 development. *J Nutr*. (2005); **135**(7): 1745-51.

145. Monk JM, Hou TY, Turk HF, McMurray DN, Chapkin RS. n3 PUFAs reduce mouse CD4+ T-cell ex vivo polarization into Th17 cells. *J Nutr*. (2013); **143**(9): 1501-8.

146. Monk JM, Hou TY, Turk HF, Weeks B, Wu C, McMurray DN, et al. Dietary n-3 polyunsaturated fatty acids (PUFA) decrease obesity-associated Th17 cell-mediated inflammation during colitis. *PLoS One*. (2012); **7**(11): e49739.

147. Allen MJ, Fan YY, Monk JM, Hou TY, Barhoumi R, McMurray DN, et al. n-3 PUFAs reduce T-helper 17 cell differentiation by decreasing responsiveness to interleukin-6 in isolated mouse splenic CD4(+) T cells. *J Nutr*. (2014); **144**(8): 1306-13.

148. Cotta-de-Almeida V, Westerberg L, Maillard MH, Onaldi D, Wachtel H, Meelu P, et al. Wiskott Aldrich syndrome protein (WASP) and N-WASP are critical for T cell development. *Proc Natl Acad Sci U S A*. (2007); **104**(39): 15424-9.

149. Padrick SB, Rosen MK. Physical mechanisms of signal integration by WASP family proteins. *Annu Rev Biochem*. (2010); **79**: 707-35.

150. Faure S, Salazar-Fontana LI, Semichon M, Tybulewicz VL, Bismuth G, Trautmann A, et al. ERM proteins regulate cytoskeleton relaxation promoting T cell-APC conjugation. *Nat Immunol*. (2004); **5**(3): 272-9.

151. Nolz JC, Medeiros RB, Mitchell JS, Zhu P, Freedman BD, Shimizu Y, et al. WAVE2 regulates high-affinity integrin binding by recruiting vinculin and talin to the immunological synapse. *Mol Cell Biol*. (2007); **27**(17): 5986-6000.

152. Eibert SM, Lee KH, Pipkorn R, Sester U, Wabnitz GH, Giese T, et al. Cofilin peptide homologs interfere with immunological synapse formation and T cell activation. *Proc Natl Acad Sci U S A*. (2004); **101**(7): 1957-62.

153. Scott CC, Dobson W, Botelho RJ, Coady-Osberg N, Chavrier P, Knecht DA, et al. Phosphatidylinositol-4,5-bisphosphate hydrolysis directs actin remodeling during phagocytosis. *J Cell Biol*. (2005); **169**(1): 139-49.

154. Hao JJ, Liu Y, Kruhlak M, Debell KE, Rellahan BL, Shaw S. Phospholipase C-mediated hydrolysis of PIP2 releases ERM proteins from lymphocyte membrane. *J Cell Biol*. (2009); **184**(3): 451-62.

155. van Rheenen J, Song X, van Roosmalen W, Cammer M, Chen X, Desmarais V, et al. EGF-induced PIP2 hydrolysis releases and activates cofilin locally in carcinoma cells. *J Cell Biol*. (2007); **179**(6): 1247-59.

156. Barda-Saad M, Braiman A, Titerence R, Bunnell SC, Barr VA, Samelson LE. Dynamic molecular interactions linking the T cell antigen receptor to the actin cytoskeleton. *Nat Immunol*. (2005); **6**(1): 80-9.

157. Ivanova PT, Milne SB, Byrne MO, Xiang Y, Brown HA. Glycerophospholipid identification and quantitation by electrospray ionization mass spectrometry. *Methods Enzymol*. (2007); **432**: 21-57.

158. Guillou H, Stephens LR, Hawkins PT. Quantitative measurement of phosphatidylinositol 3,4,5-trisphosphate. *Methods Enzymol*. (2007); **434**: 117-30.

159. Harder T, Kuhn M. Immunoisolation of TCR signaling complexes from Jurkat T leukemic cells. *Sci STKE*. (2001); **2001**(71): pl1.

160. Ledgerwood LG, Lal G, Zhang N, Garin A, Esses SJ, Ginhoux F, et al. The sphingosine 1-phosphate receptor 1 causes tissue retention by inhibiting the entry of peripheral tissue T lymphocytes into afferent lymphatics. *Nat Immunol*. (2008); **9**(1): 42-53.

161. Labno CM, Lewis CM, You D, Leung DW, Takesono A, Kamberos N, et al. Itk functions to control actin polymerization at the immune synapse through localized activation of Cdc42 and WASP. *Curr Biol*. (2003); **13**(18): 1619-24.

162. Higgs HN, Pollard TD. Activation by Cdc42 and PIP(2) of Wiskott-Aldrich syndrome protein (WASp) stimulates actin nucleation by Arp2/3 complex. *J Cell Biol*. (2000); **150**(6): 1311-20.

163. Hill EE, Husbands DR, Lands WE. The selective incorporation of 14C-glycerol into different species of phosphatidic acid, phosphatidylethanolamine, and phosphatidylcholine. *J Biol Chem*. (1968); **243**(17): 4440-51.

164. Hill EE, Lands WE. Incorporation of long-chain and polyunsaturated acids into phosphatidate and phosphatidylcholine. *Biochim Biophys Acta*. (1968); **152**(3): 645-8.

165. Shikano M, Masuzawa Y, Yazawa K. Effect of docosahexaenoic acid on the generation of platelet-activating factor by eosinophilic leukemia cells, Eol-1. *J Immunol*. (1993); **150**(8 Pt 1): 3525-33.

166. Inoue M, Murase S, Okuyama H. Acyl coenzyme a:phospholipid acyltransferases in porcine platelets discriminate between omega-3 and omega-6 unsaturated fatty acids. *Arch Biochem Biophys*. (1984); **231**(1): 29-37.

167. Fan YY, Monk JM, Hou TY, Callway E, Vincent L, Weeks B, et al. Characterization of an arachidonic acid-deficient (Fads1 knockout) mouse model. *J Lipid Res*. (2012); **53**(7): 1287-95.

168. Nair SS, Leitch J, Garg ML. N-3 polyunsaturated fatty acid supplementation alters inositol phosphate metabolism and protein kinase C activity in adult porcine cardiac myocytes. *J Nutr Biochem*. (2001); **12**(1): 7-13.

169. Yamamoto M, Hilgemann DH, Feng S, Bito H, Ishihara H, Shibasaki Y, et al. Phosphatidylinositol 4,5-bisphosphate induces actin stress-fiber formation and inhibits membrane ruffling in CV1 cells. *J Cell Biol*. (2001); **152**(5): 867-76.

170. Quintana A, Schwindling C, Wenning AS, Becherer U, Rettig J, Schwarz EC, et al. T cell activation requires mitochondrial translocation to the immunological synapse. *Proc Natl Acad Sci U S A*. (2007); **104**(36): 14418-23.

171. Samstag Y, Eibert SM, Klemke M, Wabnitz GH. Actin cytoskeletal dynamics in T lymphocyte activation and migration. *J Leukoc Biol*. (2003); **73**(1): 30-48.

172. Turk HF, Monk JM, Fan YY, Callaway ES, Weeks B, Chapkin RS. Inhibitory effects of omega-3 fatty acids on injury-induced epidermal growth factor receptor transactivation contribute to delayed wound healing. *Am J Physiol Cell Physiol*. (2013); **304**(9): C905-17.

173. Damsgaard CT, Frokiaer H, Lauritzen L. The effects of fish oil and high or low linoleic acid intake on fatty acid composition of human peripheral blood mononuclear cells. *Br J Nutr*. (2008); **99**(1): 147-54.

174. Feskens EJ, Kromhout D. Epidemiologic studies on Eskimos and fish intake. *Ann N Y Acad Sci*. (1993); **683**: 9-15.

175. Kim W, McMurray DN, Chapkin RS. n-3 polyunsaturated fatty acids--physiological relevance of dose. *Prostaglandins Leukot Essent Fatty Acids*. (2010); **82**(4-6): 155-8.

176. Kang JX, Wang J, Wu L, Kang ZB. Transgenic mice: fat-1 mice convert n-6 to n-3 fatty acids. *Nature*. (2004); **427**(6974): 504.

177. Hou TY, Monk JM, Fan YY, Barhoumi R, Chen YQ, Rivera GM, et al. n-3 polyunsaturated fatty acids suppress phosphatidylinositol 4,5-bisphosphate-dependent actin remodelling during CD4+ T-cell activation. *Biochem J*. (2012); **443**(1): 27-37.

178. Kim W, Barhoumi R, McMurray DN, Chapkin RS. Dietary fish oil and DHA down-regulate antigen-activated CD4+ T-cells while promoting the formation of liquid-ordered mesodomains. *Br J Nutr*. (2014); **111**(2): 254-60.

179. Calder PC. Lipids for intravenous nutrition in hospitalised adult patients: a multiple choice of options. *Proc Nutr Soc*. (2013); **72**(3): 263-76.

180. Chaki SP, Barhoumi R, Berginski ME, Sreenivasappa H, Trache A, Gomez SM, et al. Nck enables directional cell migration through the coordination of polarized membrane protrusion with adhesion dynamics. *J Cell Sci*. (2013); **126**(Pt 7): 1637-49.

181. Rivera GM, Vasilescu D, Papayannopoulos V, Lim WA, Mayer BJ. A reciprocal interdependence between Nck and PI(4,5)P(2) promotes localized N-WASp-mediated actin polymerization in living cells. *Mol Cell*. (2009); **36**(3): 525-35.

182. Chichili GR, Westmuckett AD, Rodgers W. T cell signal regulation by the actin cytoskeleton. *J Biol Chem*. (2010); **285**(19): 14737-46.

183. Byrum JN, Van Komen JS, Rodgers W. CD28 Sensitizes TCR Ca2+ Signaling during Ag-Independent Polarization of Plasma Membrane Rafts. *J Immunol*. (2013).

184. Lee J, Sadelain M, Brentjens R. Retroviral transduction of murine primary T lymphocytes. *Methods Mol Biol*. (2009); **506**: 83-96.

185. Koushik SV, Chen H, Thaler C, Puhl HL, 3rd, Vogel SS. Cerulean, Venus, and VenusY67C FRET reference standards. *Biophys J*. (2006); **91**(12): L99-L101.

186. Brzostowski JA, Meckel T, Hong J, Chen A, Jin T. Imaging protein-protein interactions by Forster resonance energy transfer (FRET) microscopy in live cells. *Curr Protoc Protein Sci*. (2009); **19**: 19.5.

187. Pralle A, Keller P, Florin EL, Simons K, Horber JK. Sphingolipid-cholesterol rafts diffuse as small entities in the plasma membrane of mammalian cells. *J Cell Biol*. (2000); **148**(5): 997-1008.

188. Nicolson GL. The Fluid-Mosaic Model of Membrane Structure: Still relevant to understanding the structure, function and dynamics of biological membranes after more than 40years. *Biochim Biophys Acta*. (2014); **1838**(6): 1451-66.

189. Simons K, Gerl MJ. Revitalizing membrane rafts: new tools and insights. *Nat Rev Mol Cell Biol*. (2010); **11**(10): 688-99.

190. Chazotte B. Fluorescent labeling of membrane lipid rafts. *Cold Spring Harb Protoc*. (2011); **2011**(5): pdb prot5625.

191. Day CA, Kenworthy AK. Mechanisms underlying the confined diffusion of cholera toxin B-subunit in intact cell membranes. *PLoS One*. (2012); **7**(4): e34923.

192. Wallace PK, Muirhead KA. Cell tracking 2007: a proliferation of probes and applications. *Immunol Invest*. (2007); **36**(5-6): 527-61.

193. Buckley CD, Gilroy DW, Serhan CN. Proresolving lipid mediators and mechanisms in the resolution of acute inflammation. *Immunity*. (2014); **40**(3): 315-27.

194. Chapkin RS, Kim W, Lupton JR, McMurray DN. Dietary docosahexaenoic and eicosapentaenoic acid: emerging mediators of inflammation. *Prostaglandins Leukot Essent Fatty Acids*. (2009); **81**(2-3): 187-91.

195. Kenworthy AK, Nichols BJ, Remmert CL, Hendrix GM, Kumar M, Zimmerberg J, et al. Dynamics of putative raft-associated proteins at the cell surface. *J Cell Biol*. (2004); **165**(5): 735-46.

196. Owen DM, Williamson DJ, Magenau A, Gaus K. Sub-resolution lipid domains exist in the plasma membrane and regulate protein diffusion and distribution. *Nat Commun*. (2012); **3**: 1256.

197. Kabouridis PS, Jury EC. Lipid rafts and T-lymphocyte function: implications for autoimmunity. *FEBS Lett*. (2008); **582**(27): 3711-8.

198. Jury EC, Kabouridis PS, Flores-Borja F, Mageed RA, Isenberg DA. Altered lipid raft-associated signaling and ganglioside expression in T lymphocytes from patients with systemic lupus erythematosus. *J Clin Invest*. (2004); **113**(8): 1176-87.

199. Chichili GR, Cail RC, Rodgers W. Cytoskeletal modulation of lipid interactions regulates Lck kinase activity. *J Biol Chem*. (2012); **287**(29): 24186-94.

200. Bijlmakers MJ. Protein acylation and localization in T cell signaling (Review). *Mol Membr Biol*. (2009); **26**(1): 93-103.

201. Hannoush RN, Sun J. The chemical toolbox for monitoring protein fatty acylation and prenylation. *Nat Chem Biol*. (2010); **6**(7): 498-506.

202. Greaves J, Chamberlain LH. DHHC palmitoyl transferases: substrate interactions and (patho)physiology. *Trends Biochem Sci*. (2011); **36**(5): 245-53.

203. Levental I, Lingwood D, Grzybek M, Coskun U, Simons K. Palmitoylation regulates raft affinity for the majority of integral raft proteins. *Proc Natl Acad Sci U S A*. (2010); **107**(51): 22050-4.

204. Crise B, Rose JK. Identification of palmitoylation sites on CD4, the human immunodeficiency virus receptor. *J Biol Chem*. (1992); **267**(19): 13593-7.

205. Lin J, Weiss A, Finco TS. Localization of LAT in glycolipid-enriched microdomains is required for T cell activation. *J Biol Chem*. (1999); **274**(41): 28861-4.

206. van't Hof W, Resh MD. Dual fatty acylation of p59(Fyn) is required for association with the T cell receptor zeta chain through phosphotyrosine-Src homology domain-2 interactions. *J Cell Biol*. (1999); **145**(2): 377-89.

207. Hannoush RN, Arenas-Ramirez N. Imaging the lipidome: omega-alkynyl fatty acids for detection and cellular visualization of lipid-modified proteins. *ACS Chem Biol*. (2009); **4**(7): 581-7.

208. Huisgen R. Proceedings of the Chemical Society. October 1961. *Proceedings of the Chemical Society*. (1961); (October): 357-96.

209. Liang X, Nazarian A, Erdjument-Bromage H, Bornmann W, Tempst P, Resh MD. Heterogeneous fatty acylation of Src family kinases with polyunsaturated fatty acids regulates raft localization and signal transduction. *J Biol Chem*. (2001); **276**(33): 30987-94.

210. Webb Y, Hermida-Matsumoto L, Resh MD. Inhibition of protein palmitoylation, raft localization, and T cell signaling by 2-bromopalmitate and polyunsaturated fatty acids. *J Biol Chem*. (2000); **275**(1): 261-70.

211. Belluzzi A, Boschi S, Brignola C, Munarini A, Cariani G, Miglio F. Polyunsaturated fatty acids and inflammatory bowel disease. *Am J Clin Nutr*. (2000); **71**(1 Suppl): 339S-42S.

212. Haglund O, Wallin R, Luostarinen R, Saldeen T. Effects of a new fluid fish oil concentrate, ESKIMO-3, on triglycerides, cholesterol, fibrinogen and blood pressure. *J Intern Med*. (1990); **227**(5): 347-53.

213. Hansson GK. Inflammation, atherosclerosis, and coronary artery disease. *N Engl J Med*. (2005); **352**(16): 1685-95.

214. Ross R. Atherosclerosis--an inflammatory disease. *N Engl J Med*. (1999); **340**(2): 115-26.

215. Loftus EV, Jr. The burden of inflammatory bowel disease in the United States: a moving target? *Clin Gastroenterol Hepatol*. (2007); **5**(12): 1383-4.

216. Choy EH, Panayi GS. Cytokine pathways and joint inflammation in rheumatoid arthritis. *N Engl J Med*. (2001); **344**(12): 907-16.

217. McInnes IB, Schett G. The pathogenesis of rheumatoid arthritis. *N Engl J Med*. (2011); **365**(23): 2205-19.

218. Querfurth HW, LaFerla FM. Alzheimer's disease. *N Engl J Med*. (2010); **362**(4): 329-44.

219. Noseworthy JH, Lucchinetti C, Rodriguez M, Weinshenker BG. Multiple sclerosis. *N Engl J Med*. (2000); **343**(13): 938-52.

220. Shulman GI. Ectopic fat in insulin resistance, dyslipidemia, and cardiometabolic disease. *N Engl J Med*. (2014); **371**(12): 1131-41.

221. Weiss R, Dziura J, Burgert TS, Tamborlane WV, Taksali SE, Yeckel CW, et al. Obesity and the metabolic syndrome in children and adolescents. *N Engl J Med*. (2004); **350**(23): 2362-74.

222. Berger NA, Dannenberg AJ. Obesity, Inflammation and Cancer. Berger NA, editor: Springer New York; 2013. 380 p.

223. Grivennikov SI, Greten FR, Karin M. Immunity, inflammation, and cancer. *Cell*. (2010); **140**(6): 883-99.

224. Grivennikov SI, Karin M. Inflammation and oncogenesis: a vicious connection. *Curr Opin Genet Dev*. (2010); **20**(1): 65-71.

225. Bertin B, Desreumaux P, Dubuquoy L. Obesity, visceral fat and Crohn's disease. *Curr Opin Clin Nutr Metab Care*. (2010); **13**(5): 574-80.

226. John BJ, Irukulla S, Abulafi AM, Kumar D, Mendall MA. Systematic review: adipose tissue, obesity and gastrointestinal diseases. *Aliment Pharmacol Ther*. (2006); **23**(11): 1511-23.

227. Kahn SE, Hull RL, Utzschneider KM. Mechanisms linking obesity to insulin resistance and type 2 diabetes. *Nature*. (2006); **444**(7121): 840-6.

228. Peyrin-Biroulet L, Chamaillard M, Gonzalez F, Beclin E, Decourcelle C, Antunes L, et al. Mesenteric fat in Crohn's disease: a pathogenetic hallmark or an innocent bystander? *Gut*. (2007); **56**(4): 577-83.

229. Statistics NCfH. Health, United States, 2013: With Special Feature on Prescription Drugs. Hyattsville (MD): National Center for Health Statistics; 2014. http://www.cdc.gov/nchs/data/hus/hus13.pdf

230. Osborn O, Olefsky JM. The cellular and signaling networks linking the immune system and metabolism in disease. *Nat Med*. (2012); **18**(3): 363-74.

231. Kim W, Barhoumi R, McMurray DN, Chapkin RS. Dietary fish oil and DHA down-regulate antigen-activated CD4+ T-cells while promoting the formation of liquid-ordered mesodomains. *Br J Nutr*. (2013): 1-7.

232. Kim W, Khan NA, McMurray DN, Prior IA, Wang N, Chapkin RS. Regulatory activity of polyunsaturated fatty acids in T-cell signaling. *Prog Lipid Res*. (2010); **49**(3): 250-61.

233. Corsetto PA, Cremona A, Montorfano G, Jovenitti IE, Orsini F, Arosio P, et al. Chemical-physical changes in cell membrane microdomains of breast cancer cells after omega-3 PUFA incorporation. *Cell Biochem Biophys*. (2012); **64**(1): 45-59.

234. McFarland CT, Fan YY, Chapkin RS, Weeks BR, McMurray DN. Dietary polyunsaturated fatty acids modulate resistance to *Mycobacterium tuberculosis* in guinea pigs. *J Nutr*. (2008); **138**(11): 2123-8.

235. Bonilla DL, Fan YY, Chapkin RS, McMurray DN. Transgenic mice enriched in omega-3 fatty acids are more susceptible to pulmonary tuberculosis: impaired resistance to tuberculosis in fat-1 mice. *J Infect Dis*. (2010); **201**(3): 399-408.

236. Woodworth HL, McCaskey SJ, Duriancik DM, Clinthorne JF, Langohr IM, Gardner EM, et al. Dietary fish oil alters T lymphocyte cell populations and exacerbates disease in a mouse model of inflammatory colitis. *Cancer Res*. (2010); **70**(20): 7960-9.

237. Gillespie PG, Walker RG. Molecular basis of mechanosensory transduction. *Nature*. (2001); **413**(6852): 194-202.

238. Pan B, Geleoc GS, Asai Y, Horwitz GC, Kurima K, Ishikawa K, et al. TMC1 and TMC2 are components of the mechanotransduction channel in hair cells of the mammalian inner ear. *Neuron*. (2013); **79**(3): 504-15.

239. Woo SH, Ranade S, Weyer AD, Dubin AE, Baba Y, Qiu Z, et al. Piezo2 is required for Merkel-cell mechanotransduction. *Nature*. (2014); **509**(7502): 622-6.

240. Shemesh T, Geiger B, Bershadsky AD, Kozlov MM. Focal adhesions as mechanosensors: a physical mechanism. *Proc Natl Acad Sci U S A*. (2005); **102**(35): 12383-8.

241. Vogel V, Sheetz M. Local force and geometry sensing regulate cell functions. *Nat Rev Mol Cell Biol*. (2006); **7**(4): 265-75.

242. Seong J, Wang N, Wang Y. Mechanotransduction at focal adhesions: from physiology to cancer development. *J Cell Mol Med*. (2013); **17**(5): 597-604.

243. Hao J, Zhang Y, Ye R, Zheng Y, Zhao Z, Li J. Mechanotransduction in cancer stem cells. *Cell Biol Int*. (2013); **37**(9): 888-91.

244. Kuo JC. Mechanotransduction at focal adhesions: integrating cytoskeletal mechanics in migrating cells. *J Cell Mol Med*. (2013); **17**(6): 704-12.

245. Kim ST, Takeuchi K, Sun ZY, Touma M, Castro CE, Fahmy A, et al. The alphabeta T cell receptor is an anisotropic mechanosensor. *J Biol Chem*. (2009); **284**(45): 31028-37.

246. Li YC, Chen BM, Wu PC, Cheng TL, Kao LS, Tao MH, et al. Cutting Edge: mechanical forces acting on T cells immobilized via the TCR complex can trigger TCR signaling. *J Immunol*. (2010); **184**(11): 5959-63.

247. Husson J, Chemin K, Bohineust A, Hivroz C, Henry N. Force generation upon T cell receptor engagement. *PLoS One*. (2011); **6**(5): e19680.

248. Puech PH, Nevoltris D, Robert P, Limozin L, Boyer C, Bongrand P. Force measurements of TCR/pMHC recognition at T cell surface. *PLoS One*. (2011); **6**(7): e22344.

249. Judokusumo E, Tabdanov E, Kumari S, Dustin ML, Kam LC. Mechanosensing in T lymphocyte activation. *Biophys J*. (2012); **102**(2): L5-7.

250. O'Connor RS, Hao X, Shen K, Bashour K, Akimova T, Hancock WW, et al. Substrate rigidity regulates human T cell activation and proliferation. *J Immunol*. (2012); **189**(3): 1330-9.

251. Engl W, Arasi B, Yap LL, Thiery JP, Viasnoff V. Actin dynamics modulate mechanosensitive immobilization of E-cadherin at adherens junctions. *Nat Cell Biol*. (2014); **16**(6): 587-94.

252. Hoffman BD, Grashoff C, Schwartz MA. Dynamic molecular processes mediate cellular mechanotransduction. *Nature*. (2011); **475**(7356): 316-23.

253. Martinac B, Adler J, Kung C. Mechanosensitive ion channels of *E. coli* activated by amphipaths. *Nature*. (1990); **348**(6298): 261-3.

254. Markin VS, Martinac B. Mechanosensitive ion channels as reporters of bilayer expansion. A theoretical model. *Biophys J*. (1991); **60**(5): 1120-7.

255. Anishkin A, Loukin SH, Teng J, Kung C. Feeling the hidden mechanical forces in lipid bilayer is an original sense. *Proc Natl Acad Sci U S A*. (2014); **111**(22): 7898-905.

256. Sreenivasappa H, Chaki SP, Lim SM, Trzeciakowski JP, Davidson MW, Rivera GM, et al. Selective regulation of cytoskeletal tension and cell-matrix adhesion by RhoA and Src. *Integr Biol (Camb)*. (2014); **6**(8): 743-54.

257. Dustin ML, Depoil D. New insights into the T cell synapse from single molecule techniques. *Nat Rev Immunol*. (2011); **11**(10): 672-84.

258. Purbhoo MA, Liu H, Oddos S, Owen DM, Neil MA, Pageon SV, et al. Dynamics of subsynaptic vesicles and surface microclusters at the immunological synapse. *Sci Signal*. (2010); **3**(121): ra36.

259. Williamson DJ, Owen DM, Rossy J, Magenau A, Wehrmann M, Gooding JJ, et al. Pre-existing clusters of the adaptor Lat do not participate in early T cell signaling events. *Nat Immunol*. (2011); **12**(7): 655-62.

260. Seo J, Barhoumi R, Johnson AE, Lupton JR, Chapkin RS. Docosahexaenoic acid selectively inhibits plasma membrane targeting of lipidated proteins. *FASEB J*. (2006); **20**(6): 770-2.

APPENDIX A

PHENOTYPING *FAT-1* MICE

Reagents:

- Acetone
- 0.1 M KCl (cold)
- Folch reagent ($CHCl_3$:MeOH at 2:1 v/v)
- 6% HCl in MeOH
- Hexane
- Dichloromethane (CH_2Cl_2)

Procedures:

Preparation of Glass Tubes

1. Add 1 mL of acetone in 12 mL of glass tube. Prepare about double the amount of tubes that is required since about half will leak.
2. Draw a line at the top of the acetone to record whether acetone evaporated.
3. Incubate for 1 hr at 80 °C.
4. If acetone evaporated, do not use those tubes for further experiments.
5. If acetone did not evaporate, discard the acetone, leave the tubes upside down, and label them well.
6. Prepare a second set of tubes. These do not need to be evaporated.
7. Prepare a set of 2 mL Eppendorf tubes for homogenization. Add 1ML of cold 0.1 M KCl into each tube and store on ice.

Homogenization of Mouse Tails and Isolation of Lipids

1. For each blade, can cut 2 samples (one sample per side). Similarly, for each glass slide, can cut 2 samples (one sample per end).
   - Must use the non-coated side for cutting.
2. Cut the tails into very small chunks (the smaller the better) with the blade. Insert the tail fragments into the 2 mL Eppendorf tube with 0.1 M KCl. Store on ice.
3. Homogenize with Polytron blade on ice for 45 sec at maximum speed. Check to ensure the all materials have been homogenized. Store on ice.
   - Note that hair won't be homogenized.
4. Transfer the homogenate into the non-leak proof glass tubes and add 5 mL of Folch reagent.
5. Vortex for 1 min, centrifuge at 300 rpm, 5 min, at 4 °C.
   - Make sure that the blue protective rubber is used when centrifuging.
6. Transfer the lower phase into the leak proof 12 mL glass tube, and dry down the solution under N_2.
   - This takes about 30 to 45 min.
7. Redissolve in 3 mL of 6% HCl in MeOH.
8. Flush the samples with N_2 before incubation.
9. Vortex the samples for 1 min and incubate at 76 °C for 15 h (overnight).
10. Prepare 4 mL glass vials with green caps. Use label markers to clearly mark the vials.

Isolation of FAME

1. Need to perform this step ASAP after the incubation. Can store at 4 °C for 2 to 4 h after incubation, but not longer than that.
2. Add to each sample 1 mL 0.1 M KCl and 2 mL hexane.
3. Vortex for 1 min. Centrifuge at 3000 rpm, 5 min, 4 °C.
4. Transfer upper layer into the 4 mL glass vials with green caps. Dry down under N_2.
   - This step takes about 15 to 20 min.
5. Redissolve in 100 µL of CH_2Cl_2.

6. Flush samples with N_2 before storage.
7. Vortex the samples and store at -20°C.

Preparation for Gas Chromatography

1. Warm up and stabilize the GC overnight. Follow the instructions on the machine.
2. Make sure the vials in A11 and WB9 are both full of CH_2Cl_2.
3. Prepare the sequence to run on GC.
4. Prepare the GC vials by putting in the inserts into the GC vials.
5. Load 25 μL of Nuchek 68A standard. You can start running the standard. Put 1 sample of standard at the end of the sequence as well.
6. Vortex the samples well. Load 25 μL of sample into each GC vial. Put it in the sequence.
7. Flush all samples (and standard) under N_2.
8. To analyze the chromatogram, follow the instructions on the machine.

APPENDIX B

ISOLATING $CD4^+$ T CELLS

Reagents:

Dry Reagents	Wet Reagents
• Scissors and forceps for animal surgery • 70 µm Cell Strainer • (BD 352350) • 30 µm MACS pre-separation filter (Miltenyi 08-771-2) • MACS separation columns (**LS** columns) (Miltenyi 130-042-401) • Syringes → just need to plunger part (BD 309585) • QuadroMACS Separation Unit (Miltenyi 130-090-976) • 100 mm Petri dish (BD 351029)	• Auto MACS Running Buffer (MACS Separation Buffer) (Miltenyi 130-091-221) • CD4 (L3T4) Microbeads, mouse (Miltenyi 130-049-201) • PBS (GIbco, 14190) • RPMI Complete Media (see below)

- Complete RPMI Media

	Vol (mL)	%	Stock Conc	Final Conc
RPMI (Irvine Scientific 9159)	200	92.94		
Heat-inactivated FBS (Irvine Scientific, 300320439)	10.8	5.02		
Glutamax (Gibco, 35050-061)	2.2	1.02	200 mM	4 mM
Pen-strep (Gibco, 15140-148)	2.2	1.02	P 10000 U/mL S 10000 µg/mL	P 100 U/mL S 100 µg/mL

Procedures:

Isolation of Cells from Spleens

1. Remove the spleen from a mouse and place the spleen in 15 mL conical tube containing 3 mL of MACS buffer.
   - Remove as much fat as possible from the spleen.
2. Place 70 µm cell strainer inside a 100 mm Petri dish and wet the membrane by adding 5 mL of MACS buffer.
3. Place a 30 µm MACS pre-separation filter on top of a new 15 mL conical tube. Wet the filter with 2 mL MACS buffer.
4. Transfer the spleen with the 3 mL MACS buffer onto the cell strainer and use the plunger to mesh (gently push, not grind) the tissue inside the Petri dish.
   - Want to keep the tissue wet at all time.
   - Continue until only connective tissue is left on the membrane.
   - Use Petri dish or else cells will adhere to the plate.
5. Wash the plate with the MACS buffer in the Petri dish.
6. Remove the cell strainer and transfer the 8 mL of buffer onto the 30 µm MACS pre-separation filter slowly (small volume at a time to prevent clogging).
7. Wash the cell strainer by washing it inside the Petri dish with 5 mL of MACS buffer. Wash the Petri dish again, and apply to the 30 µm MACS pre-separation filter.
8. Remove the filter, close the lid, and gently invert the tube. Take 20 µL and count using Coulter counter (4 µm cut off).

9. Centrifuge cell suspension at 300 g for 10 min and aspirate off the supernatant.
    - Use plastic tip attached to glass pipette to reduce the suction force.

Isolation of $CD4^+$ T Cells

1. Tap the bottom of the tube to loosen the pellet and then add 90 μL/10^7 total cells of MACS buffer to get a good suspension.
    - Know the amount of cells by using the Coulter counter. The approximate volume of cells is 13.5 mL (some is lost in wetting the membranes).
    - Can only load up to 2 x 10^9 total cells (10^8 labeled cells) per LS column.
    - Make sure to record the starting cell numbers for calculating yields.
2. Add 10 μL/10^7 total cells of CD4 (L3T4) microbeads directly into the suspension.
3. Mix well by pipetting and incubate for 15 min at 4 °C (use refrigerator, do not shake).
4. Wash cells by filling up the 15 mL conical tube with cold MACS buffer. Mix by inversion, centrifuge at 300 g for 10 min, and then aspirate off the supernatant.
    - Use plastic tip attached to glass pipette to reduce the suction force.
5. Tap the bottom of the tube to loosen the pellet and then add 500 μL/10^8 total cells of MACS buffer to get a good suspension.

Running the LS Column

1. Snap the LS column into the QuadroMACS Separator. Place a basin under the column for waste. Pre-wet the LS column with 1 mL of cold MACS buffer. Let the buffer slowly drip through.
2. Apply the cell suspension onto the column.
    - Can collect the flow-through to collect $CD4^-$ cell population.
3. To rinse column, first wash the tube from Step 5 (Isolation of $CD4^+$ T Cells) with 9 mL of cold MACS buffer and then apply 3 mL to the column. Allow the buffer to run through the column before applying an additional 3 mL twice.
    - This washes the unlabeled cells through the column.
4. Remove the columns from the separator and place it on 15 mL conical tube for collection.
5. Pipette 5 mL of cold MACS buffer onto the column. Immediately flush out by applying the plunger supplied with the column. Push the plunger into the column all the way.
    - This fraction contains the magnetically labeled cells.
6. Fill the tube with an additional 5 mL of cold MACS buffer. Invert to wash well.
7. Centrifuge the elution at 300 g for 10 min. Aspirate off the supernatant.
8. Fill the tube with 10 mL of ice cold PBS. Wash by inversion. Take 20 μL of the suspension and count using the Coulter Counter.
9. Centrifuge the elution at 300 g for 10 min. Aspirate off the supernatant. Proceed to downstream applications.

Notes:

- All the steps are performed in cell culture hood except the removal of the spleen from the mouse.
- Store and use MACS buffer on ice, but perform rest of procedure at room temperature.
- Pour out 50 mL of MACS buffer into a conical tube so that the stock MACS does not get contaminated.
- Remember to prepare the Coulter Counter solution the day before (dispense into the cuvette).

APPENDIX C

PI(4,5)P_2 EXTRACTION

Purpose: To extract acidic phospholipids (i.e. PI(4,5)P_2) from non-adherent cells for further analysis (see ***Quantification of PIP_2 Using Abcam Anti-PIP_2 (ab11039)***).

Reagents:

- 1:1 MeOH:$CHCl_3$ (20 mL MeOH and 20 mL $CHCl_3$)
- 80:40:0.5 MeOH:$CHCl_3$:12N HCl (40 mL MeOH, 20 mL $CHCl_3$, 0.25 mL 12 N HCl)
- 12 N HCl (concentrate)
- 1 N HCl (4.2 mL 12 N HCl in 50 mL ddH_2O)

Procedures:

- All reagents and cells should be on ice.
- Cells should be in low-retention 1.5 mL Eppendorf tubes (Phenix, MH-815SA).

Cell Collection and Extraction of Neutral Lipids

1. Spin down the cells at 4000 g, 5 min, 4 °C. Aspirate off the supernatant.
    - With 0.3 x 10^6 cells, should be able to see a pellet that resembles an RNA pellet.
2. Wash the cell with PBS to remove any residual medium/serum by resuspending the pellet with 1 mL of ice-cold PBS. Spin down at 4000 g, 5 min, 4 ºC. Aspirate off the supernatant.
3. Add 800 µL (1:1) MeOH:$CHCl_3$ and vortex for 1 min. Centrifuge at 7500 g for 5 min at 4 °C. Aspirate off the supernatant.
    - With 0.3 x 10^6 cells, should be able to see a pellet that resembles an RNA pellet.
    - The pellet may actually be at the bottom of the tube rather than the side.

Extraction of Acidic Lipids and Phase Split

11. Add 400 µL (80:40:0.5) MeOH:$CHCl_3$:12 N HCl to the pellet, and vortex for 5 minutes (30 sec on, 30 sec off). Pulse to 3000 g at 4 °C to get all solvents down to the bottom.
12. Add 80 µL of 1 N HCl to the 400 µL of solvents from the above step and vortex for 15 seconds. Centrifuge at 18000 g for 2 min at 4°C to separate the organic and aqueous phases.
    - The aqueous layer is very small (just beneath the meniscus), so be very careful.
13. Collect the organic layer (lower phase) and put into a clean low-retention 1.5 mL Eppendorf tubes and dry under N_2.
    - Can use normal fine glass pipet once comfortable in controlling the speed of the suction, but if need to, can make homemade extra fine glass pipette:
    1. Turn on the Bunsen burner in the fume hood.
    2. Take the glass pipette and hold the top of the pipette with hand, and the bottom of the pipette with pliers.
    3. Warm the pipette very briefly over the flame (5 seconds max).
    4. Once the pipette becomes pliable, pull the pipette with the pliers to elongate the pipette.
    5. The pipette will be extended, but it will be closed at the end. Clip a few centimeters above the ending to create an opening for the elongated, extra fine glass pipette.

Storage Conditions of Products/Reagents:

- All solvents should be chilled on ice until cooled before using.

Notes:

- This protocol was modified from Ivanova PT *et al* (2007), Methods in Enzymology.

APPENDIX D

PI(4,5)P_2 QUANTIFICATION USING ABCAM ANTI-PIP_2

Purpose: To quantify the amount of PI(4,5)P_2 after acidic extraction (see ***Extraction of PI(4,5)P_2 from Non-adherent Cells***).

Reagents:

- PBS Buffer (Gibco, 21600-069).
  - Filter PBS buffer through a sterile cup (Nalgene, 450-0080).
- 96 well flat bottom polystyrene microplate, not-treated (Corning, 9017)
- Plate sealers (Genemate, T-3021-7)
- IgG free bovine serum albumin (Roche, 03 116 956 001).
- 50 µM PIP_2 Standard (Echelon Biosciences, P-4502)
- Protein Stabilizer (Echelon Biosciences, K-GS01) – Add 50 µL of PS to 20 mL of PBS.
- Anti-PIP_2 (Abcam, ab11039)
- Goat anti-mouse secondary antibody (KPL, 074-1806)
- TMB High Sensitivity Substrate Solution (BioLegend, 421501)
- 1N H_2SO_4 Stop Solution (Sigma, 258148)
  - Dilute stock 18M H_2SO_4 by adding 2.8 mL of stock H_2SO_4 and 47.2 mL of ddH_2O.

Procedures:

Preparation of Samples and Standards

1. Prepare 50 µM PI(4,5)P_2 by dissolving a vial of PI(4,5)P_2 (K-4502) with 400 µL of PBS-PS Vortex the sample extremely well and sonicate for 1 minutes in ice-cold water bath. Spin down the samples briefly and leave on ice.
2. Prepare 6 tubes corresponding to 7.5 µM, 5 µM, 2.5 µM, 1 µM, 0.5 µM, 0.2 µM, and 0.1 µM
3. Make 7.5 µM by adding 27 µL of 50 µM and 153 µL of PBS-PS.
4. Make 5 µM by adding 18 µL of 50 µM and 162 µL of PBS-PS. Make subsequent 5-fold serial dilution (1 µM and 0.2 µM) by adding 30 µL of standard and 120 µL of PBS.
5. Make 2.5 µM by adding 9 µL of 50 µM and 171 µL of PBS-PS. Make subsequent 5-fold serial dilution (0.5 µM and 0.1 µM) by adding 30 µL of standard and 120 µL of PBS.
6. Dissolve your phospholipid samples in appropriate amount of PBS (each well requires 150 µL of sample). Vortex very well and sonicate for 1 minutes in ice-cold water bath. Spin down the samples briefly and leave on ice.

Sample Coating and Blocking

1. Set up the standards by adding 55 µL/well. Add an additional 95 µL/well of PBS for the standards.
2. Set up the samples by adding 150 µL/well.

	1	2	3	4	5	6	7	8	9	10	11	12
A	7.5 µM	7.5 µM										
B	5 µM	5 µM										
C	2.5 µM	2.5 µM										
D	1 µM	1 µM										
E	0.5 µM	0.5 µM										
F	0.2 µM	0.2 µM										
G	0.1 µM	0.1 µM										
H	Blank	Blank										

3. Seal the plate and incubate for 1.5 hour at room temperature on a shaker at 800 rpm. Wrap the plate in aluminum foil.

4. Wash the plate with sterile PBS 3X. Discard the solution in the well and add 200 µL/well of PBS. Tap the plate gently 10 times and discard the solution. Dry the plate by tapping the plate gently on a piece of paper towel. Repeat two more times.
5. Block the well by adding 100 µL/well of 5% BSA in PBS. Seal the plate and incubate for overnight at 4 °C. Wrap the plate in aluminum foil.

Primary Antibody Incubation
1. Wash the plate with sterile PBS 3X.
2. Dilute the primary anti-PIP_2 1:2500 in 5% BSA in PBS. Add 100 µL/well of diluted primary antibody. Seal the plate and incubate for 1.5 h at room temperature on a shaker at 800 rpm. Wrap the plate in aluminum foil.

Secondary Antibody Incubation
1. Wash the plate with sterile PBS 3X.
2. Dilute the secondary goat anti-mouse 1:5000 in 5% BSA in PBS. Add 100 µL/well of diluted secondary antibody. Seal the plate and incubate for 1 hr at room temperature on a shaker at 800 rpm. Wrap the plate in aluminum foil.

Detection
1. Wash the plate with sterile PBS four times.
2. After the last PBS wash, add 100 µL of TMB solution to each well in the dark.
3. Allow the colour to develop for 5 to 10 minutes by covering the plate with aluminum foil and in the dark
4. Stop the colour development by adding 100 µL of 1N H_2SO_4 stop solution.
5. Read absorbance at 450 nm.

Expected Results:
- Note that the standard curve is a nonlinear regression curve fitted with sigmoidal dose response. This means to use the 4-parameter or 5-parameter curve fit; there are very subtle differences (eg. an additional parameter in 5-parameter) between the two models, but does not make real differences in the absolute values.

Storage Conditions of Products and Reagents:
- Place all diluted primary and secondary antibodies on ice before use.

Notes:
- Always have the next reagent ready in basins – do not allow the plate/strip to dry!
- This protocol is adopted from the Abcam protocol for indirect ELISA.

APPENDIX E

IMMUNOFLUORESCENCE

Purpose: To examine actin morphology in unstimulated and stimulated $CD4^+$ T cells.

Reagents:

- Keep all wet reagents at 4 °C, except antifade at -20 °C.

Dry Reagents	Wet Reagents
• Coverglass (Corning, 2935-225) • Lab-Tek II 2-well glass chamber slide (Nalge, 154461)	• Anti-CD3 (eBioscience, 16-0031-85) • Anti-CD28 (eBioscience, 14-0281) • Rabbit anti-WASp (Santa Cruz, #) • Alexa 568-Phalloidin (Invitrogen, A12380) • FITC-Cholera Toxin B (Sigma, C1655) • Alexa 647-TCRβ (BioLegend, 109218) • Alexa 488-Zap 70 (Invitrogen, MHZap7020) • Goat anti-Rabbit Alexa 647(Inviroten, A21246) • Coverglass antifade reagent medium (Invitrogen, P36934) • 100 mM glycine (Sigma, G7126) o Make 100 mM by dissolving 7.507 g of glycine in 1 L PBS • 0.1%(w/v) Poly-L-Lysine solution (Sigma, P8920) • 20% PFA in PBS (EMS, 15713-S) • 10% Triton X-100 (Fluka, 93443) • Blocking solution o 1% IgG-free BSA (Roche, 03116956001) o 0.1% NaN_3 (Sigma, S2002) o 98.3% PBS (Gibco, 21600-069)

- Complete RPMI Media

	Vol (mL)	%	Stock Conc	Final Conc
RPMI (Irvine Scientific, 9159)	200	92.94		
Heat-inactivated FBS (Irvine Scientific, 300320439)	10.8	5.02		
Glutamax (Gibco, 35050-061)	2.2	1.02	200 mM	2 mM
Pen-strep (Gibco, 15140-148)	2.2	1.02	P 10000 U/mL S 10000 µg/mL	P 100 U/mL S 100 µg/mL

Procedures:

Precoating chamber slides for seeding cells

1. Must perform this the day before the assay.
2. Dilute 10X poly-L-Lysine solution with sterile H_2O to 1X (0.1% w/v to 0.01% w/v).
3. Precoat Lab-Tek II 2-well glass chamber slides with 0.01% poly-L-lysine by adding 2 mL of 0.01% poly-L-Lysine/well for 30 min at room temperature. Replace the lids

Precoating chamber slides for plated CD3/CD28 activation

1. Must perform this the day before the assay.
2. Dilute 10X poly-L-Lysine solution with sterile H_2O to 1X (0.1% w/v to 0.01% w/v).
3. Precoat Lab-Tek II 2-well glass chamber slides with 0.01% poly-L-lysine by adding 2 mL of 0.01% poly-L-Lysine/well for 30 min. Replace the lids back on while the chamber slides are incubating.
4. Aspirate excess solution and sterile the slides under

back on while the chamber slides are incubating.
4. Aspirate excess solution and sterile the slides under UV light for 1 hr. Leave the lids off.
5. The next day, wash chamber slides with 1 mL of warm complete RPMI once time. Add warm complete RPMI into each chamber, shake gently by hand, and then aspirate off the media.
6. Prewarm the coated chamber slides with 200 µL of warm complete RPMI 3 times at 37 °C for 30 min at least. Leave in the incubator until seeding.

UV light for 1 hr. Leave the lids off.
5. Dilute anti-CD3 (stock 1 mg/mL) 1:1000 and anti-CD28 (stock 1 mg/mL) 1:100 in PBS in a single tube.
   - Example, if need 1 mL, add 1 µL of anti-CD3, 10 µL of anti-CD28, and 989 µL of PBS.
   - Add 200 µL of antibodies per chamber slide. For control (unstimulated), add 200 µL of PBS per chamber slide.
6. Incubate chamber slides on a shaker (gently) in the 4 °C walk-in cold room at a speed setting of 4, overnight. Replace the lids back on to ensure sterility.
7. The next day, wash chamber slides with 1 mL of warm complete RPMI once time. Add warm complete RPMI into each chamber, shake gently by hand, and then aspirate off the media.
8. Prewarm the coated chamber slides with 200 µL of warm complete RPMI 3 times at 37 °C for 30 min at least. Leave in the incubator until seeding.

Isolation of $CD4^+$ T Cells

1. Follow Isolation of T cells protocol.
2. After isolation of T cells, resuspend the $CD4^+$ T cells with warm complete RPMI to get a final concentration of T cells at 5×10^6 cells/mL in RPMI media.
3. Seed 1 mL/well dropwise by adding the cell suspension onto the 200 µL complete media in the well. This equates to 5×10^6 cells per well.
   - Final anti-CD3 concentration = 0.17 µg/mL (but is actually higher since plated, not suspended).
   - Final anti-CD28 concentration = 0.83 µg/mL (but is actually higher since plated, not suspended).
4. Incubate at 37 °C for 30 minutes.

Fixing the Cells

1. Make 4% PFA by combining 4 mL of 20X PFA and 16 mL of PBS.
   - Always make PFA fresh (i.e. the same day of experiment).
2. Wash the cells on the chamber slides with PBS 3 times for 2 min each, then immediately fix the cells in the freshly made 4% PFA for 20 min at room temperature.
3. Rinse the samples with PBS 2 times for 2 min each, and incubate cells with 10 mM glycine in PBS for 10 min at room temperature.
   - This step is performed to quench aldehyde groups.
   - Stock at 100 mM, so dilute 1:10 in PBS.
4. Wash the chamber slides with PBS 2 times for 2 min each, and permeabilize the cells by using 0.2% Triton X-100 in PBS for 5 min at room temperature.
   - Stock at 10%, so dilute 1:50 in PBS.
5. Wash the chamber slides with PBS 3 times for 2 min each.
6. Incubate cells in blocking solution at 4 °C overnight in a humid chamber.
   - Humid chamber consists of the plastic slide holders. Alternate between slide and wet Kimwipe PBS.

Applying Antibody

1. Wash the chamber slides with PBS 3 times for 2 min each.
2. Dilute the antibody in the following manner in the dark.

Antibody	Stock	Dilution	Final	Per well
Anti-cholera toxin B	250 µg/mL	1:25	10 µg/mL	8 µL antibody + 192 µL Blocking

Phalloidin	200 U/mL	1:10	20 U/mL	20 µL antibody + 180 µL Blocking
Anti-TCRβ	500 µg/mL	1:10	50 µg/mL	20 µL antibody + 180 µL Blocking
Anti-Zap70	200 µg/mL	1:15	13µg/mL	13 µL antibody + 187 µL Blocking
Anti-WASp	200 µg/mL	1:50	4 µg/mL	4 µL antibody + 196 µL Blocking

3. Incubate each chamber slide with 200 µL per well at room temperature for 1 hr in a humid chamber. The slides much be protected from light.
    - Wrap aluminum foil around the humid chamber and put in a drawer for extra protection against light exposure.
    - Cells are labeled much better when antibodies applied sequentially. This means that only one antibody is incubated in each well for 1 hr, followed by 2 washes with PBS for 2 min each, and then add the second antibody. The order of application does not seem to affect the fluorescence, but typically if one antibody is much stronger, apply that one first.
4. **(If required)** Dilute the secondary antibody in the following manner in the dark.

Antibody	Stock	Dilution	Final	Per well
Goat anti-Rabbit Alexa 647	2 mg/mL	1:300	6 µg/mL	0.67 µL antibody + 199.4 µL Blocking

5. Incubate each chamber slide with 200 µL per well at room temperature for 1 hr in a humid chamber. The slides much be protected from light.
    - Wrap aluminum foil around the humid chamber and put in a drawer for extra protection against light exposure.
6. Prepare the ProLong medium during the last 1 hr antibody incubation by thawing at room temperature for 1 hr (stored in -20 °C freezer).
7. Wash the chamber slides with PBS 3 times for 2 min each.

Preparation for Wash

1. Use slide separator to remove the chamber. Put slides on a slide holder for subsequent washes.
2. Incubate the slides in 70% ethanol once for 2 min.
3. Incubate the slides in 95% ethanol once for 2 min.
4. Incubate the slides in 100% ethanol once for 2 min.
5. Incubate slides in fresh xylene twice for 2 min each. This means that one would need two fresh xylenes.
6. Apply a small amount of antifade reagent medium mixture to the coverglass. Cover the slide while it is still wet.
    - Use a glass rod to line the antifade reagent medium on the side of the coverglass, and then cover the slide at a 45° angle to avoid bubbles.
    - Use a razor blade to help with the coverslip.
7. Place the slide on a flat surface in the dark to dry overnight at room temperature in the fume hood. Protect from light.

Finalizing the Slides

1. Seal the coverglass to the slide with fingernail polish to prevent shrinkage of mounting medium and subsequent sample distortion.
2. After sealing, let it dry for at least 15 min, then store the slide upright in a slide box at -20°C. Desiccant may be added to the box to ensure that the slide remains dry.
3. Examine sample under fluorescence microscopy.

Expected Results/Outcome

- Actin fluorescence should be high in stimulated and low in unstimulated, with localization at the periphery of the cells.
- Zap70 should be recruited to the periphery of the cells upon stimulation.

Storage Conditions of Products/Reagents

- Antibodies should be stored at the appropriate temperature (check the product sheet); however, stored diluted antibodies on ice before applying them onto the chamber slides.
- Blocking solution should be stored on ice after preparation.

Notes

- When imaging, always do a 3D z-stack to ensure that fluorescence is contributed to the plasma membrane, and not cytoplasm. Actin should be recruited to the plasma membrane upon stimulation
- If use the Chapkin lab microscope, excitation and emission are already set up. The buttons for them are the following:

Antibody	Fluorophore	Excitation/Emission for Chapkin Lab Microscope
Anti-cholera toxin B	FITC	FITC
Phalloidin	Alexa 568	TRITC
Anti-TCRβ	Alexa 647	Cy3
Anti-Zap70	Alexa 467	FITC

APPENDIX F

T CELL STIMULATION USING ANTI-CD3/ANTI-CD28 COATED BEADS

Purpose: To examine the recruitment of proteins in unstimulated and stimulated $CD4^+$ T cells upon anti-CD3/anti-CD28 coated beads.

Reagents:

- Keep all wet reagents at 4 °C, except antifade at -20 °C.

Dry Reagents	Wet Reagents
• Coverglass (Corning, 2935-225) • Lab-Tek II 2-well glass chamber slide (Nalge, 154461)	• Anti-CD3/anti-CD28 coated beads (Invitrogen, #114.53D) • 0.1%(w/v) Poly-L-Lysine solution (Sigma, P8920)

- Complete RPMI Media

	Vol (mL)	%	Stock Conc	Final Conc
RPMI (Irvine Scientific, 9159)	200	92.94		
Heat-inactivated FBS (Irvine Scientific, 300320439)	10.8	5.02		
Glutamax (Gibco, 35050-061)	2.2	1.02	200 mM	2 mM
Pen-strep (Gibco, 15140-148)	2.2	1.02	P 10000 U/mL S 10000 µg/mL	P 100 U/mL S 100 µg/mL

Procedures:

Precoating chamber slides for seeding cells

9. Must perform this the day before the assay.
10. Dilute 10X poly-L-Lysine solution with sterile H_2O to 1X (0.1% w/v to 0.01% w/v).
11. Precoat Lab-Tek II 2-well glass chamber slides with 0.01% poly-L-lysine by adding 2 mL of 0.01% poly-L-Lysine/well for 30 min at room temperature. Replace the lids back on while the chamber slides are incubating.
12. Aspirate excess solution and sterile the slides under UV light for 1 hr. Keep the sterilized slide with lid on at RT overnight in the hood.
13. The next day, wash chamber slides with 1 mL of warm complete RPMI once.
14. Dynabeads come at a concentration of 4×10^7 beads/mL. Since the bead:cell ratio is 1:1, want to use 3.5×10^6 beads. This equates to approximately 87.5 µL of beads per well.
15. To wash the beads take the appropriate amount of beads into a 1.5 mL Eppendorf tube. Add at least an equal amount of cold PBS. Vortex for 5 sec, and then set it on the Dynabead magnet (Life Tech, #12321D) for 1 min. Aspirate off the supernatant with the tube still on the magnet.
16. Remove the bead/tube from the magnet, then resuspend the beads in 200 µL per well of complete RPMI media, and then add the beads into the wells. Incubate at 37 °C for 30 min at least.

Isolation of $CD4^+$ T Cells

5. Follow Isolation of T cells protocol.
6. After isolation of T cells, resuspend the $CD4^+$ T cells with warm complete RPMI to get a final concentration of T cells at 3.5×10^6 cells/mL in RPMI media.
7. Seed 1 mL/well dropwise by adding the cell suspension onto the 200 µL complete media in the well. This equates to 3.5×10^6 cells per well.
8. Incubate at 37 °C for 30 minutes.
9. Continue to Immunofluorescence.

APPENDIX G

IMMUNOISOLATION

Purpose: To isolate immunological synapse from $CD4^+$ T cells to detect signaling complex formations upon T cell activation.

Reagents:

- Keep all wet reagents at 4 °C.

Dry Reagents	Wet Reagents
• 15 mL conical tube • 2 mL microcentrifuge tube • 1.5 mL microcentrifuge tube • BioMag separator (Polyscience, #84102S-1) • DynaMag separator (Invitrogen, #123-21D) • N_2 cavitation apparatus (Parr Instrument, #4635)	• Homogenization buffer • Dynabeads mouse T-activator CD3/CD28 (Invitrogen, #114.53D) • PBS (Gibco, 21600-069)

- Homogenization buffer A (store at – 20 ^{0}C)

Components	Amount for 500 mL	Final Conc
250 mM Sucrose	42.75 g	250 mM
1 M Sodium HEPES, pH = 7.2 26.03 g/100 mL (Acros, 32726100)	5 mL	10 mM
1 M $MgCl_2$ In solution (Sigma, M-1028)	1 mL	2 mM
500 mM NaF 2.10 g/100 mL	10 mL	10 mM
ddH_2O	484 mL	

- Complete homogenization buffer
  - Dilute 10 mM activated sodium orthovanadate 1:100 in homogenization buffer A
  - Dilute protease inhibitor cocktail 1:25 in homogenization buffer A
- Complete RPMI Media

	Vol (mL)	%	Stock Conc	Final Conc
RPMI (Irvine Scientific, 9159)	200	92.94		
Heat-inactivated FBS (Irvine Scientific, 300320439)	10.8	5.02		
Glutamax (Gibco, 35050-061)	2.2	1.02	200 mM	2 mM
Pen-strep (Gibco, 15140-148)	2.2	1.02	P 10000 U/mL S 10000 μg/mL	P 100 U/mL S 100 μg/mL

Procedures

Isolation of $CD4^+$ T Cells

1. Follow Isolation of T cells protocol.
2. After isolation of T cells, resuspend the $CD4^+$ T cells with warm complete RPMI to get a final concentration of T cells at 1.5 x 10^7 cells/1 mL in RPMI media.

Preparation of Dynabeads and Cell-Bead Conjugates

10. Dynabeads come at a concentration of 4 x 10^7 beads/mL. Since the bead:cell ratio is 1:2, want to use 7.5 x 10^6 beads.

- This equates to approximately 187.5 µL of beads per sample.

11. Transfer an appropriate amount of beads into a new tube, and wash the beads by adding an equal volume of PBS. Vortex the sample for at least 5 seconds.
    - Normal tip should be sufficient for transferring the beads.
12. Place the tube on the DynaMag separator for 1 min, then discard the supernatant. Remove the tube from the magnet and resuspend the washed Dynabeads in 500 µL per 187.5 µL of beads using culture medium.
13. Transfer 1 mL of cell suspension into a 2 mL microcentrifuge tube. Add 500 µL of beads. Mix well by pipetting gently.
14. Allow for cell-bead conjugates to form by leaving on ice for 7 minutes. Flick the tube occasionally.
15. Transfer the bead-cell conjugate to 37 ^{0}C and incubate for 30 min.
    - Can do shorter time if desired.
    - Conjugate formation can be monitored under microscope.
16. After incubation, immediately add 1 mL of ice cold complete homogenization buffer.
17. Spin the cells at 2000 rpm for 1 min at 4 ^{0}C.
18. Resuspend in the cells in 1 mL of ice cold complete homogenization buffer.
19. Transfer the cells into the cavitation chamber.

Cavitation Bomb Apparatus (Parr Instrument, #4635) and Cavitation of the Sample

1. Install the whole apparatus in the 4 ^{0}C overnight.
2. The outlet of the cavitation bomb apparatus needs to be fitted with a silicone tube that allows for the sample to be discharged into a 15 mL conical tube. Insert the tube through a hole in the cap of a 15 mL conical tube. Punch 5 to 10 holes in the cap with an 18 gauge syringe needle to allow the release of over-pressure from the sample.
    - Make sure that the tube is in tight fit with the cap, but not obstructed.
3. Refer to the following figure for the valves:

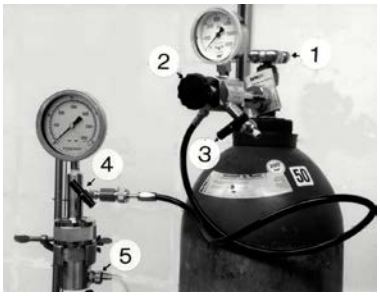

4. Ensure that valve 5 is closed. Apply 1 mL of the sample to the conical bottom of the chamber and stir at full speed on the magnetic stir plate.
5. Close the bomb and attach the hose from the filling connection (black tubing in the figure). Confirm that valves 1, 2, 3, and 5 are closed. Open valve 4.
6. Pressurize the bomb by slowly turning valve 1 until the pressure guage on the filling connections indicates full pressure (i.e. > 1500 psi).
7. Carefully open control valve 2 of the filling connection. Fill the cavitation bomb to the desired pressure (i.e. 800 psi) and then close valve 2.
8. As the nitrogen dissolves into the sample within the next 15 seconds, the pressure will drop. Readjust the pressure to the desired level (i.e. 800 psi) and then close inlet valve 4.
9. Close valve 1 on the N_2 tank.
10. Release the pressure from the filling connection and the hose by opening valves 3 and 2 in that order.
11. Detach the filling hose from the cavitation bomb and incubate the bomb for 7 minutes.
12. Screw the cap of the 15 mL tube that is already connected to the tube onto a new 15 mL conical tube to collect the sample.
    - Although there are small holes in the cap to release overpressure, use caution when collecting the sample because overpressure could cause silicon tube to pop off the cap, causing loss of sample.

13. Release the sample by slowly opening valve 5. Ensure that the sample flows at a rate of a few drops per second.
14. After the sample has been released into the tube, transfer the sample to 1 new 1.5 mL microcentrifuge tube. Fill the 15 mL conical tube with 3 mL of complete homogenization buffer.
15. Release the excess pressure from the cavitation bomb by opening valve 4.
16. Rinse the bomb with PBS and wipe the inside dry.

Preparation of Samples for Analysis

1. Conduct the following in 4 ^{0}C.
2. Retrieve the beads by placing the 1.5 mL microcentrifuge tube with the samples in the Dynabead magnet for 5 minute. During the 5 min incubation, gently invert the tube together with the magnet several times to release as many beads as possible trapped in the foam.
3. Take 100 µL of the homogenate for determining the yield.
4. Remove the foam first then the supernatant with a Pasteur pipette attached to a vacuum pump and a bottle trap. Keep the samples on ice.
5. Wash the samples 3X by resuspending in 1 mL of ice cold homogenization buffer in the 1.5 mL microcentrifuge tube (step 14 from above) and retrieve as in Step 2 after each wash.
6. After the last wash, resuspend the beads in 100 µL of ice cold complete homogenization buffer.
7. Proceed to Commassie blue assay and Western blot.

Notes:

- Instead of making sodium pervanadate, use the "activated" sodium orthovanadate available in the -20 ^{0}C at 1:100 dilution.
  - 100 mM sodium vanadate (Sigma-Aldrich)
    1. Dissolve 950 mg of sodium orthovanadate in 40 mL of ddH_2O.
    2. Adjust pH to 10.2 with HCl. Solution should be orange.
    3. Heat in a microwave until solution starts to boil. Solution should be clear.
    4. Adjust pH to 10.2 with 1 M NaOH **carefully**.
    5. Heat in a microwave until solution starts to boil.
    6. Check the pH is between 9.9 and 10.1. Repeat Steps 2 through 5 if necessary.
    7. Store in aliquots at -20 ^{0}C.
  - 10 mM pervanadate
    1. 10 µL of 100 mM sodium vanadate (see above)
    2. 10 µL of 30% H_2O_2
    3. 80 µL of ddH_2O
    4. Leave the solution at room temperature for 10 min, then use immediately to prepare the homogenization buffer
- Instead of making 1000X CLAP, use the protease inhibitor cocktail (Sigma) available in the -20 ^{o}C at 1:25 dilution
  - 1000X CLAP (Sigma-Aldrich)
    1. 5 mg of chymostatin
    2. 5 mg of leupeptin
    3. 5 mg of antipain
    4. 5 mg of pepstatin
    5. Dissolve in 500 µL of DMSO. Store at -20 ^{0}C in 50 µL aliquots

APPENDIX H

CLONING

Overall Flowchart:

Day	Steps
1	PCR insert
	Gel purification of insert
	Restriction digest of vector and insert
	Verification of digest using agarose gel
	Gel Purification of digested vector and insert
	Ligation of vector and insert
2	Bacterial transformation of plasmid
3	Overnight Culture
4	Miniprep of plasmid
5	Verification of plasmid using sequencing

Day 1 (PCR, Gel Purification, Restriction Digest, Gel Purification, Ligation):

Generation of Insert with Unique Restriction Cut Sites

Reagents:

- Keep all wet reagents at 4 °C.

Dry Reagents	Wet Reagents
	• 5' and 3' primers diluted in nuclease-free water • 25 mM $MgCl_2$ • 10 mM dNTPs • 10X reaction buffer • Pfu polymerase • Nuclease-free water

Procedures:

1. Use CLC sequence viewer to determine the restriction cut sites that you are going to use. In general, pick 2 restriction cut sites that are in the multiple cloning sites of the vector (MSCV for retrovirus and pLenti for lentivirus).
2. Check to make sure that these multiple cloning sites do not exist in your coding sequence (CDS). If they do exist, then you are just cutting your CDS and thus would give you fragments.
3. In the end, you will choose two restriction sites that are present in the multiple cloning sites of the vector but absent in your coding sequence.
4. Design primers for your coding sequence that contain your chosen restriction cut sites.
   a. Upstream (5', forward) primers
      i. Start with 5 x C
      ii. Restriction site sequence
      iii. If including fluorescent tag at the C-terminus, then add Kozak sequence (ACC ATG).
      iv. If including fluorescent tag at the N-terminus, then omit the Kozak sequence since it will be present before the fluorescent tag. Verify that this is the case using CLC sequence viewer.
      v. 12 to 15 complementary nucleotides from the 5' region of your CDS.
      vi. Should have 5'-CCCCC-(Cut Site)-(Kozak Sequence, if needed)-(12/15 of CDS)-3'
   b. Downstream (3', reverse) primers
      i. Start with 5 x C
      ii. Restriction site sequence

iii. If including fluorescent tag at the N-terminus, then add STOP codon (5'-3': ATC, ATT, or ACT).
iv. If including fluorescent tag at the C-terminus, then omit STOP codon since it will be present after the fluorescent tag. Verify using CLC sequence viewer.
v. 12 to 15 complementary nucleotides from the 3' region of your CDS.
vi. Should have 3'-(12/15 of CDS)-(STOP, if needed)-(Cut site)-CCCCC-5'

5. Make sure the primers adhere to the following rules:
   a. Use http://www.idtdna.com/analyzer/applications/oligoanalyzer/ for analysis. Use Default Settings and we will alter Mg^{2+} concentrations in our PCR reactions to optimize the reactions.
   b. 18-30 oligonucleotides long. The longer end of this range allows higher specificity and gives more space to add restriction enzyme sites and additional sequences.
   c. Melting temperature (Tm) between 65 to 70 °C. Make sure the primers are not more than 5 °C different from each other. Equation for Tm: Tm = 4(G+C) 2(A + T)
   d. Annealing temperature (Ta) of 10 to 15 °C lower than the Tm.
   e. GC content of each primer between 40 to 60%.
   f. In the CDS, have uniform distribution of G and C nucleotides, as clusters of G's or C's can cause non-specific priming.
   g. Avoid long runs of the same nucleotide.
   h. Ensure that there are no self- or cross-complementary sequences. Complementary sequences will encourage formation of hairpins and primer dimmers and will compete with template for use of primer and reagent.
   i. If possible, terminate the primers at the 3' end with C or A since neither C nor A nucleotide wobbles, allowing specificity and stability.
   j. If possible, make the 3' end slightly AT rich to avoid mispriming.
6. Dilute the primers by the following protocol:
   a. Add appropriate nuclease-free H_2O to the lyophilized primers to make the final concentration of 100 µM.
   b. Flick the tube a few times and then allow the tube to sit at room temperature for 10 minutes. Flick the tubes a few more times and spin down briefly.
   c. Aliquot 100 µL of the primer into 0.6 mL Eppendorf tubes. Label with the date, primer name, and initial.
   d. Store the primers in -80 °C.
   e. To make a working solution, dilute the stock 1:10 (i.e. add 30 µL of stock into 270 µL of nuclease-free water). This makes a 10 µM working concentration (100 µg/mL).
7. Make the following reaction tubes of $MgCl_2$, primers, and nuclease free water.

	Tube 1 (Control)	Tube 2 (Control)	Tube 3 (No Template)	Tube 4 (No $MgCl_2$)	Tube 5	Tube 6
5' primer	5	0	5	5	5	5
3' primer	0	5	5	5	5	5
25 mM $MgCl_2$	4	4	4	0	4	8
ddH_2O	9	9	6	8	4	0

8. Make the master mix containing the following components.

Reagents	Amounts
10X Buffer	35
10 mM dNTPs	7
DMSO (if required)	35
Nuclease-free H_2O	165 (135 if DMSO included)
Pfu (2.5 U/µL)	3
Total	210

- If product has high secondary structure (G-C rich), then add DMSO to a final concentration of 10% to destabilize secondary structures.

9. Add 30 µL of master mix into each reaction tube. Final volume at this point is 48 µL.

10. Add 2 µL of template DNA into each reaction tube except for Tube 3 (no template control). Template concentration should be around 10 to 20 ng/µL (this concentration can be varied depending on the amplification efficiency).
11. Use the following cycling program:

Temperature	Time	Cycles
95 °C	30 sec	5
40 °C	30 sec	
72 °C	72 sec	
95 °C	30 sec	30
60 °C	30 sec	
72 °C	2 min	
72 °C	10 min	1
8 °C	O/N	1

- Pfu polymerase has an elongation rate of 1000 base/min. Adjust the 72 °C elongation step time (in grey) to allow for Pfu polymerase to extend. For example, if product is 1500 bases, then 1500/1000 = 1.5 min. Round 1.5 min to 2 min to allow for full extension.
- For particularly long products (≥2 kb), can increase number of cycles, amount of polymerase, amount of template DNA.

Agarose Gel Electrophoresis

Reagents:

Dry Reagents	Wet Reagents
• Agarose gel electrophoresis • Visi-Blue Converter plate (Bioexpress, U-2202)	• Agarose (Phenix, RXA-2100MS) • 10X TAE buffer (Sigma, T9650) • Hyperladder IV 1 kb Ladder (Bioline, BIO-33029) • 5X sample buffer (Bioline, BIO-33029) • Gel-Green (RGB-4105)

- 1X TAE buffer
  - Dilute 10X TAE buffer in nuclease-free ddH_2O. Store at 4 ºC.

Procedures:

1. Make 0.75% agarose gel:
   a. Weigh 0.75 g of agarose and transfer into a 250 mL conical flask.
   b. Add 100 mL of 1X TAE and twirl a few times to allow for some mixing.
   c. Microwave for 90 seconds. Swirl the mixture and microwave for an additional 30 sec. Check again and microwave as required. Prepare the gel rig while agarose is dissolving.
   d. Allow the gel to cool to 60 °C, and add 7 µL of Glow-green.
   e. Pour the agarose into the tray, making sure no bubbles are formed. Use a P10 tip to either pop the bubbles or move it to the end of the gel. Insert the 10 well comb.
   f. Allow the agarose to solidify and cool down.
2. Prepare sample by adding 5 µL of sample buffer to the reaction.
3. Load the sample (all 20 µL) in the 0.75% agarose gel and run the sample for 45 min at 100 V in the cold room.
4. Place the Visi-Blue converter plate on top of the UV transilluminator, and place a glass plate on the top of the coverter plate for cutting the gel. Wear dark reader glasses or place the amber screen over the gel in order to visualize the bands.
5. To determine whether the PCR was successful, look for the appropriate size band for the product. If the bands are at the correct size, and the intensity is good (i.e. don't have to expose the gel for a long time), continue to the next step.
6. Excise the gel with the appropriate size PCR product band, and continue with PCR product purification.

PCR Product Purification

Reagents:

Dry Reagents	Wet Reagents
• Supplied by Qiagen PCR Purification Kit #28104 • If need additional columns, can order from Denville CM500-250, which are compatible with Qiagen buffers	• Supplied by Qiagen PCR Purification Kit #28104

Procedures:

1. Follow the protocol provided by Qiagen PCR Purification Kit #28104.
2. Elute the DNA with warm (i.e. 50 °C) nuclease-free H_2O so that the buffer won't affect the ligation.
3. After elution, make sure to quantify the amount of DNA By using the Nandrop.

Restriction Digest

Reagents:

- Keep all wet reagents at 4 °C.
- Make sure the NEBuffer does not have any precipitates

Dry Reagents	Wet Reagents
• 0.2 mL PCR tube (GeneMate, C-3328-2)	• 10X NEBuffer (NEB, depends on which restriction enzymes you use). • 10X BSA (NEB, B9001S), if required. • Restriction Enzymes (NEB, depends on which ones you use). • Nuclease-free H_2O

Procedures:

1. Use CLC sequence viewer to determine the restriction cut sites that you are going to use.
2. Set up the following reaction in a sterile microcentrifuge tube, adding the restriction enzyme last.

Reagents	Amounts
DNA (0.5 to 1 µg)	1 to 5 µL
10X NEBuffer	2 µL
10X BSA (if needed)	2 µL
Restriction Enzymes	0.3 to 1 µL (1 to 4 units per enzyme)
Nuclease-free H_2O	to 20 µL
Total	20 µL

   - Always make a master mix and aliquot into the samples.
   - Check the compatibility of the buffer with the restriction enzyme by looking up https://www.neb.com/tools-and-resources/interactive-tools/double-digest-finder
   - Make sure to use the buffer that has the highest % activity for the two enzymes chosen.
   - Check if BSA is required for a particular pair of restriction enzymes.
   - Always try to get High Fidelity enzymes (HF). These enzymes have reduced star activity (non-specific digestion), and have 100% activitiy in Buffer 4 (CutSmart Buffer in May 2013).
   - Include a negative control of no enzyme (uncut)
3. Gently mix the reaction flicking the reaction and then centrifuge briefly to collect the reagents to the bottom of the tubes.
4. Incubate at the recommended temperature and time. The reaction is usually at 37 °C for 1 hour. If using High Fidelity enzymes (HF), can incubate as short as 15 min.
5. Terminate the reaction by heat inactivation if mentioned for the reaction enzyme. This can be found at https://www.neb.com/tools-and-resources/interactive-tools/enzyme-finder and search for your specific enzyme. This is usually 65 ºC for 20 min, or 80 ºC for 20 min.
6. Run the whole sample on a 0.75% gel. Make sure to load the negative control for both the vector and the insert to verify that the restriction digest has worked.

7. Repeat **PCR Product Purification** and **PCR Product Purification**.

Ligation Reaction

Reagents:

- Keep all wet reagents at 4 °C.
- Make sure the NEBuffer does not have any precipitates

Dry Reagents	Wet Reagents
• 0.5 mL low DNA-binding microcentrifuge tubes	• Promega T4 DNA Liganse (Cat# 26808109) • Promega Ligase Buffer (Cat# 27464304) • Nuclease-free H_2O

Procedures:

1. Briefly centrifuge the digested vector and insert, ligase buffer, and ligase to collect the reagents to the bottom of the tubes.
2. Set up a 1:1, 2:1, 3:1 molar ratio of insert:vector DNA by the following calculations:

$$\frac{\text{ng of vector x kb (size of insert)}}{\text{kb (size of vector)}} \times \text{Molar ratio of } \frac{\text{Insert}}{\text{Vector}} = \text{ng of insert}$$

   - Example: if the insert is 1500 bp, and vector is 7031 bp, and want to use 50 ng of vector, then how much ng of insert is needed for a 2:1 reaction?

$$\frac{\text{50 ng of vector x 1500 bp (insert)}}{\text{7031 bp (vector)}} \times \text{Molar ratio of } \frac{\text{2 Insert}}{\text{1 Vector}} = \text{21.3 ng of insert}$$

3. Set up the following reactions, adding the enzyme last. Note that the volume can be scaled up linearly if required.

Reaction Components	**Control**	**1:1**	**2:1**	**3:1**
10X Ligation Buffer, T4 DNA ligase	1 µL	1 µL	1 µL	1 µL
Linear Vector (50 ng)	1 µL	Variable	Variable	Variable
PCR product (Insert)	0 µL	Variable	Variable	Variable
T4 DNA ligase (3 Weiss U/µL)	0.5 µL	0.5 µL	0.5 µL	0.5 µL
ddH2O	5.5 µL	Variable	Variable	Variable
Total	10 µL	10 µL	10 µL	10 µL

4. Mix the reactions by pipetting up and down.
5. Incubate the reactions for 3 hour at room temperature.
   - After the reactions are complete, can store at -20 °C if required for a maximum of 1 week.
   - If positive control for the transformation worked, but the transformations from the ligations did not, can set up higher ligation ratios if required (i.e. 10:1, or even 30:1).
6. Heat inactivate by placing the reactions at 65 °C for 10 minutes to inactivate any proteins in the mixture and to dissociate noncovalently ligated DNA ends.

Day 2 (Transformation):

Transformation

Reagents:

- Keep all wet reagents at 4 °C.

Dry Reagents	Wet Reagents
• Spreading loop	• Competent DH5α bacterial cells • LB broth, no antibiotic

Procedures:

1. Preheat the following equipments
   a. Heat block: 42 °C

b. Shaking incubator: 37 °C
c. Appropriate drug resistant agar plate (i.e. ampicillin or kanamycin): warm to room temperature.

2. Bring competent bacterial cells out of the –80 °C and thaw it on ice. Should take around 10 minutes.
3. Add 5 µL of the ligation reaction to the 1.5 mL tube containing the competent cells (should contain 50 µL). Mix gently with the pipette by stirring, not pipetting up and down.
   - Add a negative control (5 µL ddH_2O instead of ligation reaction), and a positive control (5 µL of complete vector, i.e. uncut vector).
4. Incubate on ice for 30 minutes.
5. Incubate at 42 °C heat block for 45 seconds.
6. Incubate on ice again for 2 minutes.
7. Add 900 µL of SOC media without drug to the 1.5 mL tubes containing the competent bacterial cells and the ligation mix.
8. Incubate for 1 h at 37 °C at 200 rpm on a shaking incubator.
   - Colour should turn from clear to cloudy.
9. Pipette 50 µL of bacterial colony onto the plate and spread using the spreading loop. Try not to poke the agar plate. Repeat with 200 µL of bacterial colony onto a second plate
10. Once the spreading is done on both halves, invert the plate and incubate at 37 °C overnight.

Day 3 (Overnight Culture):

Overnight Culture (Small Scale)

Reagents:

- Keep all wet reagents at 4 °C.

Dry Reagents	Wet Reagents
• Inoculation loop • 15 mL polypropylene culture tube	• LB broth with antibiotic (ampicillin or kanamycin)

Procedures:

1. The next morning, check to see whether there are colonies.
   - Look for white and cloudy colonies.
   - Very small clear colonies are bad.
   - Also check to see whether negative control (i.e. ddH_2O) has any colonies.
2. If enough colonies are found (i.e. 2 to 4 colonies for one sample), circle around the colonies that you want to pick.
3. Saran wrap or parafilm the plates and place in 4 °C. Will not pick the colonies until approximately 4:30 pm because don't want the culture to overgrow.
4. Prepare growth media by adding 5 mL of LB medium with antibiotic (ampicillin at final concentration of 50 µg/mL) into each 15 mL polypropylene bacterial culture tube.
   - Label clearly with the plasmid and the number.
   - Make one tube of negative control (i.e. no colony).
5. At 4:30 pm, use a inoculation loop, and (literally) pick a colony from the agar. Move the loop up and down in the LB medium to ensure that the colony has transferred into the liquid medium.
6. Label clearly with the plasmid and the number.
7. Make one tube of negative control (i.e. no colony).
8. Cap the tubes loosely to allow for air flow.
9. Incubate overnight on a shaker at 37 °C at 200 rpm.

Day 4 (Miniprep)

Miniprep

Reagents:

- Keep all wet reagents at 4 °C.

Dry Reagents	Wet Reagents
• Spreading loop • Qiagen Mini Kit #12125	• LB broth • 50 mg/mL stock ampicillin • 50% glycerol in ddH_2O

Procedures:

1. The next day, take 500 µL of the bacterial culture and combine it with 500 µL of 50% glycerol. Vortex, and store at – 80 °C. Make sure that this culture is labeled precisely how the original culture is labeled, since if the clone is confirmed in later stages, the large scale growth will come from the glycerol stock.
2. With the remaining bacterial culture, follow the protocol from Qiagen Mini kit #12125 to obtain plasmids from each colony.

APPENDIX I

CALCIUM PRECIPITATION – 293T CELL TRANSFECTION

Day 1 (around 9 am) – Plating of 293T Cells

Reagents:

Dry Reagents	Wet Reagents
• 100 mm cell culture plate (BD Bioscience, 353803)	• Complete DMEM media (see below) • Dulbecco's phosphate buffered saline (Gibco, 14190) • 0.05% Trypin-EDTA (Gibco, 25300)

- Complete media

	Vol (mL)	%	Stock Conc	Final Conc
DMEM, high glucose formula (Gibco, 10569-010)	500	88.34		
FBS (Hyclone, SH30070.03)	55	9.72		
Pen-strep(Gibco, 15140-148)	5.5	0.97	P 10000 U/mL S 10 mg/mL	P 100 U/mL S 0.1 mg/mL

Procedures:

1. Warm all media, DPBS, and trypsin to room temperature.
2. Put complete media into plate. Incubate at 37 ºC incubator until seeding.

Size of Plate	Amount of media
6 wells	1.5 mL
12 wells	500 µL

3. From the master flask (T175) of 293T cells (i.e. this is the flask that is continuously passaged), aspirate off the media and then wash the cells with ~5 mL of DPBS.
4. Aspirate off the DBPS, and add 3 mL of trypsin to the flask. Incubate in the 37 ºC incubator for 3 min. Move the flask around so that trypsin can be distributed around the plate. Check under a microscope to see whether all the cells have been dislodged. This should take no more than 5 minutes.
5. Harvest the cells by adding 7 mL of media to the flask, and transferring the 10 mL into a 50 mL conical tube. Add an additional 5 mL of complete media to the flask to wash. Combine with the previous 10 mL to have a final volume of 15 mL of media.
6. Count cell concentration using a hemacytometer.
7. Centrifuge cells at 100 g for 5 min. Aspirate off the supernatant.
8. Resuspend the 293T cells in complete media. Plate 293T cells by seeding 500 µL dropwise into each plate. This will allow the density of the cells to reach around 80% confluent.

Size of Plate	Cell Concentration for Seeding
6 wells	5×10^5 cells/500 µL
12 wells	2.5×10^5/500 µL

   a. Density is very important because transfection efficiency goes down if cells are too clumped together.

Day 2 – 4 (start around 9 am) – Virus preparation in 293T cells

Reagents:

Dry Reagents	Wet Reagents
• 1.5 mL Eppendorf tube • 0.45 µm Acrodisc® Syringe Filter with HT Tuffryn® Membrane (Pall Life Science, 4184)	• Complete DMEM media (see above) • Dulbecco's phosphate buffered saline (Gibco, 14190) • 0.05% Trypin-EDTA (Gibco, 25300) • 2M $CaCl_2$, filtered. Stored in -20 °C

	• 50 mM chloroquine, filtered. Stored in -20 °C • 2X Transfection Buffer (see below)

- 2X Transfection Buffer
  - Adjust pH to 7.5 (very critical for the success of the infection). pH will drift over time, so make fresh batch if problems arise.
  - Filter sterilize after pH is adjusted.
  - Store in -20 °C. Buffer can freeze-thaw a couple of times without compromising transfection efficiency.

	Amount	Final Conc
HEPES	6.5 g	50 mM
NaCl	8.0 g	270 mM
Na_2HPO_4	0.106 g	1.5 mM
ddH2O	500 mL	

Procedures:

1. Warm complete media and DPBS to room temperature.
2. Take out the 100 mm plate that contains the plated 293T cells.
3. Aspirate off the media and wash with ~5 mL of DPBS.
4. Aspirate off the DPBS and add complete media into the wells.

Size of Plate	Amount of media
6 wells	2 mL
12 wells	750 µL

5. Prepare 1.5 mL Eppendorf tubes for each plasmid that will be transfected (see table below).

Size of Plate	DNA	ddH_2O
6 wells	5 µg	Up to 94 µL
12 wells	2 µg	Up to 37.5 µL

6. Add 2M $CaCl_2$ into the Eppendorf tube. Mix well by vortexing.

Size of Plate	2M $CaCl_2$
6 wells	31.25 µL
12 wells	12.5 µL

7. Set the vortexer to a speed of 6, vortex the Eppendorf tube containing i) DNA; ii) ddH_2O; and iii) $CaCl_2$; and add 500 µL of transfection buffer dropwise to the plasmid tube while the tube is vortexing.

Size of Plate	Transfection Buffer
6 wells	125 µL
12 wells	50 µL

8. Add 50 mM chloroquine into the plate immediately before adding the DNA content from 3.

Size of Plate	50 mM chloroquine
6 wells	1 µL
12 wells	0.4 µL

9. Add the mixture from Step 3 into the appropriate plate dropwise with gentle swirl of the plate. Quickly replace the dish in the incubator once the batch is complete.
   - Add dropwise to spread the DNA around the plate. Cells die easily if DNA is too concentrated in one area.
   - There may be a pH change (i.e. colour change). This is normal.
10. After 6 hours, replace the media with fresh complete media. Do not wash with DPBS.

Size of Plate	Amount of media
6 wells	2 mL
12 wells	1 mL

11. Incubate for 24 hours. The next day, can check for transfection efficiency under the microscope.

APPENDIX J

GENERATING LENTIVIRUS

Purpose: To generate lentivirus to transducer plasmids into cells. Lentiviral transduction has been tested on NIH 3T3 cells and primary $CD4^+$ T cells.

Day 1 (around 9 am) – Plating of 293T Cells

Reagents:

Dry Reagents	Wet Reagents
• 100 mm cell culture plate (BD Bioscience, 353803)	• Complete DMEM media (see below) • Dulbecco's phosphate buffered saline (Gibco, 14190) • 0.05% Trypin-EDTA (Gibco, 25300)

- Complete media

	Vol (mL)	%	Stock Conc	Final Conc
DMEM, high glucose formula (Gibco, 10569-010)	500	88.34		
FBS (Hyclone, SH30070.03)	55	9.72		
Pen-strep(Gibco, 15140-148)	5.5	0.97	P 10000 U/mL S 10 mg/mL	P 100 U/mL S 0.1 mg/mL

Procedures:

9. Warm all media, DPBS, and trypsin to room temperature.
10. Put 10 mL of media into each P100 mm plate. Incubate at 37 ºC incubator until seeding.
11. From the master flask (T175) of 293T cells (i.e. this is the flask that is continuously passaged), aspirate off the media and then wash the cells with ~5 mL of DPBS.
12. Aspirate off the DBPS, and add 3 mL of trypsin to the plate. Incubate in the 37 ºC incubator for 3 min. Move the flask around so that trypsin can be distributed around the plate. Check under a microscope to see whether all the cells have been dislodged. This should take no more than 5 minutes.
13. Harvest the cells by adding 7 mL of media to the flask, and transferring the 10 mL into a 50 mL conical tube. Add an additional 5 mL of complete media to the flask to wash. Combine with the previous 10 mL to have a final volume of 15 mL of media.
14. Count cell concentration using a hemacytometer.
15. Centrifuge cells at 800 rpm for 3 min. Aspirate off the supernatant.
16. Resuspend the 293T cells to a final concentration of 6×10^6 cells/mL in complete media. Plate 293T cells in 100 mm plate by seeding 1 mL (6×10^6 cells) dropwise into each plate. This will allow the density of the cells to reach around 80% confluent by Day 2.
    a. Density is very important because infection efficiency goes down if cells are too clumped together.

Day 2 – 4 (start around 9 am) – Virus preparation in 293T cells

Reagents:

Dry Reagents	Wet Reagents
• 1.5 mL Eppendorf tube • 0.45 μm Acrodisc® Syringe Filter with HT Tuffryn® Membrane (Pall Life Science, 4184)	• Complete DMEM media (see below) • Dulbecco's phosphate buffered saline (Gibco, 14190) • 0.05% Trypin-EDTA (Gibco, 25300) • 2M $CaCl_2$ (Fisher, C79-500), filtered. Stored in -20 °C • 50 mM chloroquine (MP Bio, 193919), filtered.

	Stored in -20 °C • 2X Transfection Buffer (see below) • pGag.pol and pHCMV-G (for MSCV plasmid) • pLP1, pLP2, and pVSV-G (for lentiviral plasmid)

- 2X Transfection Buffer
  - Adjust pH to 7.5 (very critical for the success of the infection). pH will drift over time, so make fresh batch if problems arise.
  - Filter sterilize after pH is adjusted.
  - Store in -20 °C. Buffer can freeze-thaw a couple of times without compromising transfection efficiency.

	Amount	Final Conc
HEPES (Acros Organics, 3272610000)	6.5 g	50 mM
NaCl (Sigma, S3014-1KG)	8.0 g	270 mM
Na_2HPO_4 (Fisher, S373-500)	0.106 g	1.5 mM
ddH2O	500 mL	

- Complete media

	Vol (mL)	%	Stock Conc	Final Conc
DMEM, high glucose formula (Gibco, 10569-010)	500	88.34		
FBS (Hyclone, SH30070.03)	55	9.72		
Pen-strep(Gibco, 15140-148)	5.5	0.97	P 10000 U/mL S 10 mg/mL	P 100 U/mL S 0.1 mg/mL

Procedures:

12. Warm complete media and DPBS to room temperature.
13. Take out the 100 mm plate that contains the plated 293T cells.
14. Aspirate off the media and wash with 3 mL of DPBS.
15. Aspirate off the DPBS and add 10 mL of complete media onto the cell.
16. Prepare 1.5 mL Eppendorf tubes for each plasmid that will be transfected (see table below).

DNA	pLP-1	pLP-2	pVSV-G	ddH_2O
24 µg	16 µg	6 µg	8 µg	Up to 375 µL

17. Add 125 µL of 2M $CaCl_2$ into the Eppendorf tube. Mix well by vortexing.
18. Set the vortexer to a speed of 6, vortex the Eppendorf tube containing i) DNA; ii) ddH_2O; and iii) $CaCl_2$; and add 500 µL of transfection buffer dropwise to the plasmid tube while the tube is vortexing.
19. Add 8.4 µL of 30 mM chloroquine into the well immediately before adding the DNA content from 3.
20. Add the mixture from Step 3 into the appropriate well dropwise with gentle swirl of the plate. Quickly replace the dish in the incubator once the batch is complete.
    - Add dropwise to spread the DNA around the plate. Cells die easily if DNA is too concentrated in one area.
    - There may be a pH change (i.e. colour change). This is normal.
21. After 6 hours, replace the media with fresh 5 mL of complete media. Do not wash with DPBS.
22. Incubate for 24 hours. Collect the media at 48 h, 52 h, and 56 hours after transfection. Collect the media by taking up the 5 mL of media and put it in a 50 mL conical tube. Replace the plate with 5 mL of fresh media, and place it back in the incubator. Store collected media at 4 °C (i.e. fridge) until all fractions have been collected. Pool all the fractions (i.e. collect the media after 48 h, 52 h, and 56 h in the same 50 mL conical tube), and
23. Once all the fractions have been collected, filter the supernatant through a 0.45 µm syringe filter into 50 mL conical tubes. Can only have approximately 30 mL of supernatant in each conical tube since will be adding additional solutions into the supernatant for concentrating.

Day 4 – 5 – Virus Concentration (Lenti-X Concentrator)

Reagents:

Dry Reagents	Wet Reagents
• 1.5 mL Eppendorf tube • 50 mL Conical tube	• Complete RPMI Media (see below) • Lenti-X Concentrator (Clontech, 631231)

- Complete RPMI Media

	Vol (mL)	%	Stock Conc	Final Conc
RPMI (Irvine Scientific, 9159)	500	88		
Heat-inactivated FBS (Irvine Scientific, 300320439)	50	10		
Glutamax (Gibco, 35050-061)	5.5	1	200 mM	2 mM
Pen-strep (Gibco, 15140-148)	5.5	1	P 10000 U/mL S 10000 μg/mL	P 100 U/mL S 100 μg/mL

Procedures:

1. After filtering the supernatant through the 0.45 μm syringe filter, add 1 volume of Lenti-X concentrator to 3 volumes of supernatant. Mix by inversion.
    - Just need a rough estimate of the volume of supernatant (some will be loss during the filtering). Divide the amount by 3 and that's the amount of Lenti-X concentrator to add.
    - For example, if you have 30 mL of viral supernatant, 30/3 = 10 mL of Lenti-X concentrator to add.
2. Incubate the mixture at 4 ºC overnight.
3. Centrifuge samples at 1500 g for 45 min at 4 ºC. After centrifugation, an off-white pellet will be visible.
4. Carefully remove supernatant while not disturbing the pellet.
5. Gently resuspend the pellet in 1:5 or 1:10 of the original volume (i.e. If start with 30 mL, resuspend in 3 mL for 1:10 concentration). The pellet will be sticky, but should go into solution quickly.
6. Incubate for 10 min in the fridge to allow the pellet to fully dissolve, then immediately aliquot the samples in 1 mL volume. Store at -80 ºC.

Day 4 – 5 – Virus Concentration (Ultracentrifuge)

Procedures:

1. Alternatively, if Lenti-X concentrator is not available, one can concentrate the virus using an ultracentrifuge.
2. Put the viral supernatants into Beckman 1X3-1/2 P.A. Tube (Beckman, 326823) or compatible tubes. Need to fill up the tube close to full so that the tube does not collapse during the spin.
3. Need to balance the tubes by adding media to the tubes.
    - Balancing is extremely important because if the tubes are not balanced properly, then the ultracentrifuge will not operate. Further, imbalance will damage the ultracentrifuge and even cause injuries!
4. Put the tubes in the SW28 rotor, and spin at 25000 rpm for 1.5 hr at 4 ºC.
    - Set the centrifuge at 1.75 h since it takes awhile for the ultracentrifuge to reach 25000 rpm.
5. After the spin, carefully take out the tubes and remove the supernatant gently. One should see a very small white pellet at the bottom of the tube.
6. If you have more supernatant (i.e. same virus), then you can repeat steps 2 – 5 again to pellet more virus until all the supernatant is concentrated.
7. Pellet can be suspended into appropriate medium. The solution is stored in the fridge overnight to allow the pellet to fully dissolve.
7. The next day, aliquot the samples in 1 mL volume. Store at -80 ºC.

APPENDIX K

LENTIVIRAL TRANSDUCTION OF $CD4^+$ T CELLS

Purpose: To infect $CD4^+$ T cells with lentivirus containing PH-PLCδ1-GFP in order to examine colocalization of $PI(4,5)P_2$ with the plasma membrane (CellMask PM marker), and the nucleus (DAPI).

Reagents:

Dry Reagents	Wet Reagents
• 6 well plates • 15 mL conical tubes • Chamber coverglass (Nunc, 155380)	• Leibovitz's media (Gibco, 21083-02) • Sterile PBS • CellMask Deep Red plasma membrane stain (Life Technologies, C10046) • DAPI (Life Technologies, D1306) • 4 mg/mL polybrene (Sigma, H9269-10G)

- Complete RPMI Media

	Vol (mL)	%	Stock Conc	Final Conc
RPMI (Irvine Scientific, 9159)	500	87		
Heat-inactivated FBS (Irvine Scientific, 300320439)	50	10		
Glutamax (Gibco, 35050-061)	5.5	1	200 mM	4 mM
Pen-strep (Gibco, 15140-148)	5.5	1	P 10000 U/mL S 10000 µg/mL	P 100 U/mL S 100 µg/mL

  - 2-mercaptoethanol (Sigma, M7522) must be added fresh to the media.
    - Dilute 1 µL of 2-mercaptoethanol in 1.43 mL of complete RPMI media. This makes a 10 mM solution.
    - Make 1:1000 dilution (i.e. if using 1 mL of media, then add 1 µL of the 10 mM solution) into the media to make a final concentration of 10 µM.
  - Recombinant mouse IL-2 (eBioscience, 14-9021). Must be added fresh to the media.
    - Stock concentration at 100 µg/mL. Make 1:2500 dilution into media to achieve a final concentration of 40 ng/mL.

Isolation of splenic $CD4^+$ T cells (Day 1)

1. Follow isolation of splenic $CD4^+$ T cell protocol.
2. Resuspend the cell pellet in warm complete RPMI media to a final concentration of 12 x 10^6 cells/mL.
3. Seed 1 mL of $CD4^+$ T cells into each well. Need the following number of wells:
4. Incubate for at least 1 hr at 37 ºC, 5% CO_2 before viral transduction.

Viral transduction of PH-PLCδ1-GFP into $CD4^+$ T cells (Day 1)

1. Dilute polybrene to 8 µg/mL in complete RPMI media. Add 20 µL of polybrene stock to 1 mL of complete RPMI media.
2. Quickly thaw the virus in the water bath and once thawed, immediately add 100 µL of diluted polybrene to 1 mL of virus.
3. Incubate for at least 36 hr at 37 ºC, 5% CO_2. Protect the cells transduced from light.

Coating (Day 2)

1. Dilute 10X poly-L-Lysine solution (Sigma, P8920) with sterile H_2O to 1X (0.1% w/v to 0.01% w/v).
2. Precoat Lab-Tek 2-well chambered coverglass (Nalge, 154461) with 0.01% poly-L-lysine by adding 2 mL of 0.01% poly-L-Lysine/well for 30 min at room temperature. Replace the lids back on while the chamber slides are incubating.
3. Aspirate excess solution and sterile the slides under UV light for 1 hr. Leave the lids off.

4. On **Day 3**, wash chambered coverglass with 1 mL of warm Leibovitz's media once. Add the warm media into each chamber, shake gently by hand, and then aspirate off the media.
5. Prewarm the coated chambered coverglass with 200 μL of warm Leibovitz's media. Leave in the incubator until seeding.

Dye Loading (Day 3)

1. Collect the cells into 15 mL conical tubes by pipetting up and down vigorously to dislodge the cells from the plastic bottom. Wash the wells with 2 mL of complete RPMI media, pipette up and down, and collect into the conical tubes. Repeat once more.
2. Check under the microscope to ensure that most of the cells have been collected. If not, repeat the wash step described above.
3. Spin down the cells at 350 g, 5 min, room temperature. Aspirate off the media.
4. Wash the cells once with PBS. Take 20 μL and count using a Coulter counter.
5. Spin down the cells at 350 g, 5 min, room temperature. Aspirate off the PBS.
6. Resuspend the cells to a final concentration of 5×10^6 cells/mL in Leibovitz's media.
7. Take the following over to Dr. Barhoumi's lab:
    1. P1000 pipette – seed cells.
    2. P1000 tips – seed cells.
    3. Coated chambered coverglass with 200 μL of Leibovitz's media.
    4. Resuspended cells in Leibovitz's media.
    5. Timer

Imaging (Day 3) – Dr. Barhoumi's Lab

1. Seed 1 mL of $CD4^+$ T cells into each well to achieve 5×10^6 cells per chamber. Incubate at 37 ºC, 5% CO_2 for 30 min to allow the cells to settle.
2. Bring to Dr. Barhoumi for imaging.

APPENDIX L

CROSSLINKING CHOLERA TOXIN B FOR IMMUNOFLUORESCENCE

Purpose: To examine the spatial relationships between specific protein of interest and GM1 ganglioside-enriched domains (i.e. lipid rafts) of the plasma membrane by crosslinking cholera toxin B.

Reagents:

Dry Reagents	Wet Reagents
• Coverglass (Corning, 2935-225) • Lab-Tek II 2-well glass chamber slide (Nalge, 154461)	• Sterile PBS (Gibco, 14190) • Vybrant Alexa Fluor 555 Lipid Raft Labeling Kit (Molecular Probes, V-34404) • 0.1%(w/v) Poly-L-Lysine solution (Sigma, P8920) • Coverglass antifade reagent medium (Invitrogen, P36934) • 100 mM glycine (Sigma, G7126) o Make 100 mM by dissolving 7.507 g of glycine in 1 L PBS • 20% PFA in PBS (EMS, 15713-S) • 10% Triton X-100 (Fluka, 93443) • Blocking solution o 1% IgG-free BSA (Roche, 03116956001) o 0.1% NaN_3 (Sigma, S2002) • 98.3% PBS (Gibco, 21600-069) • Rabbit anti-WASp (Santa Cruz, #sc-8353) • Alexa 568-Phalloidin (Invitrogen, A12380) • Goat anti-Rabbit Alexa 647(Invitrogen, A21246)

- Complete RPMI Media

	Vol (mL)	%	Stock Conc	Final Conc
RPMI (Irvine Scientific, 9159)	500	87		
Heat-inactivated FBS (Irvine Scientific, 300320439)	50	10		
Glutamax (Gibco, 35050-061)	5.5	1	200 mM	4 mM
Pen-strep (Gibco, 15140-148)	5.5	1	P 10000 U/mL S 10000 µg/mL	P 100 U/mL S 100 µg/mL

  - 2-mercaptoethanol (Sigma, M7522) must be added fresh to the media.
    - Dilute 1 µL of 2-mercaptoethanol in 1.43 mL of complete RPMI media. This makes a 10 mM solution.
    - Make 1:500 dilution (i.e. if using 1 mL of media, then add 2 µL of the 10 mM solution) into the media to make a final concentration of 20 µM.
  - Recombinant mouse IL-2 (eBioscience, 14-9021). Must be added fresh to the media.
    - Stock concentration at 100 µg/mL. Make 1:1250 dilution into media to achieve a final concentration of 80 ng/mL.
- PBS (from Vybrant Lipid Raft Labeling Kit)
  - Add 2 mL of 10X PBS to 18 mL of ddH2O.
  - Store a 4 ºC.
- Cholera Toxin subunit B (CTxB) Conjugate (from Vybrant Lipid Raft Labeling Kit).
  - Dissolve one vial of CTxB conjugate with 100 µL of PBS. This generates 1 mg/mL stock solution.
  - Aliquot into 5 µL and store at -20 ºC for 6 months.

- Anti-CTxB antibody (from Vybrant Lipid Raft Labeling KT).
  - Aliquot into 11 µL and store at -20 ºC for 6 months.

Procedures

Precoating chamber slides for seeding cells

1. Must perform this the day before the assay.
2. Dilute 10X poly-L-Lysine solution with sterile H_2O to 1X (0.1% w/v to 0.01% w/v).
3. Precoat Lab-Tek II 2-well glass chamber slides with 0.01% poly-L-lysine by adding 2 mL of 0.01% poly-L-Lysine/well for 30 min at room temperature. Replace the lids back on while the chamber slides are incubating.
4. Aspirate excess solution and sterile the slides under UV light for 1 hr. Leave the lids off.
5. The next day, wash chamber slides with 1 mL of warm complete RPMI once time. Add warm complete RPMI into each chamber, shake gently by hand, and then aspirate off the media.
6. Prewarm the coated chamber slides with 200 µL of warm complete RPMI at 37 °C for 30 min. Leave in the incubator until seeding.

Precoating chamber slides for plated CD3/CD28 activation

1. Must perform this the day before the assay.
2. Dilute 10X poly-L-Lysine solution with sterile H_2O to 1X (0.1% w/v to 0.01% w/v).
3. Precoat Lab-Tek II 2-well glass chamber slides with 0.01% poly-L-lysine by adding 2 mL of 0.01% poly-L-Lysine/well for 30 min. Replace the lids back on while the chamber slides are incubating.
4. Aspirate excess solution and sterile the slides under UV light for 1 hr. Leave the lids off.
5. Dilute anti-CD3 (stock 1 mg/mL) 1:1000 and anti-CD28 (stock 1 mg/mL) 1:100 in PBS in a single tube.
   - Example, if need 1 mL, add 1 µL of anti-CD3, 10 µL of anti-CD28, and 989 µL of PBS.
   - Add 200 µL of antibodies per chamber slide. For control (unstimulated), add 200 µL of PBS per chamber slide.
6. Incubate chamber slides on a shaker (gently) in the 4 °C walk-in cold room at a speed setting of 4, overnight. Replace the lids back on to ensure sterility.
7. The next day, wash chamber slides with 1 mL of warm complete RPMI once time. Add warm complete RPMI into each chamber, shake gently by hand, and then aspirate off the media.
8. Prewarm the coated chamber slides with 200 µL of warm complete RPM, at 37 °C for 30 min. Leave in the incubator until seeding.

Isolation of splenic $CD4^+$ T cells (Day 2)

1. Follow isolation of splenic $CD4^+$ T cell protocol.
2. Resuspend the cell pellet in warm complete RPMI media to a final concentration of 5×10^6 cells/mL.
3. Seed 1 mL/well dropwise by adding the cell suspension onto the 200 µL complete media in the well. This equates to 5×10^6 cells per well.
   - Final anti-CD3 concentration = 0.17 µg/mL (but is actually higher since plated, not suspended).
   - Final anti-CD28 concentration = 0.83 µg/mL (but is actually higher since plated, not suspended).
4. Incubate at 37 °C for 30 minutes.

Cholera Toxin B Labeling (Day 2)

1. Prepare Cholera Toxin B conjugate.
   - Dilute CTxB conjugate 1:1000 in chilled RPMI media. Each sample requires 2 mL of working conjugate, so add 2 µL of conjugate in 2 mL of chilled RPMI media per sample.
2. Prepare CTxB antibody.
   - Dilute the antibody 1:200 in chilled RPMI media. Each sample requires 2 mL of working CTxB antibody, so add 10 µL of working CTxB antibody in 2 mL of chilled RPMI media per sample.

3. After the 30 min incubation at 37 ºC, wash the cells in the chamber slides with ice cold PBS 3 times for 2 min each.
4. Add 2 mL of working CTxB conjugate into each well and incubate for 10 min at 4 ºC.
5. Wash the cells in the chamber slides with ice cold PBS 3 times for 2 min each.
6. Add 2 mL of working CTxB antibody into each well and incubate for 15 min at 4 ºC.
7. Wash the cells in the chamber slides with ice cold PBS 3 times for 2 min each.

Fixing the Cells (Day 2)

Protect the samples from light at this point.

7. Make 4% PFA by combining 4 mL of 20X PFA and 16 mL of PBS.
   - Always make PFA fresh (i.e. the same day of experiment).
8. Fix the cells in the freshly made 4% PFA for 20 min at 4 ºC.
9. Rinse the samples with PBS 2 times for 2 min each, and incubate cells with 2 mL of 10 mM glycine in PBS for 10 min at room temperature.
   - This step is performed to quench aldehyde groups.
   - Stock at 100 mM, so dilute 1:10 in PBS.
10. Wash the chamber slides with PBS 2 times for 2 min each, and permeabilize the cells by using 2 mL of 0.2% Triton X-100 in PBS for 5 min at room temperature.
    - Stock at 10%, so dilute 1:50 in PBS.
11. Wash the chamber slides with PBS 3 times for 2 min each.
12. Incubate cells in blocking solution at 4 °C overnight in a humid chamber.
    - Humid chamber consists of the plastic slide holders. Alternate between slide and wet Kimwipe PBS. Cover with foil paper to prevent evaporation.

Applying Antibody (Day 2 – 3)

8. Wash the chamber slides with PBS 3 times for 2 min each.
9. Dilute the antibody in the following manner in the dark.

Antibody	Stock	Dilution	Final	Per well
Phalloidin	200 U/mL	1:10	20 U/mL	20 µL antibody + 180 µL Blocking
Anti-WASp	200 µg/mL	1:50	4 µg/mL	4 µL antibody + 196 µL Blocking

10. Incubate each chamber slide with 200 µL per well at room temperature for 1 hr in a humid chamber. The slides much be protected from light.
    - Wrap aluminum foil around the humid chamber and put in a drawer for extra protection against light exposure.
    - Cells are labeled much better when antibodies applied sequentially. This means that only one antibody is incubated in each well for 1 hr, followed by 2 washes with PBS for 2 min each, and then add the second antibody. The order of application does not seem to affect the fluorescence, but typically if one antibody is much stronger, apply that one first.
11. **(If required)** Dilute the secondary antibody in the following manner in the dark.

Antibody	Stock	Dilution	Final	Per well
Goat anti-Rabbit Alexa 647	2 mg/mL	1:300	6 µg/mL	0.67 µL antibody + 199.4 µL Blocking

12. Incubate each chamber slide with 200 µL per well at room temperature for 1 hr in a humid chamber. The slides much be protected from light.
    - Wrap aluminum foil around the humid chamber and put in a drawer for extra protection against light exposure.
13. Prepare the ProLong medium during the last 1 hr antibody incubation by thawing at room temperature for 1 hr (stored in -20 °C freezer).
14. Wash the chamber slides with PBS 3 times for 2 min each.

Preparation for Wash (Day 3)

8. Use slide separator to remove the chamber. Put slides on a slide holder for subsequent washes.

9. Incubate the slides in 70% ethanol once for 2 min.
10. Incubate the slides in 95% ethanol once for 2 min.
11. Incubate the slides in 100% ethanol once for 2 min.
12. Incubate slides in fresh xylene twice for 2 min each. This means that one would need two fresh xylenes.
13. Apply a small amount of antifade reagent medium mixture to the coverglass. Cover the slide while it is still wet.
    - Use a glass rod to line the antifade reagent medium on the side of the coverglass, and then cover the slide at a 45° angle to avoid bubbles.
    - Use a razor blade to help with the coverslip.
14. Place the slide on a flat surface in the dark to dry overnight at room temperature in the fume hood. Protect from light.

Finalizing the Slides (Day 3)

4. Seal the coverglass to the slide with fingernail polish to prevent shrinkage of mounting medium and subsequent sample distortion.
5. After sealing, let it dry for at least 15 min, then store the slide upright in a slide box at -20°C. Desiccant may be added to the box to ensure that the slide remains dry.
6. Examine sample under fluorescence microscopy.

Notes:

- Vybrant Lipid Raft Labeling Kit → excitation (555 nm) and emission (565 nm). We use Alexa 647-CTxB to avoid bleedthrough of Alexa 555-CTxB into the green channel.
- Adopted from Vybrant Lipid Raft Labeling Kits product information. Published protocol from Chazotte B., (2011), *Cold Spring Harb Protoc* **5**: 576-578.
- Please see van Zanten TS *et al.* PNAS (2010) for comments on why labeling and crosslinking CTxB is conducted at 4 ºC. Also see Tanaka KA *et al* Nat Methods (2010) for comments on mobility of molecules (proteins and lipids) even after chemical fixation.

APPENDIX M

CFSE LABELING OF $CD4^+$ T CELLS

Objective: To measure T-cell proliferation by dilution of CFSE dye in daughter cells.

Materials:

Dry Reagents	Wet Reagents
• Titertube Micro Test Tubes (Bio-Rad, #223-9391).	• BSA, IgG free (Boehringer Mannheim Laboratory Reagents, #100018) • PBS/0.1% BSA (see below). • CellTrace CFSE Cell Proliferation kit (Invitrogen #C34554) • RPMI Complete Media (see below)

- PBS/0.1% BSA: Filter thorough 0.2 µm filter to sterilize.
- CFSE:
  - Not light-sensitive until bound to amino acids in cells.
  - To prepare 5 mM CFSE working stock, dissolve one vial (component A) in 18 µl DMSO (component B) immediately before use.
- Complete RPMI Media

	Vol (mL)	%	Stock Conc	Final Conc
RPMI (Irvine Scientific, 9159)	500	87		
Heat-inactivated FBS (Irvine Scientific, 300320439)	50	10		
Glutamax (Gibco, 35050-061)	5.5	1	200 mM	4 mM
Pen-strep (Gibco, 15140-148)	5.5	1	P 10000 U/mL S 10000 µg/mL	P 100 U/mL S 100 µg/mL

  - 2-mercaptoethanol (Sigma, M7522) must be added fresh to the media.
    - Dilute 1 µL of 2-mercaptoethanol in 1.43 mL of complete RPMI media. This makes a 10 mM solution.
    - Final concentration of 10 µM in the culture is required.

Procedures:

Preparation of anti-CD3/anti-CD28 Stimulation Plate (Day 0)

1. The day before labeling, precoat 96 well round bottom culture plate with anti-CD3 by diluating anti-CD3 in PBS 1:1000. Add 200 µL per well.
2. Seal the plate, store at 4°C overnight.
3. The next day, discard the anti-CD3 solution, and add anti-CD28 diluted in complete media (with 2-mercaptoethanol) at 1:100 dilution (final concentration in culture = 5 µg/mL). Incubate at 37 °C until ready to seed.

Labeling $CD4^+$ T cells with CFSE

10. Follow isolation of splenic $CD4^+$ T cell protocol.
11. Resuspend cells at 1 x 10^6 cells in 1 mL PBS/0.1% BSA (need 2 x 10^6 cells/in 2 mL PBS/0.1%BSA).
12. Add 2µl of 5 mM CFSE/ 1x10^6 cells in the tube containing cells (add **4** µL to the 2 x 10^6 cell vial). Vortex immediately at highest setting for 3 sec. **Now, CFSE is light-sensitive!**
13. Incubate at 37 ^oC. (in water bath) for 10 min .
14. Add 5x volume of **ice-cold** RPMI 1640/10% HI-FBS into the cell suspension (so add **10** mL to the 2 ml cells), swirl the tube 2-3 times, and incubate for 5 min on ice.
15. Centrifuge at 350 g for 5 min to pellet the cells. Aspirate the supernatant.

16. Resuspend the cell pellet in sterile PBS at RT (use 5 mL), spin down (350 g, 5 min at RT) and aspirate supernatant.
17. Resuspend cells in 1 mL complete media with 2-mercaptoethanol. (final cell density at 2 x10^6 cells/ml)

Culture and Flow

1. Add 100 µL cells (0.2 x 10^6 cells per well) to each well so that the final volume is 200 µL.
2. Incubate at 37 °C for 3 days.
3. After culture, spin down culture plate at 350 g for 5 min at RT. Using 200 uL multi-channel pippette, aspirate supernatant.
    - You don't need to aspirate all the supernatant. Instead, leave a little bit of supernatant to avoid touching the plate bottom.
    - Tip: Angle the plate slightly and pipette against the wall to avoid touching the bottom of the plate.
4. Tap plate to resuspend the cells with residual medium. Add 200 uL staining buffer into each culture well and spin down at 350 rpm for 5 min at RT.
5. Aspirate supernatant as described in step 3.
6. Resuspend cells in 100 uL staining buffer.
7. Transfer cell suspension into the small flow Titertubes.
8. Keep samples on ice until analysis.
9. Run flow cytometery. CFSE is detected in FL-1 channel.

APPENDIX N

MONITORING POST-TRANSLATIONAL MODIFICATIONS IN $CD4^+$ T CELLS

USING IMMUNOPRECIPITATION

Purpose: To immunoprecipitate azido-palmitic acid-labeled proteins generated from $CD4^+$ T cells incubated with the probe for downstream detection of specific proteins of interest (i.e. LAT, LCK, FYN, CD4).

Reagents:

Dry Reagents	Wet Reagents
• 15 mL conical tube • 1.5 mL microcentrifuge tube • 35 mm plates • NMWL 3000 centrifugal filter device (Millipore, UFC500396)	• Complete RPMI media (with FBS) • Complete RPMI media, serum free (without FBS) • Click-iT palmitic acid, azide (Invitrogen, C10265) • Pierce BCA Protein Assay Kit (Thermo Scientific, 23225 or 23227) • ddH2O • Methanol (CH_3OH) • Chloroform ($CHCl_3$) • Protein G Dynabeads (Invitrogen, #100.04D) • DynaMagnet (Invitrogen, #123.21D, #123.22D) • Rabbit polyclonal IgG anti-Lck (Millipore, #06-583) • Rabbit polyclonal IgG anti-LAT (Millipore, #06-807) • 5X Pyronin • Biotinylated molecular weight marker (Sigma, B2787) • Streptavidin conjugated horseradish peroxidase (Invitrogen, S911)

- Complete RPMI Media

	Vol (mL)	%	Stock Conc	Final Conc
RPMI (Irvine Scientific, 9159)	500	89.2		
Heat-inactivated FBS (Irvine Scientific, 300320439)	50	8.9		
Glutamax (Gibco, 35050-061)	5.5	0.98	200 mM	2 mM
Pen-strep (Gibco, 15140-148)	5.5	0.98	P 10000 U/mL S 10000 μg/mL	P 100 U/mL S 100 μg/mL

- Complete RPMI Media with 2% FBS

	Vol (mL)	%	Stock Conc	Final Conc
RPMI (Irvine Scientific, 9159)	500	96.1		
Heat-inactivated FBS (Irvine Scientific, 300320439)	10	1.9		
Glutamax (Gibco, 35050-061)	5.1	0.98	200 mM	2 mM
Pen-strep (Gibco, 15140-148)	5.1	0.98	P 10000 U/mL S 10000 μg/mL	P 100 U/mL S 100 μg/mL

- Click-iT palmitic acid, azide (Invitrogen, C10265)
  a. Since want the final concentration of the probe to be at 50 μM, stock concentration will be made at 50 mM (1000X stock).

$$0.001\ \text{g} \times \frac{\text{mol}}{283.41\ \text{g}} \times \frac{\text{L}}{0.05\ \text{mol}} \times \frac{\mu\text{L}}{10^{-6}\text{L}} = 70.6\ \mu\text{L}$$

- Since final volume will be at 4 mL (20 x 10^6 cells in 4 mL in 35 mm plate), will be using 4 µL.
- Aliquot into 5 µL aliquots, and store in -80 ºC.

- Homogenization buffer A (can be prepared beforehand and store at 4 °C, good for 3 months).

Components	Amount for 5 mL	Final Conc
1M Tris-HCl, pH = 8.0	0.25 mL	50 mM
20% (w/v) SDS 20 g of SDS in 100 mL of ddH_2O	0.25 mL	1%
ddH_2O	4.2 mL	

- On the day of the protein extraction, add the following components (Homogenization buffer B).

Components	Dilution Factor	Amount for 5 mL	Final Conc
10 mM Sodium Orthovanadate 1.839 mg/mL	1:100	50 µL	100 µM
Sigma Protease Cocktail	1:25	200 µL	
Benzonase Nuclease (Sigma, E1014-5KU)	Lot Dependent	Lot Dependent (~ 1 µL)	250 units

- Click-iT biotin, alkyne (Invitrogen, B10185)
  a. Since want the final concentration of the probe to be at 40 µM, stock concentration will be made at 4 mM (100X stock).

$$0.001\ \text{g} \times \frac{\text{mol}}{528.66\ \text{g}} \times \frac{\text{L}}{0.004\ \text{mol}} \times \frac{\mu\text{L}}{10^{-6}\text{L}} = 472.9\ \mu\text{L}$$

  - Since dilute 1:100 in 100 µL, will be using 10 µL per reaction.
  - Aliquot into 12 µL aliquots, and store in -80 ºC.

- Immunoprecipitation buffer A

Components	Volume (µL) for 5 mL	Final Conc
500 mM Tris-HCl (pH = 7.5), Fisher #BP153 6.1 g/100 mL	500 µL	50 mM
100 mM EGTA (pH = 7.5), Sigma #E4378 0.38 g/10 mL Add NaOH to get it to dissolve and bring pH up to 7.5	750 µL	15 mM
500 mM NaCl, Sigma #S3014 0.168 g/10 mL	1 mL	100 mM
10% Triton X-100, Sigma #X100 2 mL in 20 mL ddH_2O	50 µL	0.1%
ddH_2O	1.75 mL	

- On the day of the protein extraction, add the following components (Homogenization buffer B).

Components	Dilution Factor	Amount for 5 mL	Final Conc
10 mM Sodium Orthovanadate, Sigma #S6508 1.839 mg/mL		250 µL	500 µM
Sigma Protease Cocktail, Sigma #P8340	1:25	200 µL	
β-mercaptoethanol, Sigma #M6250 14.2 M		3.5 µL	10 mM

Procedures

Isolation of $CD4^+$ T Cells

20. Follow Isolation of T cells protocol.
21. After isolation of T cells, resuspend the $CD4^+$ T cells with warm complete RPMI to get a final concentration of T cells at 15 x 10^6 cells/1 mL in complete RPMI media.
22. Leave the cells in the 15 mL conical tubes, and incubate at 37 °C for 1 hr.
23. Prepare 35 mm plate by adding 3 mL of RPMI media with 2% FBS per plate. Incubate at 37 °C until use.

24. Seed 1 mL of cells per 35 mm plate. Incubate overnight at 37 ºC, 5% CO_2.

Incubation with Fatty Acid Probes

1. The next morning, add 4 µL of 50 mM ω-alkyl probes into each plate (50 µM final concentration). Incubate at 37 ºC, 5% CO_2 for 24 h.
2. Collect cells by transferring the media into a 15 mL conical tube. Wash the plate with 3 mL of RPMI media with 2% FBS twice to try to collect as many cells as possible. Pipette up and down in order to dislodge cells that are stuck on the plate. Spin at 350 g, 5 min.
3. Pool 2 wells per sample by washing 2 wells of cells with 1mL of PBS and transfer into 1.5 mL microcentrifuge tube. Count the number of viable cells using Trypan Blue. Spin at Spin at 350 g, 5 min.
4. Resuspend the pellet in 500 µL of complete homogenization buffer (i.e. A + B).
    - Because of the high number of cells, the lysate will be very viscuous due to the DNA. Treatment with Benzonase will digest the nucleic acids and eliminate any precipitate.
5. Incubate on a rotator for 30 min at 4 ºC.
6. Vortex the lysate for 5 minutes to further solubilize proteins and disperse the DNA.
7. Centrifuge at 14000 g for 20 min at 4 °C.

Protein Concentration

1. First insert the Millipore YM-3 centrifugal filter reservoir into the provided vial. This concentrator has a molecular weight cut-off of 3 kDa.
2. Load 500 µL of lysate into the sample reservoir without touching the membrane with the pipette tip. Seal the reservoir with attached cap.
3. Spin the concentrator at 14000 g, at 4 ºC for 30 min. Check to see the amount of sample retained in the sample reservoir. Should aim for approximately 50 ~100 µL.
4. If the sample volume in the sample reservoir is more than desired, spin at 14000 g at 4 ºC for more time, and check the volume. Can keep on repeating until the volume in the reservoir is the right volume.
5. Once the volume is optimized, turn the reservoir upside down into a new 1.5 mL microcentrifuge tube. Spin at 1000 g at 4 ºC for 10 min.
6. Proceed to Pierce BCA Protein Assay Kit (Thermo Scientific, 23225) or store at -80 ºC.

BCA Protein Assay

1. Preheat an incubator at 37 ºC.
2. Start by preparing 7 protein standards.

Final BSA Concentration (µg/mL)	Volume of Homogenization Buffer (A) (µL)	Volume and Source of BSA (µL)
2000	0	Remaining volume of 2 mg/mL stock
1500	125	375 µL of 2 mg/mL stock
1000	325	325 µL of 2 mg/mL stock
750	175	175 µL of 1500 µg/mL
500	325	325 µL of 1000 µg/mL
250	325	325 µL of 500 µg/mL
125	325	325 µL of 250 µg/mL
0	400	0

3. In a 96-well microplate, pipette 10 µL of standards and samples.

	1	2	3	4	5	6	7	8	9	10	11	12
A	2000	2000	2000									
B	1500	1500	1500									
C	1000	1000	1000									

D	750	750	750									
E	500	500	500									
F	250	250	250									
G	125	125	125									
H	0	0	0									

4. Prepare the BCA working solution by mixing 50 parts of reagent A with 1 part of reagent B. Vortex to mix the components well. Transfer into a reservoir.
   - That means add 50 mL of reagent A and 1 mL of reagent B. Adjust accordingly.
5. Using a multichannel pipette, add 200 µL of BCA working solution into each well. Mix thoroughly with a plate shaker for 30 sec.
6. Cover the plate with an adhesive plate cover and incubate at 37 ºC for 30 min.
7. Measure the absorbance at 562 nm on a plate reader.

Click Chemistry

1. Prepare Component C (additive 1) and Component D (additive 2) of Click-iT kit. These can be stored as stock solutions.
   - Component C → add 500 µL of deionized water to Component C and mix until fully dissolved. Store at -20 ºC. Stabile for up to 1 year. If the colour turns from colourless to brown, it is oxidized. Discard.
   - Component D → add 540 µL of deionized water to Component D mix until fully dissolved. Store at 4 ºC. Stabile for up to 1 year.
2. Prepare Click-iT reaction buffer.
   - Dilute biotin-alkyne 1:100 in Component A by adding 10 µL of 4 mM biotin-alkyne and 90 µL of Component A.
   - The above is for one reaction, so scale up as required.
3. To set-up the reaction, add the following reagents **<u>in sequence</u>** in 1.5 mL microcentrifuge tube (see next page for the complete table).
4. Rotate end-over-end or vortex continuously for 30 min. Protect from light.

Reagent	Volume (µL)
Cell Lysate (<200 µg/µL)	50
Prepared Click-iT reaction buffer (with biotin-alkyne)	100
ddH_2O	10
Vortex for 5 sec at high setting	
$CuSO_4$ (Component B)	10
Component C	10
Vortex for 5 sec at high setting Wait for 3 min.	
Component D	20
Total Volume	200

Protein Precipitation

1. Add 600 µL of methanol to the reaction mixture and vortex for 5 seconds.
2. Add 150 µL of chloroform and vortex for 5 seconds.
3. Add 400 µL of ddH_2O and vortex for 5 seconds.
4. Centrifuge for 5 min at 18000 g. Remove and discard as much upper aqueous phase as possible while leaving the interface layer containing the protein precipitate intact.
5. Add 450 µL of methanol and vortex for 5 seconds.
6. Centrifuge 5 min at 18000 g to pellet the protein. Discard the supernatant.
7. Wash the protein pellet by adding an additional 450 µL of methanol and vortex for 5 seconds. Centrifuge for 5 min at 18000 g to pellet the protein again, Discard the supernatant.

8. Allow the pellet to air dry by keeping the tube open covered with a lint-free tissue. Time length is approximately 5 min. Do not over-dry since this will make solubilizing the proteins difficult.
9. Store the samples at -20 ºC.

Immunoprecipitation using Streptavidin Dynabeads

1. Prepare complete immunoprecipitation buffer by combining component A and component B. Store on ice.
2. Resuspend the protein pellet stored at -20 ºC with 100 µL of complete immunoprecipitation buffer. Gentle heat while vortexing can help with the solubilization process.
3. Determine the protein concentration using Coomassie assay.
4. Make the following standards in glass tubes.

Protein µg	BSA 0.25 µg/µL	BSA 1 µg/µL	BSA 2 µg/µL	ddH_2O	Homogenization Buffer	Coomassie Reagent
0	0 µL			497.5 µL	2.5 µL	500 µL
0.5	2 µL			495.5 µL	2.5 µL	500 µL
1.0	4 µL			493.5 µL	2.5 µL	500 µL
2.0		2 µL		495.5 µL	2.5 µL	500 µL
4.0		4 µL		493.5 µL	2.5 µL	500 µL
10.0		10 µL		487.5 µL	2.5 µL	500 µL
20.0			10 µL	487.5 µL	2.5 µL	500 µL

5. Make the samples in glass tubes. Need to make samples for each aliquot.

Sample Amount	ddH_2O	Coomassie Reagent
2.5 µL	497.5 µL	500 µL

6. Perform the assay in triplicates (both samples and standards). For each standard or sample, load 3 wells/sample. Transfer 300 µL to a microtiter plate.
7. Read at $A_{595\ nm}$ immediately.
8. Combine the following amount of proteins with antibody to a final volume of 500 µL.

Protein Amount (µg)	Antibody	Antibody Range (µg)
100	Anti-LAT at 1 µg/µL	8 – 10
	Anti-Lck at 1 µg/µL	4

9. Place the samples by rotating the tubes on an orbital shaker at 4 ºC for 90 min.
10. At this time, prepare the Protein G Dynabeads by place the beads on an orbital shaker for 5 min at room temperature to completely resuspend the beads. Transfer 50 µL of Dynabeads to a 1.5 mL microcentrifuge tube. Separate on the magnet for 1 min (or until the supernatant is clear), and remove the supernatant.
11. After 90 min incubation of the samples, quickly spin down the samples and add the antibody-antigen (Ab-Ag) mixture to the Dynabeads. Rotate the samples on an orbital shaker at 4 ºC overnight.
12. The next day, place the samples on the DynaMagnet for 1 min to clear the supernatant. Save the supernatant as flow-through.
13. Wash the samples by adding 200 µL of immunoprecipitation buffer and resuspending by gentle pipetting. Separate on the magnet and remove the supernatant (discard). Repeat the wash two more times.
14. Resuspend the samples in 100 µL of immunoprecipitation buffer and transfer into a new 1.5 mL microcentrifuge tube. This is recommended to avoid co-elution of proteins bound to the tube wall.
15. Place the tube on the magnet and remove the supernatant.
16. Add 35 µL of 2X pyronin and gently pipette to resuspend the sample. Heat the samples at 98 ºC for 10 min.
17. Place the tube on the magnet and remove the supernatant to a new tube. Keep the supernatant in a new tube.
18. Resuspend the beads in 100 µL of immunoprecipitation buffer and transfer into a new 1.5 mL microcentrifuge tube. Place the tube on the magnet and remove the supernatant.

19. Resuspend the beads in 35 μL of immunoprecipitation buffer and combine with the supernatant from Step 13.

Notes:

- The protein concentration for T cells is approximately 65 μg/10^7 cells (May 2011, Liem & Logan's T cell isolation and protein quantification).
- Immunoprecipitation is from HFT's Dissertation (Current Protocols in Protein Science 19.4.5).